Optimisation of a non-linear tuned vibration absorber in a hand-held impact machine

Master's Thesis in Applied Mechanics

MATTIAS JOSEFSSON
SNÆVAR LEÓ GRÉTARSSON

Department of Applied Mechanics
CHALMERS UNIVERSITY OF TECHNOLOGY
Göteborg, Sweden 2015

MASTER'S THESIS IN APPLIED MECHANICS

Optimisation of a non-linear tuned vibration absorber in a hand-held impact machine

MATTIAS JOSEFSSON
SNÆVAR LEÓ GRÉTARSSON

Department of Applied Mechanics
Division of Dynamics
CHALMERS UNIVERSITY OF TECHNOLOGY

Göteborg, Sweden 2015

Optimisation of a non-linear tuned vibration absorber in a hand-held impact machine
MATTIAS JOSEFSSON
SNÆVAR LEÓ GRÉTARSSON

Master's Thesis 2015:19
ISSN 1652-8557
Department of Applied Mechanics
Division of Dynamics
Chalmers University of Technology
SE-412 96 Göteborg
Sweden
Telephone: +46 (0)31-772 1000

Cover:
Previous pneumatic breaker prototype made by Swerea IVF, standing in a stone in Ävja quarry. In the background is one of the older machines without any vibration reduction.

Chalmers Reproservice
Göteborg, Sweden 2015

Optimisation of a non-linear tuned vibration absorber in a hand-held impact machine
Master's Thesis in Applied Mechanics
MATTIAS JOSEFSSON
SNÆVAR LEÓ GRÉTARSSON
Department of Applied Mechanics
Division of Dynamics
Chalmers University of Technology

Abstract

Traditionally, hand-held impact machines (HHIM) such as pneumatic breakers have little or no means of vibration reduction. Consequently, vibration injuries are a common problem for individuals working with them on a daily basis. Some existing HHIM utilise vibration isolation between the handle and the impact mechanism, but the vibrations are still above the levels defined by health standards.

Swerea IVF is currently running a project with the long-term goal to prevent all vibration injuries in industry. A breakthrough towards that goal was to successfully implement a non-linear tuned vibration absorber (TVA) on a pneumatic HHIM prototype and thereby lowering the vibrations significantly on a wide frequency band. Some electric machines have previously been fitted with a TVA but the varying operating frequency of pneumatic machines has been a problem since traditional linear TVAs are only effective in a very narrow frequency range.

This thesis investigates how the new non-linear TVA parameters can be optimised to minimise the vibrations of the prototype while keeping the suppression band wide enough. An efficient, verified and validated simulation model of a pneumatic breaker utilising a non-linear TVA is developed and implemented in Matlab. The model is used to optimise the 3 parameters of the TVA and to investigate the sensitivity of the solution to different model parameters. It is also investigated how the mass ratio of the TVA affects the optimal solution. The results show that using a non-linear TVA can significantly reduce the vibration of a pneumatic HHIM over a broad frequency range and thereby reduce the risk of vibration injuries significantly.

Keywords: Impact machine, Non-linear, Tuned vibration absorber, Tuned mass damper, Multi-body simulation, Hand-arm vibration

Preface

This thesis work is submitted as the final requirement for our MSc degrees in Applied Mechanics from Chalmers University of Technology. The work was carried out during a period of 20 weeks, from January to June 2015. It was conducted on behalf of and in close cooperation with Swerea IVF, a Swedish research institute within production and product development. Hans Lindell was our supervisor at IVF and Professor Viktor Berbyuk was our examiner at Chalmers.

Acknowledgements

There are two people we would like to thank for the opportunity to be part of this exciting work and for great help along the way to successfully finishing this thesis. Our first thanks goes to our examiner Viktor Berbyuk, for his good feedback, ideas and endless help. Secondly, we are truly grateful to Hans Lindell, our supervisor at Swerea IVF, for consistently being there with insightful thoughts and unsurpassed enthusiasm for this technology and engineering thinking in general. Many thanks to both of you.

Göteborg, June 2015

Mattias Josefsson

Snævar Leó Grétarsson

Nomenclature

Symbol	Unit	Description
m_{m}	kg	Main mass
m_{a}	kg	Auxiliary mass
m_{h}	kg	Housing mass
m_{pist}	kg	Piston mass
k_{m}	N/m	Stiffness between main mass and ground
k_{a}	N/m	Stiffness between main mass and auxiliary mass
k_{h}	N/m	Stiffness between main mass and housing
k_{p}	N/m	Hand-arm stiffness between housing and ground
c_{m}	N s/m	Damping between main mass and ground
c_{a}	N s/m	Damping between main mass and auxiliary mass
c_{h}	N s/m	Damping between main mass and housing
c_{p}	N s/m	Hand-arm damping between housing and ground
a	m	Gap of auxiliary spring
F_0	N	Preload of auxiliary spring
b	m	Compression length of auxiliary spring
F_{e}	N	Exciting force from piston acting on main mass
$\lvert F_{\mathrm{e}}\rvert$	N	Amplitude of exciting force
F_k	N	Non-linear auxiliary spring force acting on main mass
x_1, x_2, x_3	m	Displacements of main mass, auxiliary mass and housing respectively
x_{rel}	m	Auxiliary mass displacement relative the main mass; $x_2 - x_1$
$\mathbf{z}(t)$		State vector as a function of time
P		Set of parameters
P_0		Set of parameters, nominal values
p		Set of normalised parameters
p_{x}		Normalised parameter x, where x is any of the model parameters
f	Hz	Operating frequency (or excitation frequency)
f_{nom}	Hz	Nominal operating frequency
f_{res}	Hz	Resonance frequency of non-linear auxiliary system
$W(f)$		Weighting as a function of frequency
L		Objective function value

Abbrevations

Abbrevation	Description
TVA	Tuned Vibration Absorber
LTVA	Linear Tuned Vibration Absorber
NLTVA	Non-Linear Tuned Vibration Absorber
HAVS	Hand-Arm Vibration Syndrome
HHIM	Hand-Held Impact Machine
DOF	Degree Of Freedom
RMS	Root Mean Square
ODE	Ordinary Differential Equation
FFT	Fast Fourier Transform

Contents

Abstract **V**

Preface **VII**

Acknowledgements **VII**

Nomenclature **IX**

Abbrevations **IX**

Contents **XI**

1 Introduction **1**
1.1 Background . . . 1
1.2 Purpose . . . 1
1.3 Limitations . . . 2

2 Theory and method **2**
2.1 Tuned vibration absorbers . . . 2
2.2 Hand-arm vibration . . . 4
2.3 The prototype machine . . . 5
2.4 Analytical formulas for the auxiliary system . . . 7
2.5 Measurements . . . 7
2.6 Computations . . . 8

3 The model **8**
3.1 Non-linear tuned vibration absorber . . . 8
3.2 Equation of motion . . . 9
3.3 Numerical model . . . 10
3.3.1 ODE solver . . . 11
3.3.2 Strategy of computation . . . 11
3.3.3 Spring force smoothing . . . 12
3.4 Model parameters and sensitivity analysis . . . 13
3.4.1 Mass of parts . . . 13
3.4.2 Stiffness . . . 13
3.4.3 Damping . . . 15
3.4.4 Optimisation parameters . . . 18
3.4.5 Exciting force . . . 18
3.5 Verification . . . 23
3.6 Validation . . . 26

4 Optimisation method **30**
4.1 Objective function . . . 30
4.2 Non-linear least squares formulation . . . 32
4.3 Optimisation algorithm . . . 32

5 Optimisation results **32**
5.1 Nominal auxiliary mass . . . 33
5.1.1 Comparison with an LTVA . . . 34
5.1.2 The solution's sensitivity . . . 36
5.1.3 Different exciting force assumptions . . . 37
5.2 Sensitivity to mass ratio . . . 40
5.2.1 Chaotic behaviour with low mass ratios . . . 42

5.3 Free damping 44
5.4 Free auxiliary mass 45
5.5 Removing a resonance with the proposed NLTVA 46

6 Conclusions **49**

7 Recommendations **50**

References **50**

A Derivation of analytical formulas for the non-linear auxiliary system **53**

B Pictures of measurement set-up **56**

C Flowchart of the optimisation routine **57**

1 Introduction

This project is performed in close cooperation with Swerea IVF, a Swedish research institute. In the project, a computational model is developed, validated against experimental results and used to minimise vibration in a hand-held impact machine. The background and goals of the project are described below.

1.1 Background

Vibration is a common issue in industrial working environments and can cause severe injuries, especially for operators of pneumatic hand-held impact machines (HHIM) such as pneumatic hammer drills and breakers. The injuries are commonly denoted Hand-Arm Vibration Syndrome (HAVS) and are often manifested as the so called "white fingers". Some of the symptoms experienced in the hands are cold intolerance, tingling sensation, impaired sensation and impaired fine motor skills [1, 2]. Reducing vibration levels in HHIMs is highly desirable.

One common strategy is to construct some sort of isolating layer of springs between the impact mechanism and the handles, but that still requires a very large mass at the handles in order to achieve satisfactory vibration levels. The isolating layer could also consist of semi-active components, e.g. MR-dampers, or actuators for active vibration control, but that increases the complexity of the machine greatly and also requires electric power. A different approach is to absorb vibration at the source using a tuned vibration absorber (TVA) attached to the impact mechanism. This can reduce vibration without significantly increasing the overall mass of the machine.

TVA is a well-known classical concept for reducing vibration in a primary structure by attaching an auxiliary system consisting of a small mass with a spring, which are tuned to a certain frequency, and thereby creating a counterforce that counteracts the vibration in the primary structure. Traditionally, this technology has been greatly restricted to operate only in a very narrow frequency range. It is therefore unsuitable for pneumatic impact machines since their operating frequency can vary considerably. However, it has been shown that the useful frequency range can be broadened substantially by introducing non-linearities into the auxiliary system [3].

Recent breakthrough concerning pneumatic HHIMs has been done at Swerea IVF using a non-linear tuned vibration absorber (NLTVA) in combination with a vibration isolating layer. The effective non-linearity is achieved by a simple construction consisting of a gap and a preload in the auxiliary spring. This has paved the way for a large project starting in 2015, run by Swerea IVF and funded by Vinnova, with the overall purpose to eliminate vibration injuries. A patent covering this technology was filed in 2012 [4]. The technique of using NLTVA in combination with vibration isolation has already been tried out in a handful of prototype machines and opens up a wide field of new possible applications [5, 6].

1.2 Purpose

The main purpose is to improve the NLTVA technology developed at Swerea IVF, in terms of minimising the vibrations experienced by operators of the machines. In order to do this, a reliable model of a pneumatic impact machine prototype as well as an optimisation routine is developed and implemented in MATLAB. The model is verified mathematically and validated experimentally against an existing prototype. It is based on an older model that has previously been validated in a specially designed test rig. The new model is more refined and efforts are made to make it more computationally efficient.

The model is used to optimise the NLTVA on pneumatic HHIMs as well as investigating its general behaviour. In particular, it is desired to answer the following questions:

- How "refined" does the model need to be in order to capture all the relevant phenomena?
- How should the model be parametrised and how does the different parameters affect performance?
- What is a suitable objective function for evaluating the level of vibration?
- How well can the NLTVA be optimised to reduce vibration?
- How does the mass ratio affect the performance of the NLTVA?

- Can the current NLTVA be used to remove resonances?

1.3 Limitations

Some specific tasks that will not be treated in this project include testing on optimised machines, building new prototypes and performing any strength or fatigue analysis on the machine.

2 Theory and method

This chapter covers basic information that is useful before developing a model and obtaining results. A brief study of tuned vibration absorbers in general is presented, followed by a section concerning hand-arm vibration including some relevant standards and regulations. The prototype machine is explained and its model parameters introduced. A few analytical results are shown. The experimental and computational set-up and methodology is described.

2.1 Tuned vibration absorbers

Tuned vibration absorbers (TVA) have been used for over a century to suppress vibrations in structures and mechanical systems. Civil applications include skyscrapers, bridges and power lines where the absorbers are tuned to suppress vibration at frequencies excited by the environment. The first patented tuned vibration absorber was Frahm's *Device for damping vibrations of bodies*, granted in 1911 [7].

The theory of the linear tuned vibration absorber (LTVA) was first published in 1928 by Den Hartog [8]. Undamped LTVAs are practical when an undamped 1-DOF system is excited at its eigenfrequency, cf. Figure 2.1. By tuning the eigenfrequency of the added auxiliary system to the main system's eigenfrequency, all vibration

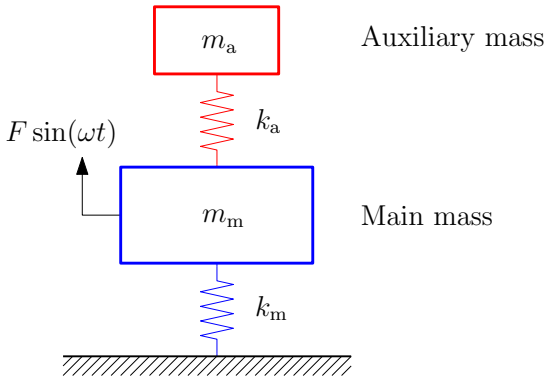

Figure 2.1: An undamped LTVA (red) applied to an undamped linear main system (blue) that is excited by a harmonic force.

of the main system is suppressed at that frequency, which is called the tuned frequency. A drawback using an undamped LTVA is that the system, now being a 2-DOF system, has two undamped eigenfrequencies, one slightly below the excitation frequency and the other slightly above it, with infinitely high resonance peaks. This is problematic when passing one of the eigenfrequencies during operation start-up and if the excitation frequency varies. A small variation can move the excitation frequency close to one of the two new resonance peaks and cause vibration in the main system to be amplified. Therefore the use of undamped LTVAs is limited to very well-controlled systems [9].

Damping can be introduced in the system to lower the two resonance peaks to finite values. Using a damped LTVA is very common in buildings and machines where the excitation frequency can vary significantly and the response at an eigenfrequency is too large for the structure to handle. The LTVA can be tuned using Den Hartog's equal-peaks method resulting in a response curve where, instead of having one unacceptably high resonance peak, you get two equally high peaks that are significantly lower [9]. The drawback of introducing damping to the system is that the vibration of the main system is no longer completely suppressed at the

tuned frequency. Typical unitless response of a 1-DOF system with and without an LTVA, for various damping ratios, tuned using the equal-peaks method, can be seen in Figure 2.2.

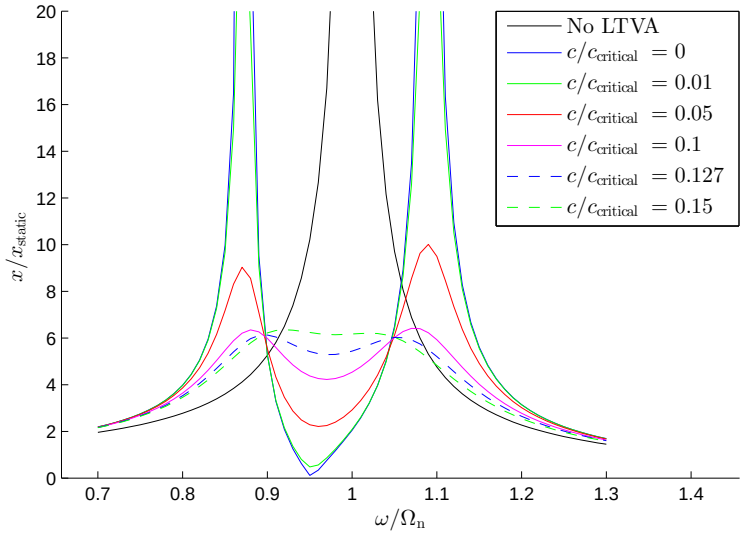

Figure 2.2: Typical unitless response of a 1-DOF main system, with and without an LTVA, around its unitless eigenfrequency. Ω_{n} is the eigenfrequency of the main system and ω is the excitation frequency. The response is shown for several damping ratios.

As can be seen in Figure 2.2, increasing the damping does not at all widen the suppression band, i.e. the band of frequencies in which the unitless response of the main system is below unity. The effect is only lowered peaks and decreased vibration suppression between the peaks, i.e. a flattening of the response curve. Note that the tuned frequency (antiresonance at the minimum in the figure) is slightly below the eigenfrequency of the system. The equal-peaks method does this to keep the resonance peaks of equal height. When the damping ratio of the LTVA in Figure 2.2 is $c/c_{\text{critical}} = 0.127$, the peaks are as low as they can get. This is often used in buildings or machines that are excited at varying frequencies and cannot handle to be excited at their eigenfrequency because that would cause too large and damaging vibration. Nor can they handle being excited at the two new high resonance peaks that would be introduced if the damping was very low. A relatively high damping is therefore needed. The trade-off is a limited vibration suppression at the main system's eigenfrequency compared to the undamped case.

Although the most obvious use of TVAs may be to suppress vibration caused by excitation at the resonance frequencies of systems, it is also common to use them to limit vibration at other excitation frequencies that are well controlled. For example, the excitation frequency ω in Figure 2.1 may be different from the eigenfrequency of the main system. A few examples are in hair clippers, electric impact machines and torsional TVAs on drive shafts. In these situations, the damping in the auxiliary system should be very low for maximum suppression. It is though very important that the excitation frequency is well controlled and can be held constantly very close to the TVA's tuned frequency. Remember that, by adding the TVA, a new resonance frequency is added just next to the tuned frequency.

A different approach to using LTVAs is to control the placement of nodes in a vibrating beam. This has recently been used by Hao et al. In 2011, they reduced the acceleration of the handle on an electric grass trimmer by 67 % by moving the nodal points of the beam closer to the handles [10]. In 2013, they showed that a similar reduction in acceleration can be achieved for a petrol engine grass trimmer [11].

Historically TVAs where linear and, as explained above, the vibration attenuation was limited to a very narrow frequency range around their eigenfrequency. Consequently, engineers have been investigating non-linear TVAs (NLTVA) for over 60 years to broaden the suppression frequency band for non-linear structures or mechanical systems with varying excitation frequencies. Roberson's synthesis from 1952 [3] showed theoretically that a TVA with cubic softening would have much broader suppressing frequency band than a linear one. Pipes showed similar results in 1953 [12] and Arnold in 1955 [13]. In 1982, Hunt and Nissen showed that the suppression

band can be doubled by using softening springs of Belleville type [14], and in 2011, Min Wang showed that switching from a linear to a non-linear TVA for chatter suppression in a milling machine would increase the critical cutting depth by around 30 % [15].

Several patents have been filed regarding the use of TVAs to reduce the vibration of HHIMs, but most of them are for electric impact machines and not pneumatic. One of those is *US20120279741* [16] where the TVA is given non-linear characteristics using two parallel springs of different length at each side of the auxiliary mass. The longer springs are always in contact with the auxiliary mass giving it normal linear characteristics. When the amplitude of vibration of the auxiliary mass becomes grater than the length difference of the springs the shorter springs come in contact with the auxiliary mass giving it increased stiffness. This increases the eigenfrequency of the auxiliary system and prevents too high loads on the longer springs. The patent also includes a centrifugal mechanism that can vary the preload of the springs with frequency to change the eigenfrequency of the TVA. There is also *US8434565* [17] where two LTVAs are tuned to slightly different frequencies to give a broader suppression band. *US8066106* [18] uses an LTVA which eigenfrequency can be increased by the operator, via a switch that connects extra springs. *US7712548* [19] covers a pneumatic power tool with an LTVA attached to both the impact mechanism and the housing, i.e. it is placed in the middle of an isolating layer between the impact mechanism and housing.

In 2012, the European Research Council started funding a 5 year long project called *The Nonlinear Tuned Vibration Absorber*, led by Prof. Gaëten Kerschen at Universite De Liege in Belgium. The project's goal is to investigate how the intentional use of non-linearities in TVAs can be used to solve non-linear vibration problems in aircraft as well as other applications [20]. Some preliminary results, where cubic non-linearity is used, include [21] where they introduced a tuning rule for NLTVAs and [22] where they showed that a 3D printed NLTVA was superior to an LTVA when applied on a non-linear primary system.

2.2 Hand-arm vibration

The amount of vibration transferred from machine, through hand, to body depends on several factors such as frequency, handling force, arm position, wrist angle and the operator's physique. Low frequency vibration tends to propagate to the entire hand-arm system, while high frequency vibration is damped closer to the handle [23].

Swedish Work Environment Authority regulations [24] and European Agency for Safety and Health at Work regulations [25] specify that hand-arm vibration exposure is assessed according to the adopted standard (ISO 5349-1:2001) [26]. A vibration value is given in terms of root mean square (RMS) of the frequency-weighted acceleration on the machine's handle surface. The RMS value corresponds to the vibration's energy content per unit time. The frequency weighting is performed to account for the human body's sensitivity to different frequencies. Effectively, frequencies below about 5 Hz and above about 1300 Hz are filtered out in the weighting. The weighting filter is also designed such that, at frequencies above about 20 Hz, acceleration is integrated to velocity to reflect the vibration energy absorption to the hand which is believed to cause the injuries. The standard frequency-weighting curve is seen in Figure 2.3.

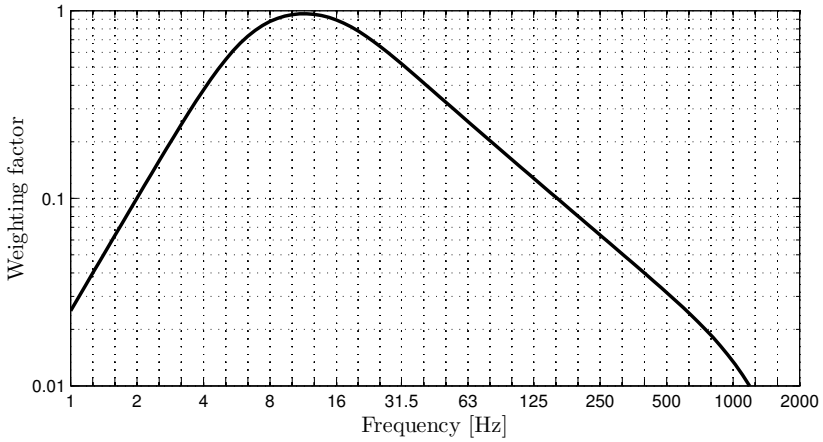

Figure 2.3: Frequency-weighting curve for hand-arm vibration.

Vibration exposure is expressed as an 8-hour energy-equivalent frequency-weighted vibration value, denoted A(8) [26]. That value is used to compare the daily exposure to the exposure action value of 2.5 m/s^2 and the exposure limit value of 5.0 m/s^2 [24]. When exceeding the action value, action on the working environment is required by the employer. The limit value should never be exceeded. A long-term goal is therefore to be able to produce machines with vibration values less than the action value 2.5 m/s^2, meaning the machine can be operated for 8 hours straight without any action required by the employer.

2.3 The prototype machine

The prototype machine that is modelled and investigated in this project is a pneumatic HHIM named P3B and manufactured by Swerea IVF, see Figure 2.4b. It comprises an impact mechanism (main mass and piston), auxiliary mass, housing and chisel, cf. Figure 2.4a. The main mass and housing is considered as the primary system, while the auxiliary mass with its damper and non-linear spring is an auxiliary system.

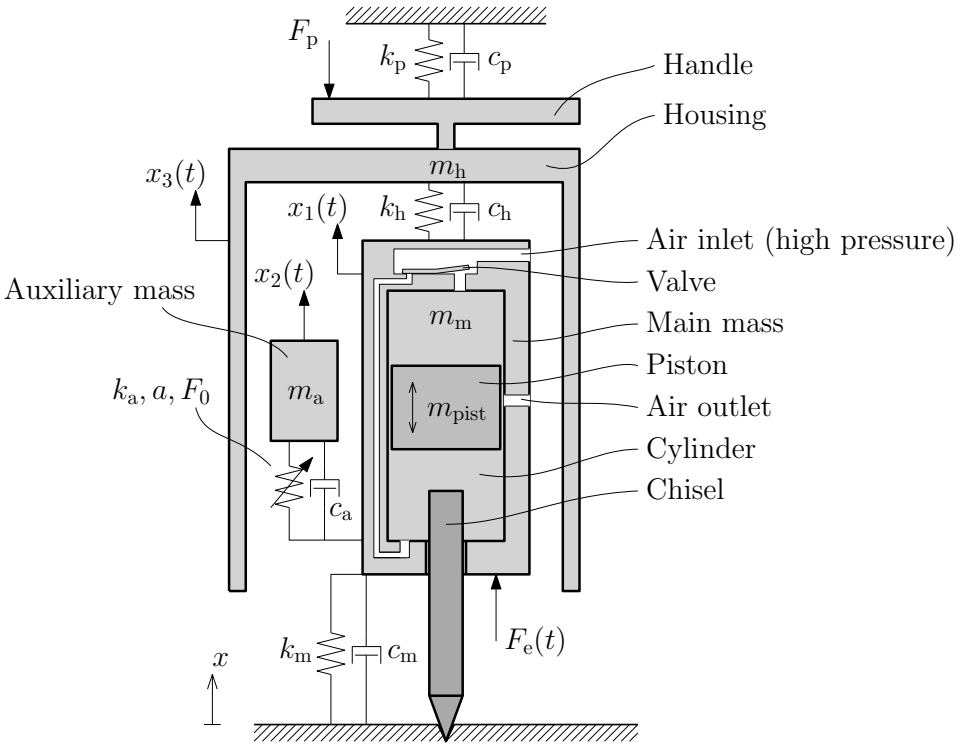

(a) Engineering model of the prototype machine, introducing model parameters.

(b) Current prototype version; P3B.

Figure 2.4: The prototype machine.

The impact mechanism is very simple. It basically consists of the piston reciprocating inside the cylinder in the main mass due to pneumatic air pressure and hitting the working tool, in this case a chisel, see Figure 2.4a. In the cylinder there are two air inlets, one at the top and one at the bottom, and one air outlet at the middle. A valve controls the inlet air flow so that it only enters either at the top or the bottom. The basic functional steps of the impact mechanism during one period of vibration are illustrated in Figure 2.5. Each time the piston passes the outlet hole, the currently active inlet becomes connected to the outlet and atmospheric pressure, cf. Figures 2.5c and 2.5f. The valve then closes that inlet due to pressure difference and at the same time opens the other inlet. The piston is then forced to accelerate in the other direction. So the point at which the shift of inlets happens is always the same. The piston hits the chisel on its way down, cf. Figure 2.5d, and the location of this impact depends on the downward feeding force from the operator. For maximum impact energy, the piston should have as great velocity as possible at impact. The feeding force must not be too small nor too large. Experienced operators are very good at finding the best operating condition for their machines. Via the air pressure, the piston exerts a periodic force on the main mass causing it to vibrate. This exciting force is

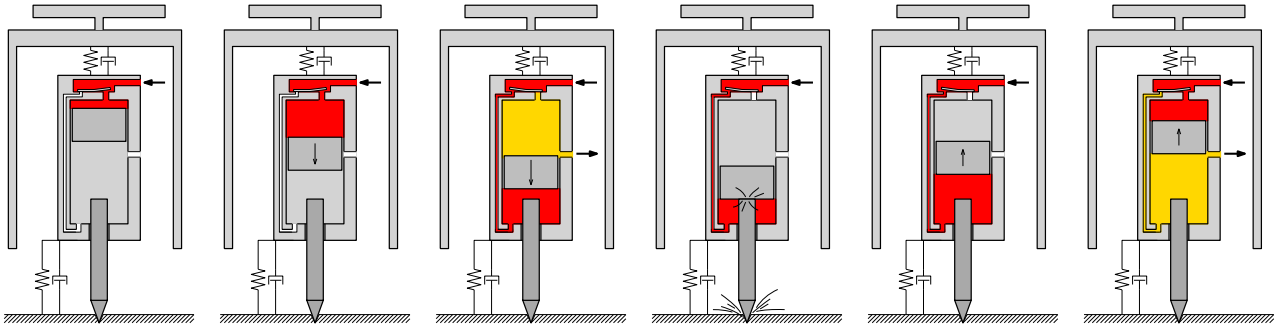

Figure 2.5: Function of the impact mechanism during one period of vibration.

approximately sinusoidal as will be seen in a later section. Note that the main mass practically has no axial connection to the chisel and the connection to ground via air pressure is very weak.

The auxiliary mass is allowed to vibrate alongside the main mass and is restricted by a non-linear spring characteristic, cf. Figure 2.4a. This is the NLTVA. It creates a force acting on the main mass that is opposite the exciting force. A more detailed description of the non-linear spring construction is given in a later section. The impact mechanism and NLTVA are encapsulated inside a housing on which the handles are attached. A spring between main mass and housing functions as a layer of isolation. The isolation acts in axial, radial and rotational direction. Most of the vibration is axial and rotational, but a portion is radial. The axial vibration is obvious since that is the working direction. Rotational vibration has been observed during high-speed filming. It consists of some very high transients and is much less regular. The cause of rotational vibration is believed to be when the shape of the stone hole and the chisel tip, which is oblong, are misaligned rotationally. Care has been taken by Swerea not to make the axial and rotational stiffness of the isolation too low which would compromise the controllability. Consistent with this, a study by Golysheva et al. concluded that the axial stiffness of the isolation would not need to be the lowest possible if a TVA was used to remove the low frequency accelerations [27]. On the other hand, the isolation cannot be too stiff for it to be effective. The resonant mode between the housing and main mass is kept at a frequency well below the operating frequency by not having the isolation too stiff. The housing also provides considerable noise reduction since it covers the air outlet of the impact mechanism.

Existing HHIMs, especially older types still in use, often have no means of vibration reduction except for being built heavy. But heavy machines are severely disadvantageous for ergonomic reasons. Some HHIMs have vibration isolation between the handles and impact mechanism [28, 29] and some electric machines utilise a linear TVA [17, 18, 30]. Since this prototype is pneumatic, the operating frequency is not well known or controllable and a linear TVA is infeasible for reasons previously discussed.

Some analytical results for an HHIM were obtained by Babitsky in 1998 to optimise the excitation from the piston by considering it as an optimal control problem [31]. The work was built on further by Golysheva et al. in 2003 where they added a flexible element to the piston to make the excitation itself more beneficial for the machine performance [32]. Their results were supported by numerical simulations in MATLAB. In 2007, Sokolov et al. considered different concepts other than TVA to suppress vibration at the handles [33]. They state that the simplest optimal solution that suppresses vibration completely is to let the housing be pushed against the ground, but severe disadvantages such as inconvenience for the operator and a high required feeding force were noted. They also suggested a theoretical zero-stiffness mechanism between the impact mechanism and housing. In other words this mechanism is a non-linear stiffness element that can transfer feeding force up to a point, above which the force does not change with displacement and thereby does not transmit any vibration. However, this mechanism turns out to be hard to realise and implement in practice.

Parameters of the prototype

The nominal model parameters of the current prototype machine can be seen in Table 2.1. If nothing else is stated, these are the model parameters that have been used in simulations. All parameters are introduced in Figure 2.4a, except $F_{\mathrm{e,ref}}$ and f_{ref} which are reference values for exciting force amplitude and corresponding

excitation frequency, respectively. Detailed descriptions of how the model parameters were determined will be presented in Section 3.4.

Table 2.1: Nominal model parameters of the prototype machine.

TVA parameters

Parameter	Value	Unit
k_a	40	kN/m
a	5	mm
F_0	190	N
m_a	1	kg
c_a	1	N s/m

Other model parameters

Parameter	Value	Unit
m_m	2.7	kg
m_h	3.1	kg
k_m	500	N/m
k_h	14000	N/m
k_p	1000	N/m
c_m	100	N s/m
c_h	20	N s/m
c_p	60	N s/m
$F_\mathrm{e,ref}$	351	N
f_ref	26.1	Hz

2.4 Analytical formulas for the auxiliary system

An exact analytical solution has been derived for the resonance frequency f_res of the non-linear auxiliary system with spring stiffness k_a, gap a and preload F_0. The assumption is that the main mass is completely still and there is no damping or gravity. The complete derivation is included in Appendix A and results in the following formula:

$$f_\mathrm{res} = \sqrt{\frac{k_\mathrm{a}}{m_\mathrm{a}}}\left[2\pi - 4\arcsin\left(\frac{F_0}{F_0 + k_\mathrm{a} b}\right) + 4a\sqrt{\frac{k_\mathrm{a}}{k_\mathrm{a} b^2 + 2F_0 b}}\right]^{-1} \tag{2.1}$$

for which the model parameters are introduced in Figure 2.4a and b is the spring compression in the NLTVA. This equation is used as a reference for verification of the mathematical and numerical model.

A solution for the spring compression b as a function of exciting force amplitude $|F_\mathrm{e}|$ acting on the main mass by the piston is also derived in Appendix A. It is based on the same assumptions as the above formula; main mass completely still and no damping or gravity. It reads

$$b = \frac{1}{k_\mathrm{a}}\left[\sqrt{\frac{k_\mathrm{a}}{m_\mathrm{a}}\left(\frac{|F_\mathrm{e}|}{2\pi f}\right)^2 + F_0^2} - F_0\right] \tag{2.2}$$

where f is the excitation frequency of the reciprocating piston.

2.5 Measurements

Measurements were performed on the prototype machine P3B mainly for two reasons; estimating model parameters, especially concerning the exciting force F_e, and for validating the developed computational model. The measurements were done running the machine in a test rig at Swerea IVF. The test rig, a so called ball absorber, is manufactured in accordance with standard ISO 28927-10 [34]. It consists of a horizontally supported chisel with its tip down in a closed cavity filled with small zirconium oxide balls. The balls absorb

the impact energy from the chisel, mainly into heat by friction, thus mimicking the rock-breaking. To support the machine vertically, either elastic bands or hands were used. The machine was pulled down with a force of approximately 80 N, which was measured with a personal scale.

Two different types of techniques were used to measure the motion of the machine running in the test rig: accelerometer and high-speed camera. The accelerometer was of type Dytran 3035B5 and the data was collected in National Instruments LabVIEW, SignalExpress module. The high-speed camera was a Casio EX-ZR1000, which is a digital camera that can film in 1000 fps at 224×64 resolution. The camera was placed about 1.5 m away from the machine to eliminate perspective distortion. It was zoomed in optically and tilted, resulting in very useful footage despite the low resolution. The footage was processed in the video analysis software Tracker 4.87. This gave the displacements of the filmed masses at a sampling frequency of 1000 Hz.

Pictures of the machine in the test rig, the accelerometer placement and an example of the video footage are shown in Appendix B.

2.6 Computations

All computations, simulations and processing of data were done in MATLAB, versions R2013b and R2014a. Only built-in MATLAB functions and code written by the authors of this thesis were used. In particular, spectral analysis was done using a Hann (Hanning) window and the built-in FFT implementation *fft* for magnitude and the cross power spectral density implementation *cpsd* for phase angles. The heavy computations during optimisation were performed using the *parfor* loop, a built-in parallel computing tool for distributing computation on several processors. Solving the system of ordinary differential equations (ODEs) was done using the solver *ode45*, which is based on an explicit Runge-Kutta formula and utilise adaptive time stepping and error control [35]. The optimisation was performed using the trust-region-reflective method and the Levenberg-Marquardt method, both implemented in the built-in *lsqnonlin* [36]. A brief description of the developed optimisation routine including a flowchart is presented in Appendix C. More information about the ODE solver and the optimisation is found in later sections.

3 The model

The following sections describe in detail how the HHIM was modelled and how its response was computed. The mathematical and numerical models are based on an earlier MATLAB code written at Swerea, which has been validated over a range of frequencies against test data from a specially designed test rig employing non-linearity from a gap [37]. This test rig has adjustable frequency, exciting force amplitude, TVA stiffness and gap so it is a much more controllable test set-up than the prototype itself. For example, it is not possible to sweep a range of operating frequencies in the prototype machine. The current model and computational implementation has been modified and improved on several points including: 1) adding the housing as a third DOF, 2) updated nominal parameters, 3) updated exciting force, 4) faster computations, e.g. by detecting limit cycles and smoothing the non-linear spring force, 5) more stringent solver tolerances for reducing errors, and 6) ensuring more accurate results by improving the code.

A few sections are then devoted to motivating the model parameter values and the exciting force used, including a sensitivity analysis of the system with respect to these parameters. The final sections cover verification and validation of the model.

3.1 Non-linear tuned vibration absorber

The non-linearities in the prototype's TVA are introduced by the gap length a as well as the preload F_0 of the auxiliary spring, cf. Figure 3.1a. The pins travel either with the auxiliary mass or the main mass depending on whether they are in contact with the main mass. This effect is not modelled since the mass of the pins is negligible in comparison with the other masses. Figure 3.1b shows the auxiliary spring force F_k acting on the main mass by the auxiliary mass as a function of their relative displacement $x_{\text{rel}} = x_2 - x_1$.

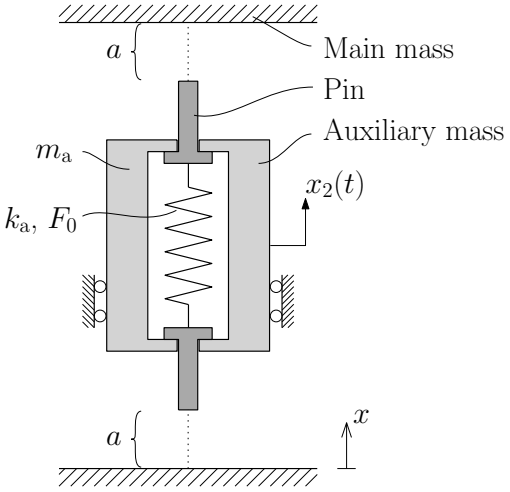

(a) Construction of the non-linear spring characteristic restricting the auxiliary mass. Ground represents the main mass.

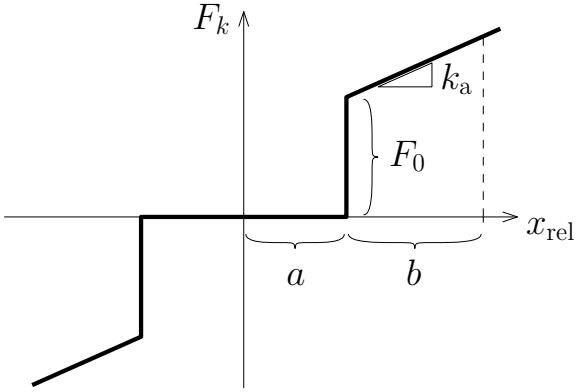

(b) Non-linear auxiliary spring force as a function of relative displacement between auxiliary and main mass.

Figure 3.1: NLTVA stiffness characteristic for the prototype machine, with spring stiffness k_a, gap length a, spring preload F_0 and spring compression b. The displacement amplitude of the auxiliary mass relative the main mass is $a + b$.

3.2 Equation of motion

The prototype machine is modelled mathematically according to Figure 3.2. Nominal model parameters were defined earlier in Table 2.1. Only axial vibration is modelled, i.e. vibration in the x-direction, since that is the direction in which the TVA functions. The behaviour of the operator's arms holding the machine is modelled as a spring and a viscous damper connected to ground in parallel. The mass of the hand-arm system is neglected for a couple of reasons. The effective mass of the hand-arm system is quite small and will have a minor influence of the TVA performance due to the housing as isolation layer. Moreover, including it would add one DOF to the model and increase computation time. The constant feeding force F_p supplied by the operator, as seen in Figure 2.4b, is neglected in the model since it would only contribute a constant downward displacement. Gravity, however, is still included in the model since it affects the behaviour of the NLTVA because of the gap and preload. Note though that the machine may sometimes be operated horizontally, which would correspond to gravity $g = 0$ in the model.

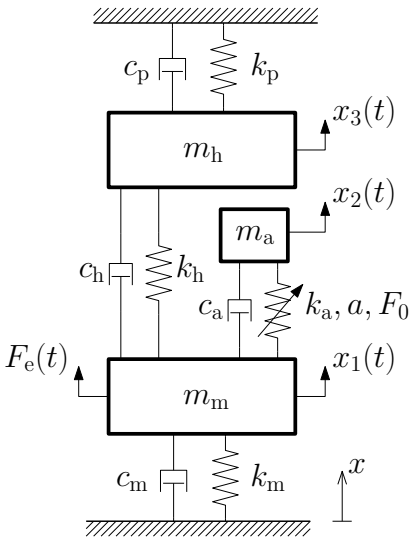

Figure 3.2: Mathematical model of the prototype P3B, a pneumatic HHIM.

The equation of motion for the 3-DOF system in Figure 3.2 is written as:

$$\begin{bmatrix} m_\mathrm{m} & 0 & 0 \\ 0 & m_\mathrm{a} & 0 \\ 0 & 0 & m_\mathrm{h} \end{bmatrix}\ddot{\mathbf{x}}+\begin{bmatrix} c_\mathrm{m}+c_\mathrm{h} & 0 & -c_\mathrm{h} \\ 0 & 0 & 0 \\ -c_\mathrm{h} & 0 & c_\mathrm{h}+c_\mathrm{p} \end{bmatrix}\dot{\mathbf{x}}+\begin{bmatrix} k_\mathrm{m}+k_\mathrm{h} & 0 & -k_\mathrm{h} \\ 0 & 0 & 0 \\ -k_\mathrm{h} & 0 & k_\mathrm{h}+k_\mathrm{p} \end{bmatrix}\mathbf{x}=\begin{bmatrix} F_\mathrm{e}(t,f)+F_k(\mathbf{x})+F_c(\mathbf{x},\dot{\mathbf{x}})-m_\mathrm{m}g \\ -F_k(\mathbf{x})-F_c(\mathbf{x},\dot{\mathbf{x}})-m_\mathrm{a}g \\ -m_\mathrm{h}g \end{bmatrix} \tag{3.1}$$

where $\mathbf{x}(t)=[x_1(t),\ x_2(t),\ x_3(t)]^\mathrm{T}$ and F_k is the non-linear auxiliary spring force acting on the main mass by the auxiliary mass and is defined as:

$$F_k(\mathbf{x})=\begin{cases} F_0+k_\mathrm{a}(x_\mathrm{rel}-a) & \text{if } x_\mathrm{rel}>a \\ -F_0-k_\mathrm{a}(-x_\mathrm{rel}-a) & \text{if } x_\mathrm{rel}<-a \\ 0 & \text{else} \end{cases} \tag{3.2}$$

where $x_\mathrm{rel}=x_2-x_1$ is the relative displacement between auxiliary mass and main mass. The auxiliary damping force F_c acting on the main mass by the auxiliary mass is here modelled as a linear viscous damper and is defined as:

$$F_c(\mathbf{x},\dot{\mathbf{x}})=c\,\dot{x}_\mathrm{rel} \tag{3.3}$$

The exciting force F_e, created by the piston and acting on the main mass, is in this machine assumed to be quadratically increasing with frequency. It is also approximated as a sinusoidal excitation. This is described and motivated in the later Section 3.4.5. The explicit expression of the exciting force that is used is

$$F_\mathrm{e}(t,f)=F_\mathrm{e,ref}\cdot(f/f_\mathrm{ref})^2\cdot\sin(2\pi ft) \tag{3.4}$$

with time t [s], excitation frequency f [Hz] and the reference values $F_\mathrm{e,ref}$ and f_ref given in Table 2.1 along with all other model parameter values.

It was considered whether to model damping as linear viscosity or friction between housing and main mass (c_h) and between auxiliary mass and main mass (c_a). It is assumed that friction is the main cause of dissipation in these two areas. But friction can be difficult to model and there exists a variety of different theories to chose from. Even a simple theory as Coulomb friction with a single friction coefficient has the disadvantage of discontinuity in the friction force. Also, no notable differences in the results of interest are expected. It was therefore decided to stay with linear viscous damping to keep the model simple and faster in computation. On an additional note, the auxiliary mass will be allowed to decrease and thus have larger amplitude in a later stage. Then viscous damping might even be closer to reality due to increased velocity and air resistance.

3.3 Numerical model

The equation of motion is non-linear so finding an analytical solution is not possible. Therefore, it is transformed to a system of first order ordinary differential equations (ODE) to be solved numerically by one of MATLAB's ODE solvers. The equation of motion (3.1) is rewritten in state-space form. The system of ODEs is stated as:

$$\begin{aligned} \dot{\mathbf{z}}(t)&=\mathbf{f}\big(t,\mathbf{z}(t),\mathbf{u}(t)\big) \\ \mathbf{z}(0)&=\mathbf{z}_0 \end{aligned} \tag{3.5}$$

where $\mathbf{z}(t)=[x_1(t),\ x_2(t),\ x_3(t),\ \dot{x}_1(t),\ \dot{x}_2(t),\ \dot{x}_3(t)]^\mathrm{T}$ is the state vector, $\mathbf{u}(t)$ is the input vector, $\mathbf{z}_0$ is the initial state and $\mathbf{f}$ is a non-linear function. The initial displacements at time $t=0$ are an approximation of the static deflection of the system when subjected to gravity: $x_\mathrm{st}=-g(m_\mathrm{m}+m_\mathrm{a}+m_\mathrm{h})/(k_\mathrm{m}+k_\mathrm{p})$. The initial velocity of the auxiliary mass is set to $-\sqrt{2ga}$, which is the free fall velocity after falling the gap length a. An initial velocity of the auxiliary mass has been seen to ease the computation in many situations. The other two masses have no initial velocity, giving the initial state vector as

$$\mathbf{z}_0=[x_\mathrm{st},\ x_\mathrm{st},\ x_\mathrm{st},\ 0,\ -\sqrt{2ga},\ 0]^\mathrm{T} \tag{3.6}$$

Note that if the machine was operated horizontally, gravity would be set to zero and the initial condition would simply be $\mathbf{z}_0=\mathbf{0}$.

Explicitly, the state equation in (3.5) reads:

$$\frac{\mathrm{d}}{\mathrm{d}t}\begin{bmatrix} x_1 \\ x_2 \\ x_3 \\ \dot{x}_1 \\ \dot{x}_2 \\ \dot{x}_3 \end{bmatrix} = \begin{bmatrix} \dot{x}_1 \\ \dot{x}_2 \\ \dot{x}_3 \\ \big(F_\mathrm{e} + F_\mathrm{k} + F_\mathrm{c} - c_\mathrm{m}x_1 + c_\mathrm{h}(\dot{x}_3 - \dot{x}_1) - k_\mathrm{m}x_1 + k_\mathrm{h}(x_3 - x_1)\big)/m_\mathrm{m} - \mathrm{g} \\ (-F_\mathrm{k} - F_\mathrm{c})/m_\mathrm{a} - \mathrm{g} \\ \big(-c_\mathrm{p}\dot{x}_3 + c_\mathrm{h}(\dot{x}_1 - \dot{x}_3) - k_\mathrm{p}x_3 + k_\mathrm{h}(x_1 - x_3)\big)/m_\mathrm{h} - \mathrm{g} \end{bmatrix} \tag{3.7}$$

where auxiliary spring force F_k (3.2), auxiliary damper force F_c (3.3) and exciting force F_e (3.4) are defined in Section 3.2.

3.3.1 ODE solver

The ODE solver used to solve the equations of motions in state-space form throughout the project was decided to be the built-in MATLAB function *ode45*. Accurate enough results was ensured by tightening both the relative and absolute error tolerances to 10^{-8} from their default values of 10^{-3} and 10^{-6} respectively. With this setting, the solver is denoted ode45x, while *ode45* indicates default settings. The solver has a medium order of accuracy, is relatively fast, designed for non-stiff ODEs and is seen as the standard first choice ODE solver in MATLAB [35]. Motivation of using *ode45* and said error tolerances is given in the model verification in Section 3.5.

3.3.2 Strategy of computation

This section presents some important details regarding how the actual computation of model response is performed. The system of ODEs (3.5) must be solved numerically, due to non-linearities, over a certain time domain. It is desired to find when the system has stabilised into a limit cycle and to then compute the required responses. A limit cycle is a closed trajectory in phase space, meaning that all states (displacements and velocities) in a limit cycle will reoccur after some time period. Such a vibration in the system is periodic and may have a time period that is any multiple of the excitation period $1/f$. The system may however not stabilise into a limit cycle, but instead continue in an irregular vibration indefinitely. An example of a vibration stabilising into a limit cycle after a few seconds is shown in Figure 3.3.

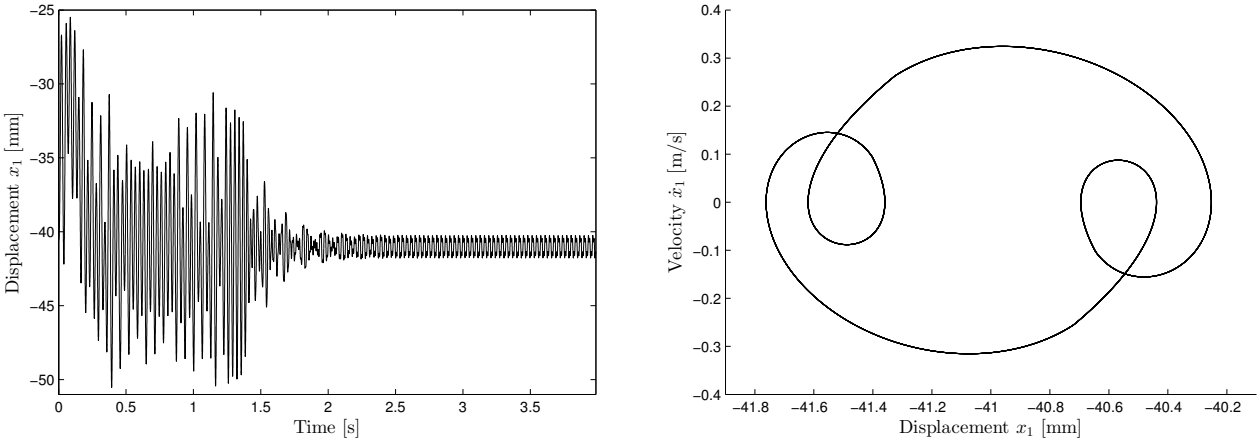

(a) Displacement signal, beginning to stabilise after about 2 s.

(b) Phase space plot of the limit cycle, for $t > 3.5$ s.

Figure 3.3: Main mass vibration in an example simulation at a single excitation frequency f.

The ODE solver is run for approximately 1 second at a time. It is made sure that this time is exactly an integer multiple of the excitation period $1/f$, so the exciting force always starts and ends the same. The resulting states after simulation are checked for limit cycles by comparing the very last state vector with previous state vectors at times that are multiples of $1/f$, using a certain relative tolerance for each state vector component. If no limit cycle is found, then continue with new simulation steps until one is found, but stop anyway if more

than 10 seconds have been simulated since the vibration may never stabilise. When resuming the simulation after each limit cycle check, the last state from previous simulation step is used as initial state in the next simulation step. The same is done when the response at the current excitation frequency f is computed and stepping to the next frequency. Thus the initial state in (3.6) is only used once when simulating the system at several excitation frequencies. Connecting the states between different excitations in this manner often helps to decrease the time it takes for the vibration to stabilise in a limit cycle a lot. Moreover, adaptive simulation time by detecting limit cycles enables major savings of computational time, since the time it takes for the vibration to stabilise in a limit cycle, if it even does, varies widely with system parameters.

System response is calculated using standard deviation of the time signals (displacements, velocities and/or acceleration). Standard deviation is the same as RMS if the vibration is about the zero level, but in this case it is not about the zero level because of gravity, cf. Figure 3.3a. System response will although be referred to as RMS response hereafter. Only the last piece of the time signals, the limit cycles, are used to calculate the response. The state vectors obtained from *ode45* are pertinent to non-equidistant time points t_k since the solver uses adaptive time step size by default. The states are interpolated to equidistant time points t_j before calculating the response with the standard deviation.

The standard deviation of a signal x sampled at N equidistant time points t_j is defined as

$$\text{std} = \sqrt{\frac{1}{N}\sum_{j=1}^{N}(x_j - \bar{x})^2} \tag{3.8}$$

where the mean value $\bar{x}$ is

$$\bar{x} = \frac{1}{N}\sum_{j=1}^{N} x_j \tag{3.9}$$

Compare this with the definition of RMS. It is the same except that the mean value is not subtracted at each time point:

$$\text{RMS} = \sqrt{\frac{1}{N}\sum_{j=1}^{N} x_j^2} \tag{3.10}$$

Phase angles for all mass displacements are calculated using cross power spectral density, the *cpsd* function in MATLAB. In particular, phase angle of a displacement signal is taken for its frequency component that corresponds to the excitation frequency, i.e. the dominating frequency component. The exciting force is always used as reference (0° phase).

A brief description of the methodology can be seen in a flowchart in Figure C.1 in Appendix C.

3.3.3 Spring force smoothing

The non-linear auxiliary spring force F_k acting between the main mass and the auxiliary mass, as it is defined in (3.2), is discontinuous at $x_{\text{rel}} = \pm a$. An accurate numerical solution in this condition requires extremely small time steps at the discontinuity and will thus be computationally expensive. To decrease computation time and errors, smoothing of the spring force was applied. The force smoothing was carried out by defining transition regions around the discontinuities for $\pm x_{\text{rel}} \in [a - \delta,\ a + \delta]$, see Figure 3.4a. In these transition regions, the spring force F_k is given by a third order polynomial. The polynomial is defined such that the spring force F_k and its first derivative is continuous and defined for all x_{rel}. The transition width parameter δ is kept as small as possible, to not distort the force curve too much, but large enough to keep the number of time steps in simulation small. The curvature of the polynomial is always kept smaller than a reference curvature $\kappa_{\text{ref}} = 4.69 \cdot 10^9$ N/m^2, that was tested to work fine. The polynomial of transition is calculated as:

$$\begin{aligned} F_{\text{k}}(x_{\text{rel}}) = -\frac{F_0}{4\delta^3}x_{\text{rel}}^3 + \text{sgn}(x_{\text{rel}})\frac{k_{\text{a}}\delta^2 + 3F_0 a}{4\delta^3}x_{\text{rel}}^2 - \frac{(a-\delta)(2k_{\text{a}}\delta^2 + 3F_0\delta + 3F_0 a)}{4\delta^3}x_{\text{rel}} \\ + \text{sgn}(x_{\text{rel}})\frac{(a-\delta)^2(k_{\text{a}}\delta^2 + 2F_0\delta + F_0 a)}{4\delta^3} \end{aligned} \tag{3.11}$$

for $a - \delta \leq |x_{\text{rel}}| \leq a + \delta$ when the normal force smoothing could be used, where:

$$\delta = \frac{k_{\text{a}}\sqrt{k_{\text{a}}^2 + 24F_0\kappa_{\text{ref}}}}{4\kappa_{\text{ref}}} \tag{3.12}$$

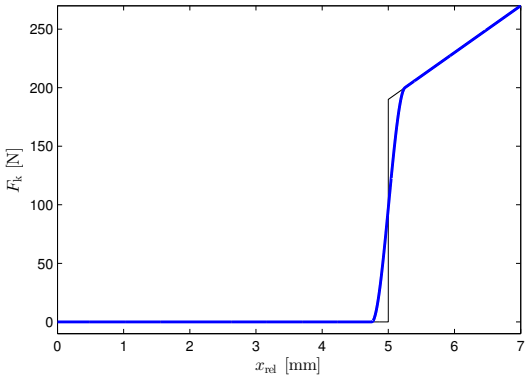

(a) Nominal spring parameters used. 3rd order transition polynomial for $x_{\text{rel}} \in [a-\delta,\ a+\delta]$. Note that the spring force is symmetric about the origin.

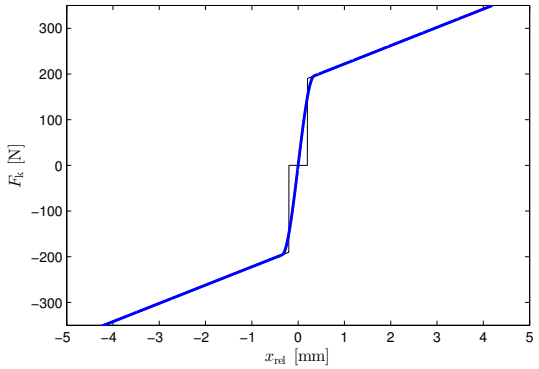

(b) Spring parameters: $k_{\text{a}} = 40$ kN/m, $a = 0.2$ mm and $F_0 = 190$ N. 3rd order transition polynomial for $x_{\text{rel}} \in [-\varepsilon,\ \varepsilon]$.

Figure 3.4: Auxiliary spring force F_k with smoothing (thick blue line) and without smoothing (thin black line).

A special case is when the gap is smaller than the transition regions, i.e. $a < \delta$, due to restrictions on the curvature. Instead of using two separate transition regions around $x_{\text{rel}} = \pm a$, one transition region is used for $x_{\text{rel}} \in [-\varepsilon,\ \varepsilon]$. The requirements on the polynomial with respect to smoothness and curvature of F_k are the same as in the above case. A typical case of smoothed spring force when the gap is very small can be seen in Figure 3.4b. The polynomial of this single transition region is calculated as:

$$F_{\text{k}}(x_{\text{rel}}) = \frac{ak_{\text{a}} - F_0}{2\varepsilon^3} x_{\text{rel}}^3 + \frac{3F_0 + k_{\text{a}}(2\varepsilon - 3a)}{2\varepsilon} x_{\text{rel}} \tag{3.13}$$

where

$$\varepsilon = \sqrt{\frac{3|F_0 - ak_{\text{a}}|}{\kappa_{\text{ref}}}} \tag{3.14}$$

3.4 Model parameters and sensitivity analysis

This section discusses the values of the different model parameters and the model's sensitivity to these parameters. In general, there are large uncertainties in the parameters. Especially for the damping coefficients, but also in the stiffness between main mass and ground as well as the hand-arm stiffness. It shall be seen though that many of these uncertainties have little or even no effect on the system's behaviour around the nominal operating frequency.

The first parts of this section regards mass, stiffness and damping in the model. This is followed by the NLTVA spring parameters that are primarily subject to optimisation. The last part regards the exciting force created by the reciprocating piston.

3.4.1 Mass of parts

All parts of the prototype were weighed prior to simulation and optimisation. The weight of the three DOFs and the piston can be seen in Table 3.1.

3.4.2 Stiffness

The only stiffness that could be obtained correctly is the stiffness of the spring between the housing and the main mass. This stiffness value was given by the supplier as $k_{\text{h}} = 14$ kN/m. Changing this stiffness affects the vibration isolation and controllability of the machine. It should also be noted that the second resonance frequency, seen just below 15 Hz in the following response plots, is mainly determined by the stiffness k_{h} and

Table 3.1: Mass of all parts of the machine.

Part	Mass [kg]
Main mass, m_{m}	2.7
Auxiliary mass, m_{a}	1.0
Housing mass, m_{h}	3.1
Piston mass, m_{pist}	0.52

it should be kept on a safe distance from the excitation frequency f. Other stiffness values are not based on measurements or data from manufacturer since they are not created by mechanical springs.

Main stiffness

The stiffness between the main mass and the ground could not be measured since this stiffness comes from the machine's hovering connection to the chisel via air pressure in the cylinder. Figure 3.5 shows how the response of the system changes for different values of the main stiffness k_{m}. Figure 3.5 clearly shows that the model is not sensitive to the value of k_{m} around the operating frequency 28 Hz. The only difference is that the lowest resonance frequency moves upwards with increased stiffness. To keep the lowest resonance frequency low, around 2 Hz as is estimated from operating the machine, the main stiffness was set to $k_{\mathrm{m}} = 500$ kN/m.

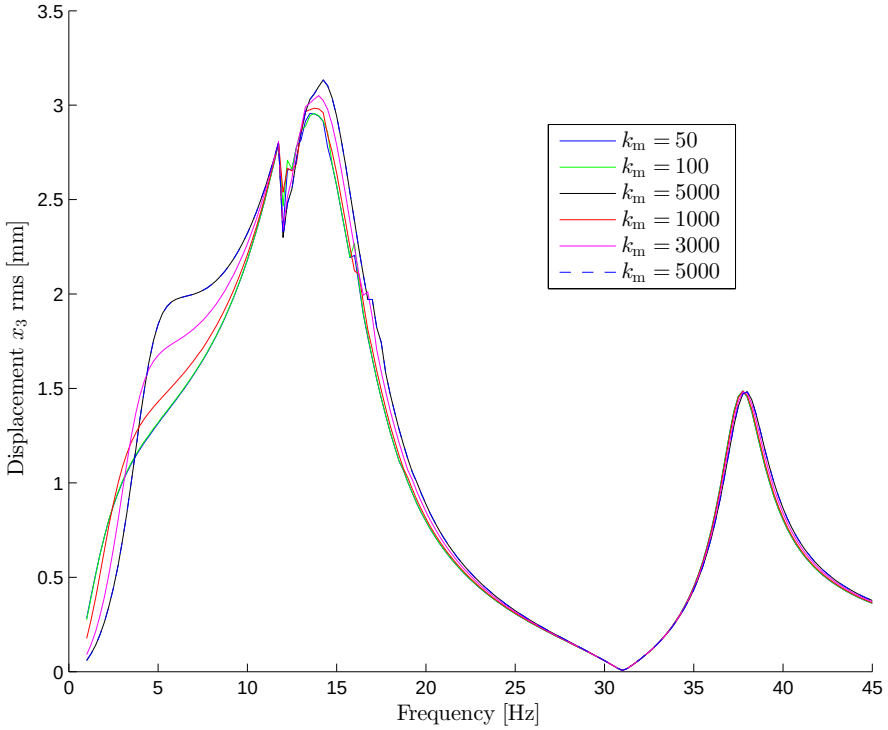

Figure 3.5: Response of the handle for different values of k_{m}. All other parameters are kept constant at their nominal values given in Table 2.1.

Operator stiffness

One of the design goals of the prototype has been to have the handle height adjustable such that the operator is standing almost straight with his arms almost straight [6]. The machine is also supposed to be constructed such that the operator does not have to put much effort into holding it down. Measuring of the arm's end point stiffness, k_{p}, is not within the scope of this thesis. Studies have been done to measure the stiffness. In 1985, Mussa-Ivaldi et al. [38] tested the arm's end point stiffness by making test subjects hold a handle that is displaced by a motor while recording the impedance of the arm. They published stiffness values of 641 and 436 N/m when the hands are in distal (horizontal, almost straight) position. A similar study conducted by Tsuji

et al. [39] in 1995 resulted in similar values of 506 and 474 N/m per hand, for two different testers. Although both these tests were performed with the arms horizontal, the results show at which order of magnitude the stiffness is when arms are in vertical position, supporting the machine.

Figure 3.6 shows how insensitive the model is to the value of k_p. Based on this insensitivity of the model and the values from the presented studies, the stiffness for each hand was chosen as 500 N/m or $k_\mathrm{p} = 1000$ N/m for both hands.

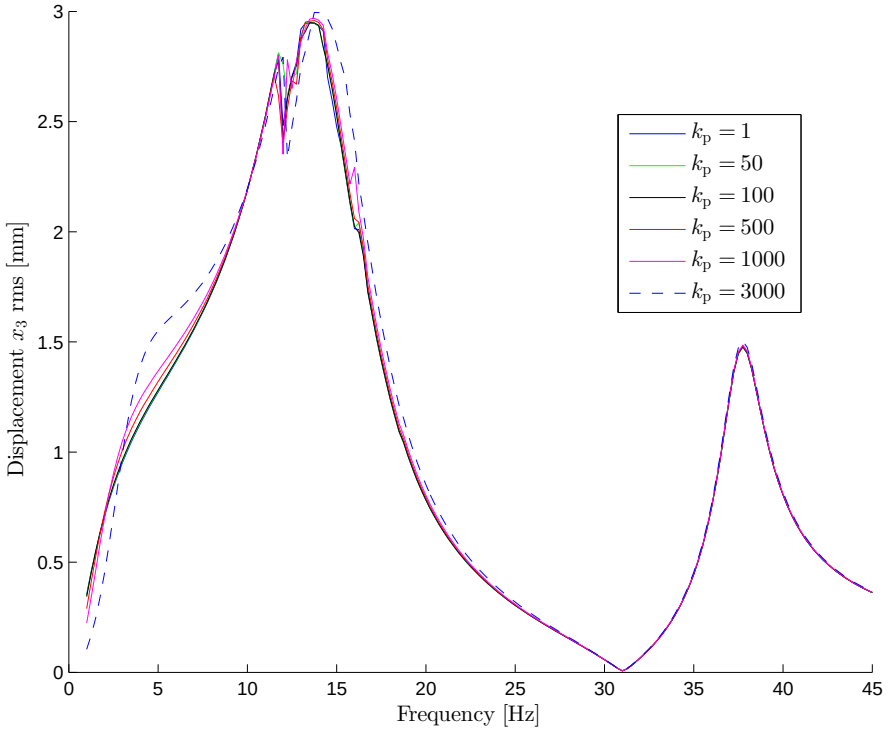

Figure 3.6: Response of the handle for different values of k_p. All other parameters were kept constant at their nominal values given in Table 2.1.

3.4.3 Damping

All damping was assumed to be continuous and viscous, not including friction as discussed in Section 3.2. This assumption was made to keep the simulation as efficient and fast as possible since the optimisation requires many simulations. The damping parameters were chosen as follows.

Main damping

The same applies for the damping to the ground as for the stiffness. The damping is similarly created by the main mass's hovering connection to the chisel. The sensitivity of the model to the main damping can be seen in Figure 3.7. One sees that the model is quite sensitive to c_m in the lower frequencies but the difference between different values disappears when we approach 25 Hz. The sensitivity increases again after 34 Hz. It is therefore safe to assume that the value for c_m can be chosen quite freely without changing the fundamental behaviour of the system in the frequency range of interest, around 28 Hz. It is also clear that higher damping will always give less vibration so it is more conservative to choose this damping value low. As a result the main damping was chosen as $c_\mathrm{m} = 100$ N s/m.

TVA damping

The damping of a TVA is an important parameter in all cases. LTVAs give the best effect at the tuned frequency when no damping is used, but the downside of having no damping is that the unwanted resonance peak, slightly above the tuned frequency becomes very large. Looking at the sensitivity to the NLTVA damping,

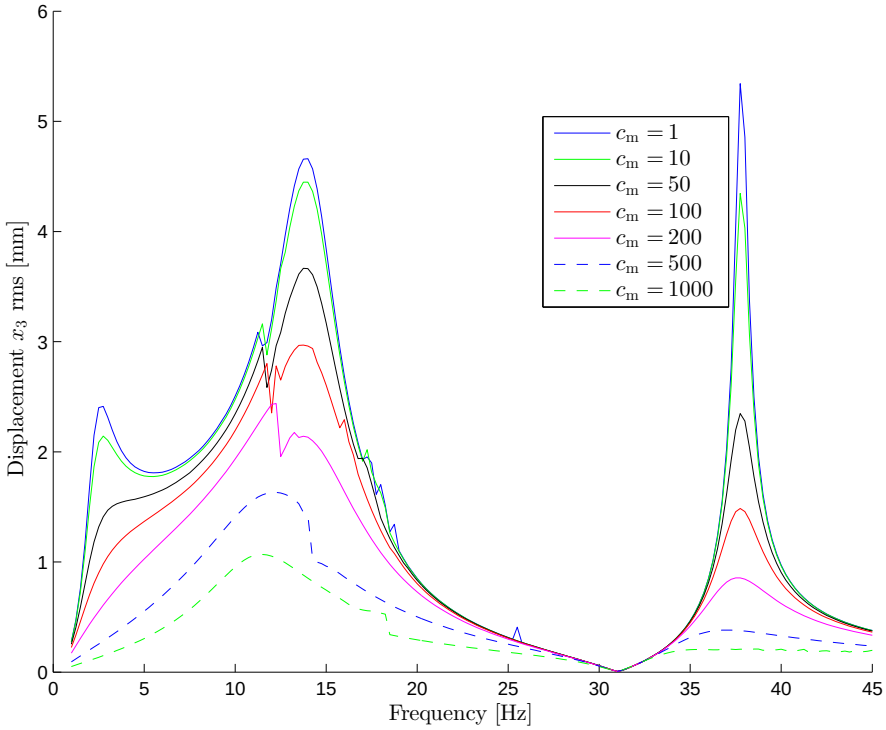

Figure 3.7: Response of the handle for different values of c_m. All other parameters are kept constant at their nominal values given in Table 2.1.

seen in Figure 3.8, one sees that the same applies here, i.e. the resonance peak around 38 Hz is lowered at the cost of reduced vibration suppression at the tuned frequency when the damping is increased. The goal with the proposed NLTVA is to widen the effective frequency range as much as possible to eliminate the risk of exciting the unwanted resonance frequency. Therefore the focus was kept on keeping the damping low with maximum suppression while optimising the non-linearities to keep the unwanted resonance frequency far enough away to safely operate below it. As a result the damping of the NLTVA was set to $c_a = 1$ N s/m.

Operator damping

The damping of the operator was decided the same way as the operator stiffness. From the study conducted by Tsuji et al. [39] in 1995, the damping of each hand of the operator can be approximated as 30 N s/m per hand. Therefore the damping of the operator's hand-arm system was chosen as $c_p = 60$ N s/m. Figure 3.9 shows how insensitive the model is to the operator damping c_p around the operating frequency 28 Hz.

Damping between housing and main mass

The damping between housing and main mass of the prototype could unfortunately not be measured. The sensitivity to this parameter can be seen in Figure 3.10. It clearly shows that keeping this value low is beneficial, since that gives lower response around the tuned frequency. It can also be seen that the response of the system is not dramatically changed in the region of interest when the damping is 100 N s/m or less. It is however obvious that this kind of machine should be designed with c_h as low as possible.

To help setting a realistic value, the following reasoning was made. Mainly friction, e.g. Coulomb friction with a friction coefficient of about 0.1, is assumed to be causing the dissipation between housing and main mass. The radial normal force is caused by imbalances from the operator's handling during operation and perhaps some small preload in between. The radial normal force is assumed not to exceed 40 N, which was chosen as a rough estimation. High-speed video measurements of housing and main mass during operation were differentiated numerically to get the relative velocity $\dot{x}_3 - \dot{x}_1$. The viscous damping force $(\dot{x}_3 - \dot{x}_1)c_h$ should exert the same absolute impulse, i.e. have the same area under a time curve, as the friction force F_{fr}.

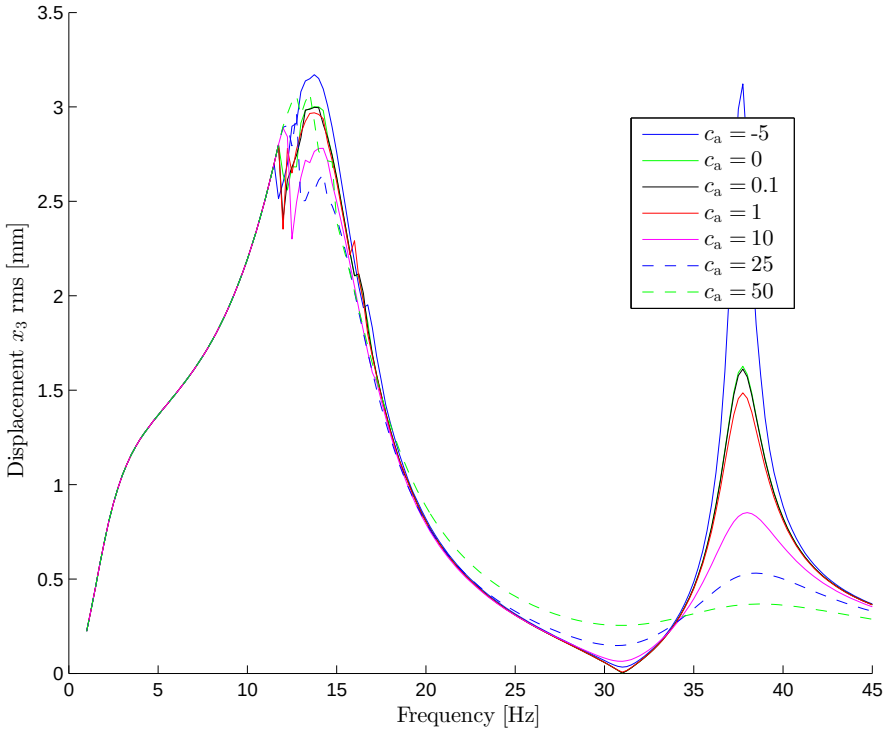

Figure 3.8: Response of the handle for different values of c_a. All other parameters are kept constant at their nominal values given in Table 2.1.

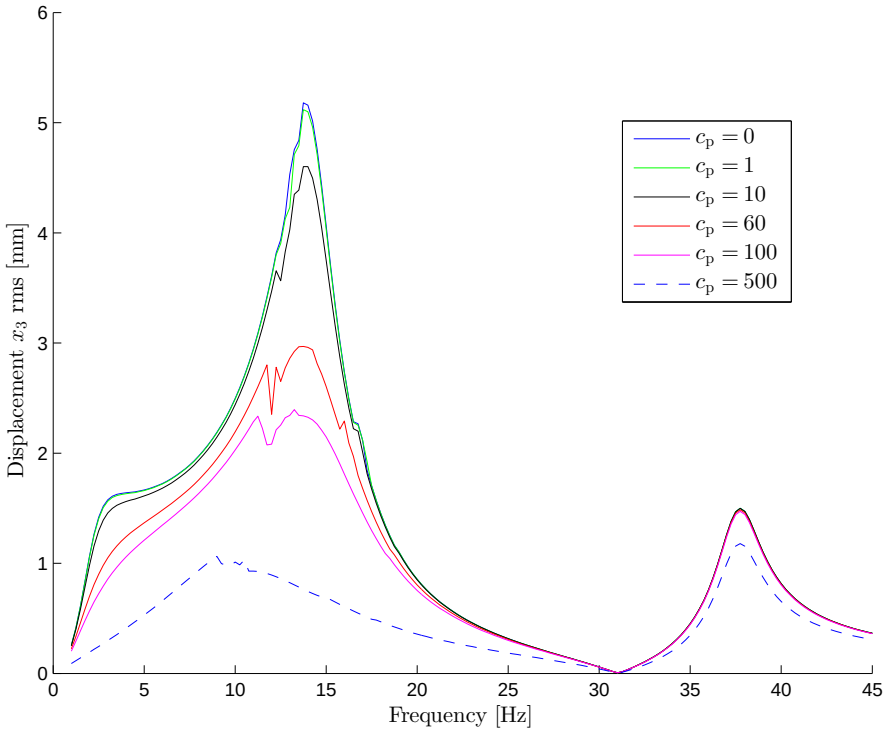

Figure 3.9: Response of the handle for different values of c_p. All other parameters are kept constant at their nominal values given in Table 2.1.

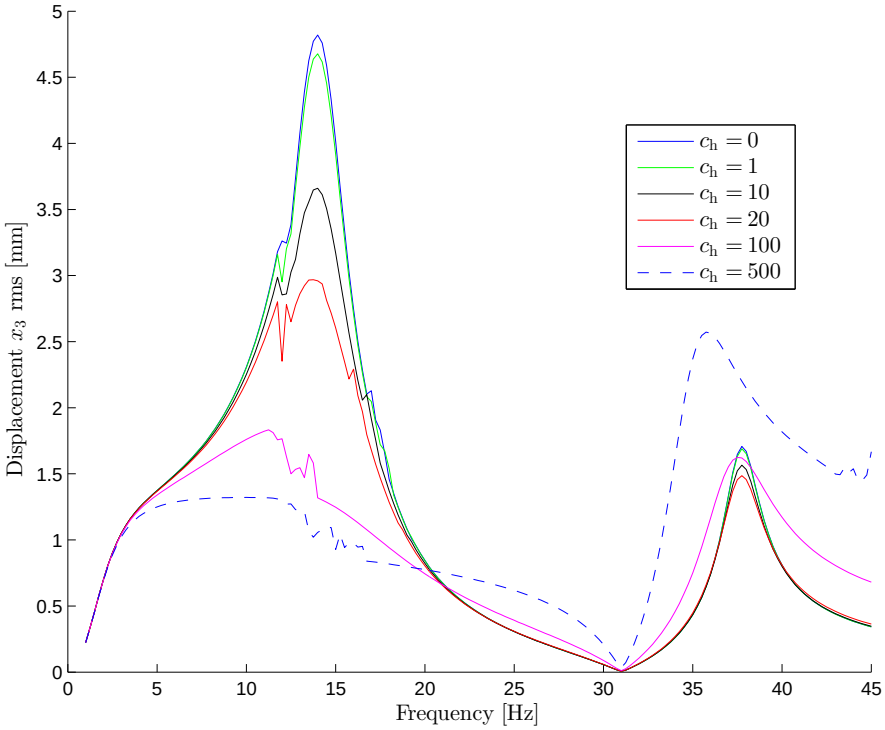

Figure 3.10: Response of the handle for different values of c_h. All other parameters are kept constant at their nominal values given in Table 2.1.

This leads to an expression for the viscous damping coefficient c_h as

$$c_h = \frac{F_{fr}}{f \cdot \left(\int_0^{1/f} |\dot{x}_3 - \dot{x}_1| \, dt \right)} \approx \frac{0.1 \cdot 40 \text{ N}}{27.95 \text{ Hz} \cdot 6.82 \text{ mm}} \approx 21.0 \text{ N s/m} \tag{3.15}$$

The damping was chosen as $c_h = 20$ N s/m.

3.4.4 Optimisation parameters

Optimisation parameters are the three NLTVA spring parameters that are primarily subject to optimisation: linear stiffness coefficient k_a, gap length a and preload F_0. The sensitivity of the model to changes in the optimisation parameters k_a, a and F_0 can be seen in Figures 3.11, 3.12 and 3.13, respectively. Looking at these figures, one clearly sees that all parameters affect the frequency where the NLTVA gives maximum vibration suppression, i.e. the tuned frequency. It can also be seen how different parameters effect the shape of the response differently. Figure 3.11 shows how increasing the stiffness k_a increases the tuned frequency as well as moves the unwanted resonance peak significantly upwards in frequency, i.e. making the safe operating zone wider. Figure 3.12 shows how decreasing the gap a increases the tuned frequency, but the unwanted resonance peak does not move as much upwards as when changing k_a. Similar behaviour can be seen in Figure 3.13 when changing F_0, i.e. the tuned frequency can be moved up and down but the resonance peak does not move that much. These results clearly show how any one of the optimisation parameters can be changed to move the tuned frequency, but the shape of the response around that frequency depends on how they are combined.

3.4.5 Exciting force

The shape and amplitude of the exciting force, i.e. the force caused by the piston periodically moving up and down, was unknown. To estimate the shape and amplitude, measurements on the prototype machine were performed. The machine was stripped of the housing and the TVA was fixed to the main mass creating a single DOF system, see Figure 3.14. The machine was then mounted in the ball absorber test rig, described in Section 2.5, and pulled down with elastic bands creating an approximately constant feeding force. An accelerometer was glued on top of the main mass, see Appendix B for pictures.

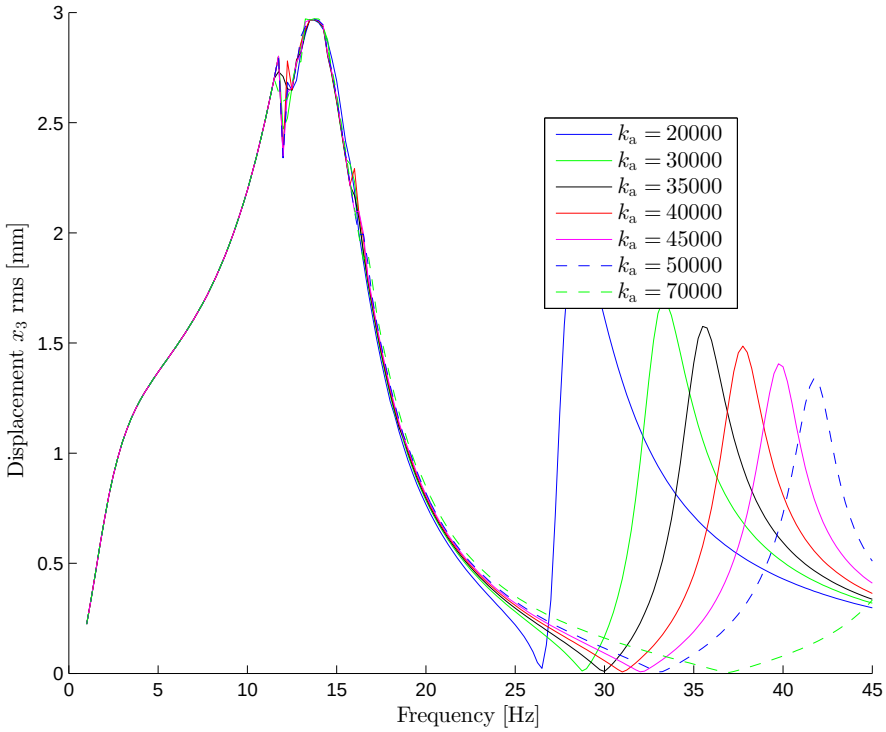

Figure 3.11: Response of the handle for different values of k_a. All other parameters are kept constant at their nominal values given in Table 2.1.

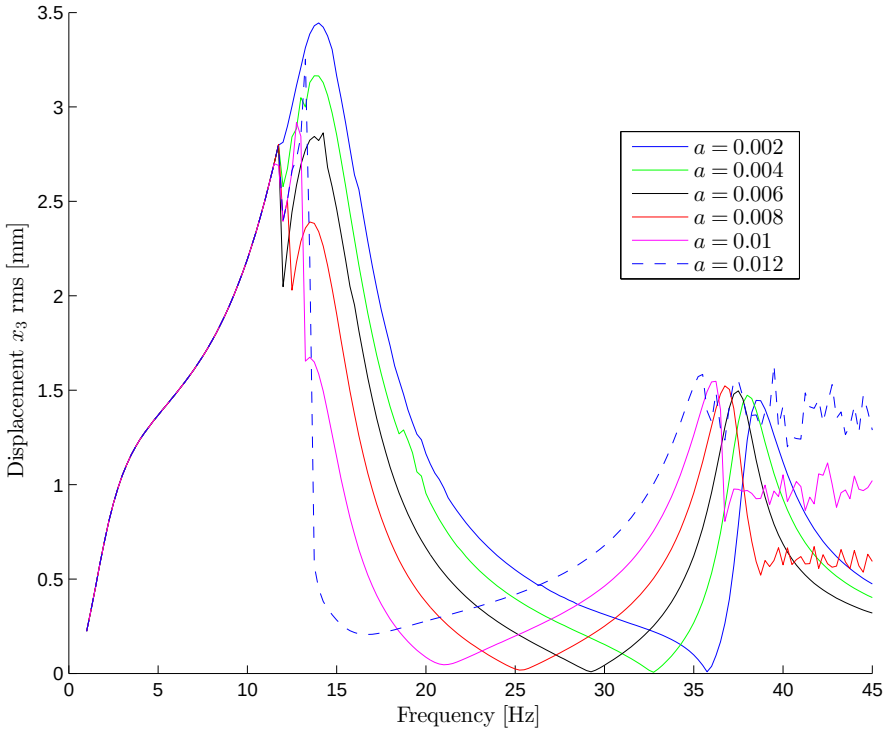

Figure 3.12: Response of the handle for different values of a. All other parameters are kept constant at their nominal values given in Table 2.1.

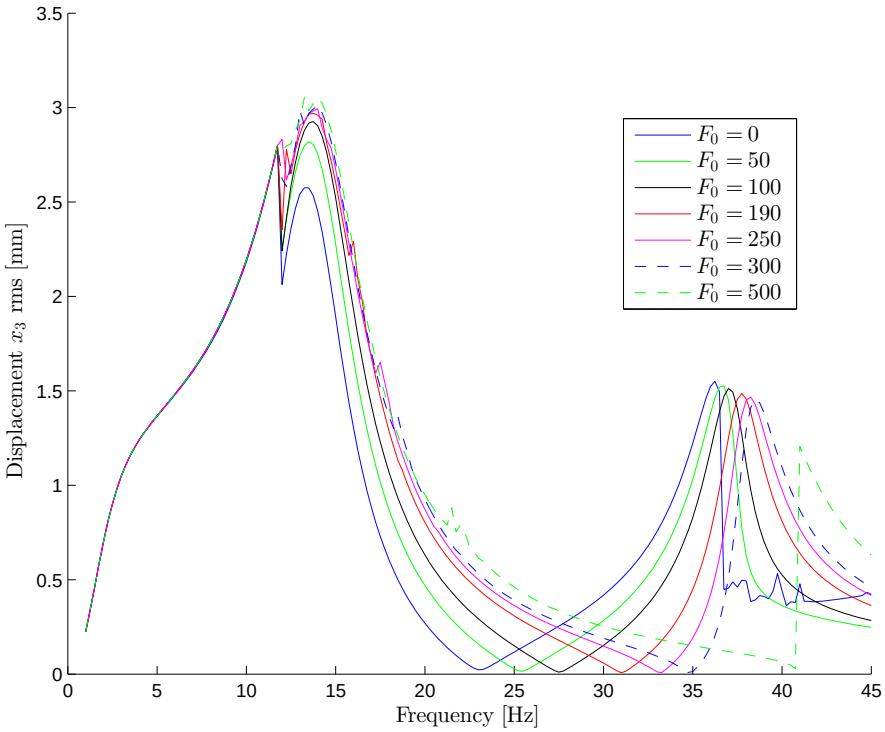

Figure 3.13: Response of the handle for different values of F_0. All other parameters are kept constant at their nominal values given in Table 2.1.

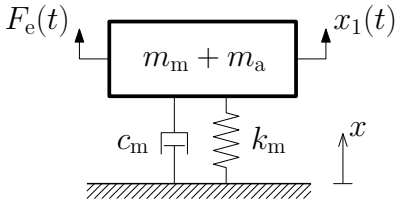

Figure 3.14: Model of the experimental set-up when measuring the exciting force.

The measured acceleration signal had large non-physical narrow peaks. Most of the peaks were removed using a moving average filter with 2 points. The measured acceleration filtered can be seen in Figure 3.15a. Remaining large noises in the valleys are believed to come from when the piston hits the chisel. A fitting of the measured acceleration using a 5-term Fourier series is also included in Figure 3.15a. The Fourier coefficients were obtained from an FFT with a Hann window performed on 1 second of the acceleration signal, see Figure 3.15b. The five terms correspond to excitation frequency, in this case 26.1 Hz, and the following four harmonics. As a result of the harmonics, the shape of the 5-term Fourier series is quite far from being a pure sine wave.

The exciting force F_e is believed to have a shape similar to that of the 5-term Fourier curve in Figure 3.15a. To get from measured acceleration to exciting force, consider the model of the experimental set-up illustrated in Figure 3.14. The exciting force can be calculated from the 1-DOF equation of motion:

$$\big(m_m + m_a\big)\ddot{x}_1(t) + c_m\dot{x}_1(t) + k_m x_1(t) = F_e(t) \tag{3.16}$$

where velocity $\dot{x}_1(t)$ and displacement $x_1(t)$ can be obtained by integrating the 5-term Fourier series for acceleration $\ddot{x}_1(t)$ once and twice respectively. The Fourier series based exciting force is then given by (3.16).

To investigate the sensitivity of the model's response to the shape of the force, a comparison was made between using a pure sinusoidal force and the Fourier series force obtained from (3.16). To make the comparison accurate and fair, the amplitude of the sinusoidal force was tuned such that the absolute impulse, i.e. the area under the curve, was the same as for the Fourier series force. The equivalent sine force amplitude and the frequency at

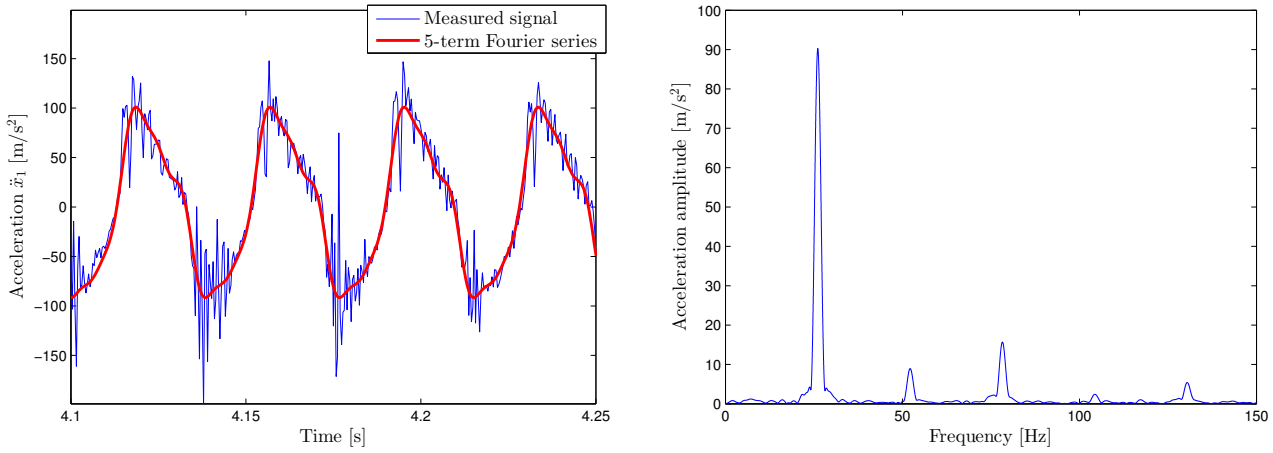

(a) The measured acceleration fitted with a 5-term Fourier series.

(b) FFT of the measured acceleration signal.

Figure 3.15: Acceleration measurements of the 1-DOF system, main and auxiliary mass fixed together.

which it was measured was

$$\begin{aligned} F_{\mathrm{e,ref}} &= 351 \text{ N} \\ f_{\mathrm{ref}} &= 26.1 \text{ Hz} \end{aligned} \tag{3.17}$$

It turns out from testing that the equivalent sinusoidal force amplitude in (3.17) is rather insensitive to the values of damping c_{m} and stiffness k_{m} used in (3.16), or if the elastic band stiffness is included, or if the damping and stiffness are neglected entirely. There are however larger experiment uncertainties in whether the used feeding force and the ball absorber test rig creates sufficiently normal operating conditions for measuring a realistic exciting force.

The stroke length of the reciprocating piston creating the exciting force F_{e} is assumed to be constant for all frequencies. With a piston mass of 0.520 kg and assuming sinusoidal motion, the piston amplitude becomes $351 \text{ N}/\big(0.52 \text{ kg}\cdot(2\pi\cdot 26.1 \text{ Hz})^2\big) \approx 25.1$ mm. The assumption of constant amplitude is not based on measurement data since it is currently not possible to measure the piston's movement within the cylinder and it is hard to control the excitation frequency in the prototype machine. It is based on the construction of the pneumatic impact mechanism, as described in Section 2.3. Since the point at which the shift of air inlets happens is always the same, the piston is somewhat geometrically conditioned. It suggests that the stroke length of the piston is approximately the same regardless of frequency. For other reciprocating machines with electric or combustion engines, the piston stroke length is always the same, and this assumption is perhaps even more realistic. The amplitude of the periodic exciting force created by the piston will thus increase quadratically with frequency. The exciting force amplitude is updated for different excitation frequencies f as:

$$|F_{\mathrm{e}}(f)| = F_{\mathrm{e,ref}} \cdot (f/f_{\mathrm{ref}})^2 \tag{3.18}$$

This quadratic scaling is used to update the amplitude of the measured exciting force in (3.17) during simulations.

A comparison of displacements for the main mass, auxiliary mass and housing can be seen in Figures 3.16a, 3.16b and 3.16c respectively. Figure 3.16 clearly shows that the difference between using a force with the measured shape and a sinusoidal force is negligible for all DOFs. There is however a significant difference in the time it takes to calculate the response. Calculating these graphs, on an average computer, with a resolution of 0.5 Hz took 64 s using a sinusoidal force versus 157 s when the measured shape was used. Therefore a sinusoidal force is used for all further simulations and optimisations. The explicit expression of the exciting force that is used is

$$F_{\mathrm{e}}(t, f) = F_{\mathrm{e,ref}} \cdot (f/f_{\mathrm{ref}})^2 \cdot \sin(2\pi f t) \tag{3.19}$$

with time t [s], excitation frequency f [Hz] and the reference values $F_{\mathrm{e,ref}}$ and f_{ref} given by (3.17). The sensitivity to variations in exciting force, cf. Figure 3.17, is solely due to the TVA non-linearity. It causes the tuned frequency to move, even though all other model parameters are constant.

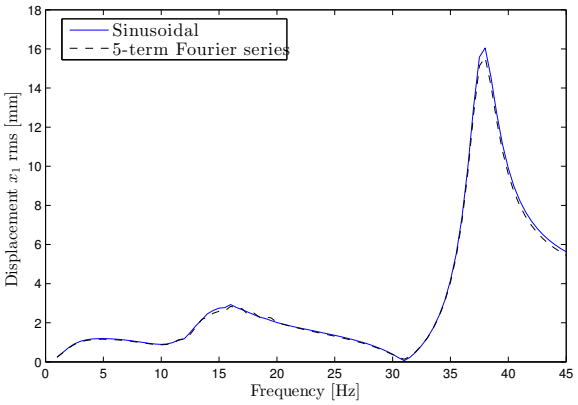

(a) Main mass.

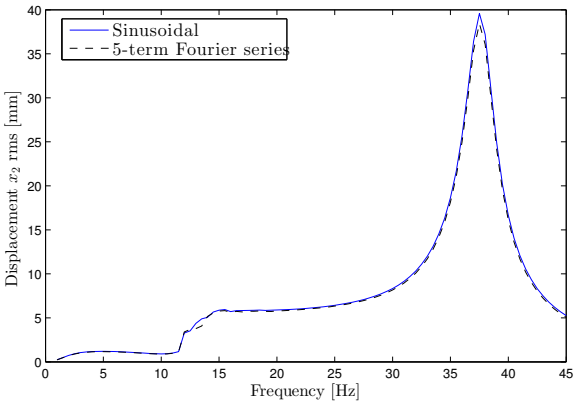

(b) Auxiliary mass.

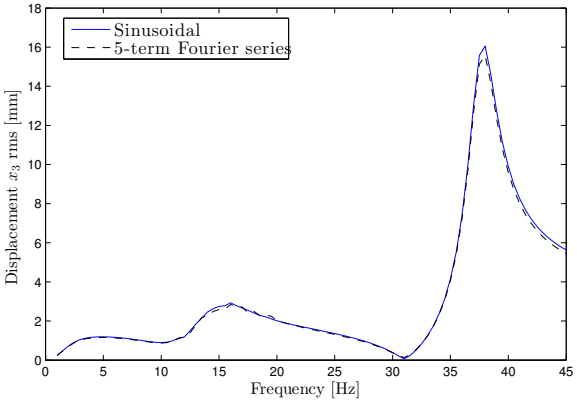

(c) Housing.

Figure 3.16: Comparison of model responses between sinusoidal force and fitting of the measured exciting force.

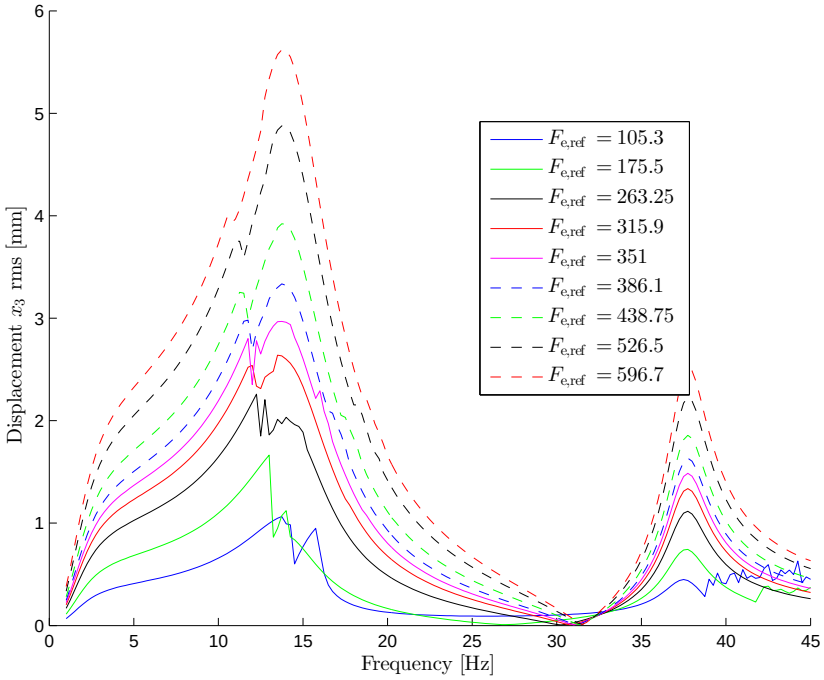

Figure 3.17: Response of the handle for different values of $F_{\mathrm{e,ref}}$. All other parameters are kept constant at their nominal values given in Table 2.1

3.5 Verification

Verifying the computational methods and the model is a required step to be able to trust its outputs. Verification, as opposed to validation, consists of ensuring the correctness and accuracy of the numerical solutions obtained from the computational model. It does not involve comparison with experimental results as in validation. Instead, comparison is done with rigorously known reference results such as analytic ones.

A thorough verification of the mathematical and computational model will be done here by comparison against analytical results. First of all, however, the developed MATLAB model is compared to the older model used previously to simulate the machine without housing, cf. Figure 3.18. Keeping the models as they are, the responses are given as seen in Figure 3.18a. There is a notable difference that is nearly entirely eliminated by a small correction in the old model, cf. Figure 3.18b. The correction consists in interpolating the signals to get samples at equidistant time points before calculating the signal's RMS. There still remain a lot of fluctuations in the response of the old model, which can be glimpsed slightly in the figure. This is explained by the lack of other precautions such as tightened error tolerances and always measuring the RMS over an integer number of periods.

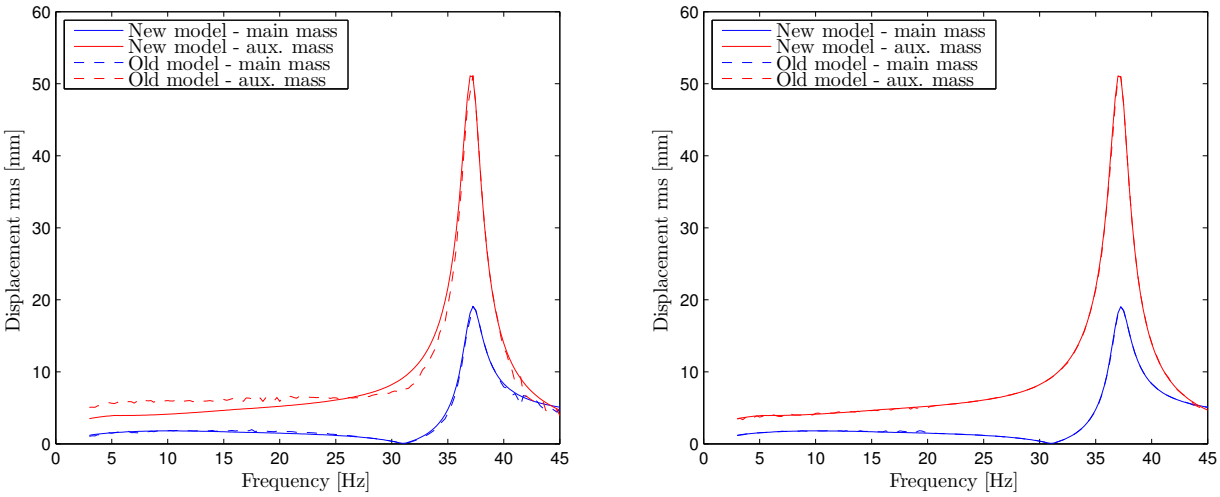

(a) The new and old models as they are.

(b) Applying a small correction to the old model.

Figure 3.18: Comparison of the new and old MATLAB model. No housing included, otherwise nominal parameters used.

Results from a numerical simulation of the 3-DOF system utilising a completely linear TVA, i.e. gap and preload $a = F_0 = 0$, is compared with the analytical solution of the same system. The analytical solution of the 3-DOF system (with damping) is obtained by considering the continuous time-invariant state-space model and deriving the transfer function from exciting force to displacements, velocities and accelerations. The state-space model is given as

$$\begin{aligned} \dot{\mathbf{z}}(t) &= \mathbf{A}\mathbf{z}(t) + \mathbf{B}\mathbf{u}(t) \\ \mathbf{y}(t) &= \mathbf{C}\mathbf{z}(t) + \mathbf{D}\mathbf{u}(t) \end{aligned} \tag{3.20}$$

Performing the Laplace transform gives

$$\begin{aligned} s\mathbf{Z}(s) &= \mathbf{A}\mathbf{Z}(s) + \mathbf{B}\mathbf{U}(s) \\ \mathbf{Y}(s) &= \mathbf{C}\mathbf{Z}(s) + \mathbf{D}\mathbf{U}(s) \end{aligned} \tag{3.21}$$

with the complex variable $s = \omega i$ and $\mathbf{Z}(s)$, $\mathbf{U}(s)$ and $\mathbf{Y}(s)$ are the Laplace transforms of the state vector $\mathbf{z}(t)$, the input $\mathbf{u}(t)$ and the output $\mathbf{y}(t)$ respectively. The transfer function is then defined and given as

$$\mathbf{H}(s) = \frac{\mathbf{Y}(s)}{\mathbf{U}(s)} = \mathbf{C}(s\mathbf{I} - \mathbf{A})^{-1}\mathbf{B} + \mathbf{D} \tag{3.22}$$

The amplitudes of the outputs are then given as

$$|\mathbf{Y}(s)| = |\mathbf{H}(s)||\mathbf{U}(s)| \tag{3.23}$$

and their phase angles are given as

$$\varphi = \arg\big(\mathbf{H}(s)\big) \tag{3.24}$$

There is only one input, the exciting force, so $|\mathbf{U}(s)|$ is simply the exciting force amplitude $|F_\mathrm{e}|$ and varies quadratically with frequency according to (3.18). Response of a linear system is always harmonic. Therefore, the RMS response is easily obtained by multiplying output amplitudes $|\mathbf{Y}(s)|$ with the factor $1/\sqrt{2}$. Analytical RMS responses are then compared to the MATLAB model's RMS response, cf. Figure 3.19a, 3.19b and 3.19c. The phase angles are corrected to produce smooth curves by adding multiples of $\pm 2\pi$ when jumps occur. See the verification of phase angles in Figure 3.19d. Analytic and numerical simulation results are practically identical.

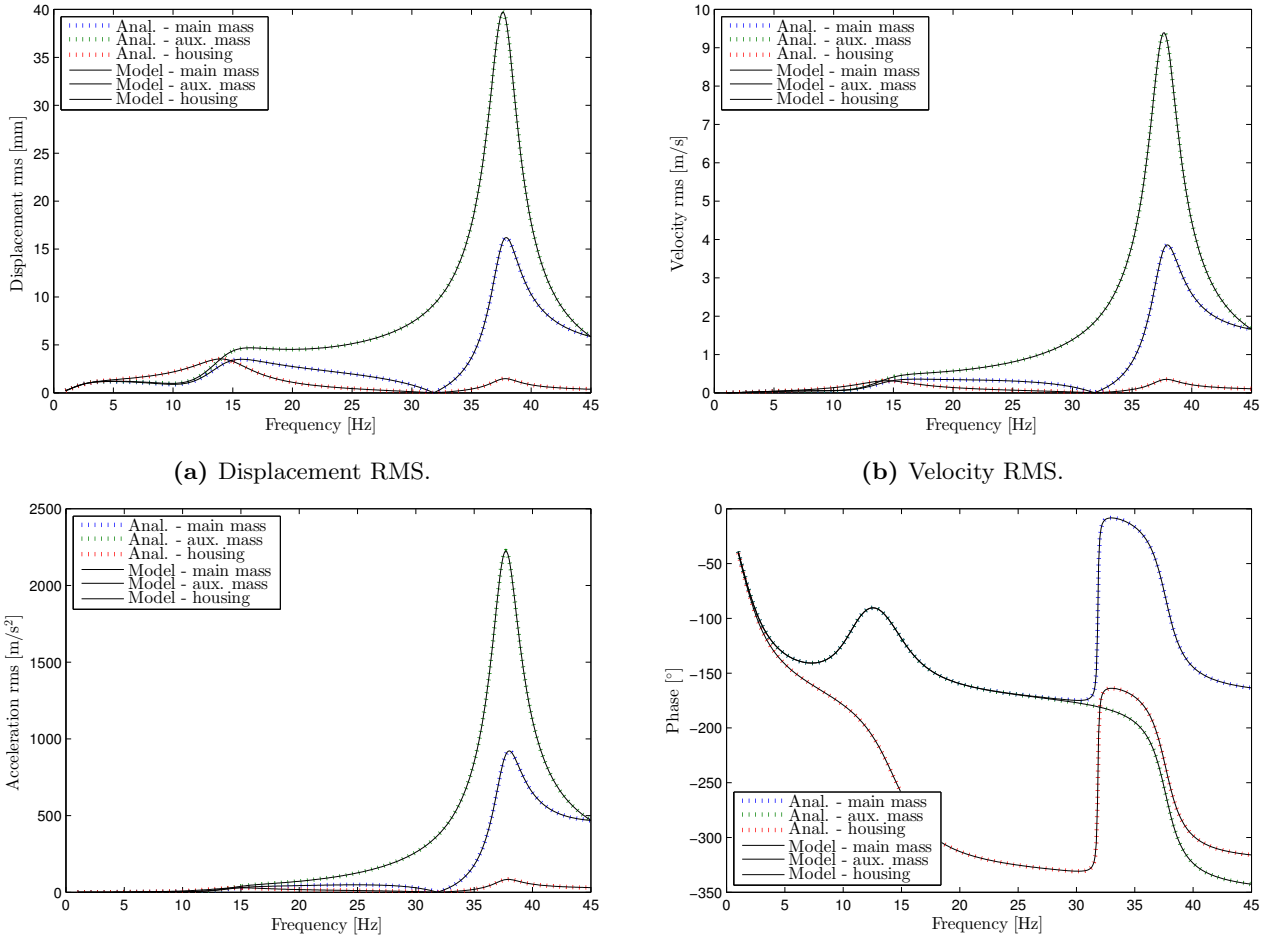

(a) Displacement RMS.

(b) Velocity RMS.

(c) Acceleration RMS.

(d) Phase angle of displacements relative exciting force.

Figure 3.19: Comparison between analytical solution and model outputs for the 3-DOF system with a linear TVA, $k_\mathrm{a} = 40$ kN/m and $a = F_0 = 0$.

To test the performance of different solvers, and especially the chosen-to-be-used *ode45*, a numerically challenging test was devised. In the test, the auxiliary system, as seen in Figure 3.1a, is simulated in free vibration without damping or gravity for 20 seconds. The resulting frequency is then compared to the analytic resonance frequency of this non-linear system according to (2.1). It is also assessed whether the response is realistic. For example, the amplitude of the auxiliary mass should stay constant since there is no dissipation or external force. The result after testing all different ODE solvers with the nominal configuration $k_\mathrm{a} = 40$ kN/m, $a = 5$ mm and $F_0 = 190$ N, and with an initial displacement amplitude of 10 mm can be seen in Table 3.2. Corresponding displacement in the beginning and end of simulation for three of the cases are shown in Figure 3.20. The

Table 3.2: Comparison of different ODE solvers as well as with and without spring force smoothing. Nominal configuration of auxiliary system used: $k_a = 40$ kN/m, $a = 5$ mm and $F_0 = 190$ N. Initial amplitude of the auxiliary mass is 10 mm. ode45x has tightened error tolerances.

Solver	**Analytical**		**Sim. (smoothing)**			**Sim. (no smoothing)**		
	Freq. [Hz]	Ampl. [mm]	Freq. [Hz]	Ampl. [mm]	Comp. time [s]	Freq. [Hz]	Ampl. [mm]	Comp. time [s]
ode45x	30.36	10.00	30.36	10.00	12.32	30.36	10.00	15.94
ode45	”	”	16.50	5.37	1.40	0.80	5.00	0.35
ode23	”	”	16.98	5.37	2.20	6.00	5.03	1.40
ode113	”	”	31.80	66.09	2.14	31.82	92.42	2.18
ode15s	”	”	31.84	98.04	8.11	31.11	13.28	14.11
ode23s	”	”	29.68	8.81	13.39	30.15	9.58	15.48
ode23t	”	”	8.98	5.07	9.84	30.43	9.94	12.66
ode23tb	”	”	29.90	9.11	10.61	30.61	10.72	13.92

results suggest that ode45x (*ode45* with tightened error tolerances) should be used in order to get correct results and that force smoothing shortens the computation time. Moreover, no sign is seen of the ODE system being stiff since the stiff solvers *ode15s*, *ode23s*, *ode23t* and *ode23tb* also have great problems to solve correctly and do not offer reduced computation time.

Table 3.3 verifies that the solver ode45x in fact gives reliable results for a few different configurations of the auxiliary system, i.e. different parameters k_a, a and F_0, and different displacement amplitudes. The conclusions that are drawn from this are:

- Force smoothing decreases computation time without affecting result.
- Numerical simulation of the auxiliary system is verified to be correct if solver's error tolerances are tightened. Otherwise, integration might very well fail.

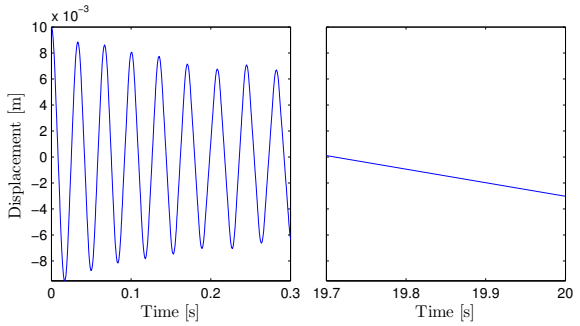

(a) Failed integration with *ode45*, default settings.

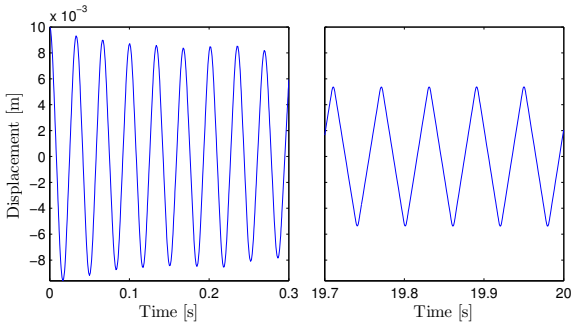

(b) Failed integration with *ode45*, default settings and force smoothing.

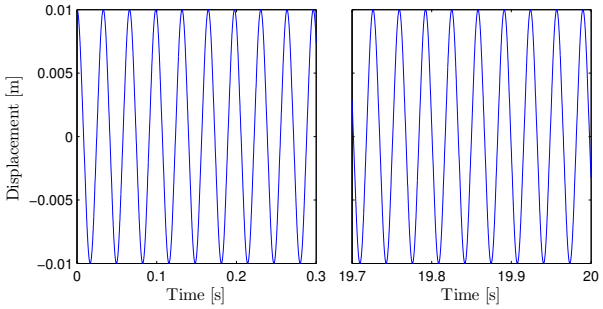

(c) Successful integration with *ode45*, tightened error tolerances and force smoothing.

Figure 3.20: Simulation of free vibrating auxiliary mass with nominal parameters $k_a = 40$ kN/m, $a = 5$ mm and $F_0 = 190$ N.

Table 3.3: Verification of the simulation of auxiliary system when using *ode45* with tightened error tolerances and spring force smoothing. The analytical amplitude is the initial auxiliary mass amplitude used in simulation.

Parameters			**Analytical**		**Sim. (smoothing)**	
k_a	a	F_0	Frequency	Amplitude	Frequency	Amplitude
[kN/m]	[mm]	[N]	[Hz]	[mm]	[Hz]	[mm]
40	5	190	30.36	10.00	30.36	10.00
40	5	190	23.38	6.00	23.40	6.00
40	5	190	31.52	20.00	31.52	20.01
40	0.5	800	150.6	1.000	156.8	1.000
40	0.5	800	76.91	5.00	76.92	5.01
200	5	190	49.51	10.00	49.52	10.00
200	5	190	61.35	20.00	61.35	20.01

3.6 Validation

A comparison of results from the MATLAB model and experimental results has been done. The experiment was done in the ball absorber test rig without housing. Both the main and auxiliary mass displacements were measured with a high-speed video camera. An accelerometer was placed on top of the main mass, next to the air inlet, to also measure the main mass acceleration. It could not be placed on the auxiliary mass due to practical reasons. Model parameters, such as excitation frequency f, gap length a etc., were adjusted as well as possible to correspond to the actual measurement performed.

First of all, an excellent correspondence is seen between accelerometer data and high-speed video data, which leads to the conclusion that the measurements are correct. A comparison of the two measurement methods, used at exactly the same occasion, is shown in Figure 3.21. Here, displacement is obtained from accelerometer data by integrating it twice, using a simple trapezoidal integration implementation in MATLAB. After each integration, a 5th order high-pass Butterworth filter with a cut-off frequency of 10 Hz was applied to remove large low frequency fluctuations.

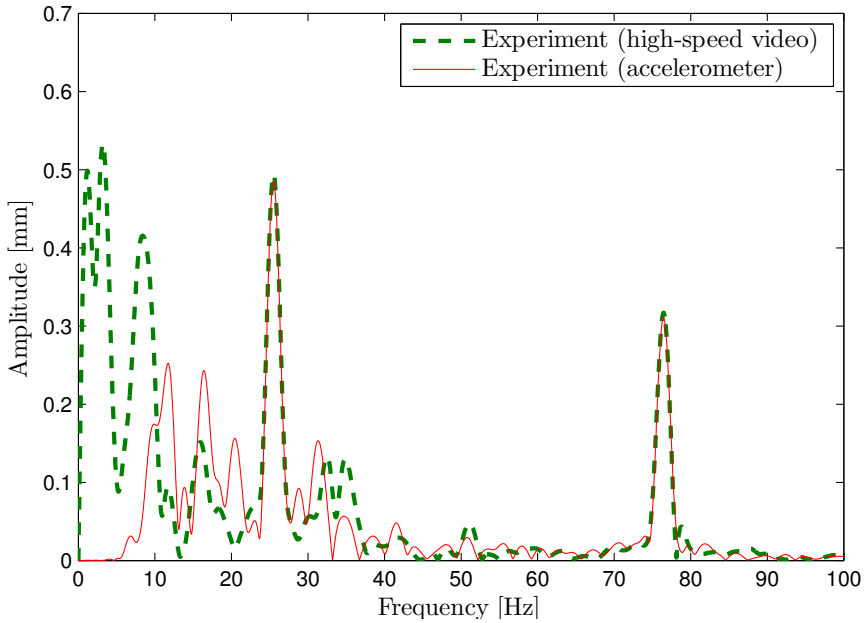

Figure 3.21: Comparison between FFT of accelerometer and high-speed video data.

The model validation was done from measurements with three different gap lengths. The gap a is by far the easiest parameter to control. The original gap in the machine at the time of measurement was $a = 9.65$ mm. Two smaller gaps, 6.07 mm and 3.15 mm, were set by gluing small aluminium blocks in the gap, see Figure 3.22.

Two plastic blocks were used to compress the large free housing spring, usually connected to the housing, to fasten it more to the main mass and to prevent it from vibrating at an overtone of the operating frequency.

Some great uncertainties in the model parameters during measurements made it impossible to run corresponding simulations for comparison. Mainly the exciting force amplitude and the preload were uncertainties having significant effect on model response at the machine's operating frequency. The preload was measured in the machine a long time before, only using a personal scale, and may have changed since. The exciting force varies with, for example, applied feeding force and inlet air pressure, both of which can vary considerably from occasion to occasion. The machine was kept in place by hand, trying to apply approximately the same feeding force during each measurement. This allowed to easier find a feeding force at which the machine worked well, i.e. ran stable without sudden jumps. On the other hand, the feeding force was not measured accurately, but on a personal scale, and may have varied for the three different gap lengths. The way to resolved the uncertainties was to use the measurement with the largest gap to calibrate both exciting force amplitude and preload. The same values were then used when running simulations for the two smaller gaps. The calibration is not explained in detail. Basically, it consisted in minimising the relative difference in amplitude at the excitation frequency (≈ 26 Hz) and the third harmonic (≈ 78 Hz), cf. Figure 3.21, since these frequency components are usually dominant. This resulted in an exciting force reference of $F_{\mathrm{e,ref}} = 508$ N and a preload of $F_0 = 228$ N. Compare with the nominal values of $F_{\mathrm{e,ref}} = 351$ N and $F_0 = 190$ N. Note that the measuring of exciting force was done at a separate time and under slightly different conditions, e.g. using elastic bands to keep the machine in place.

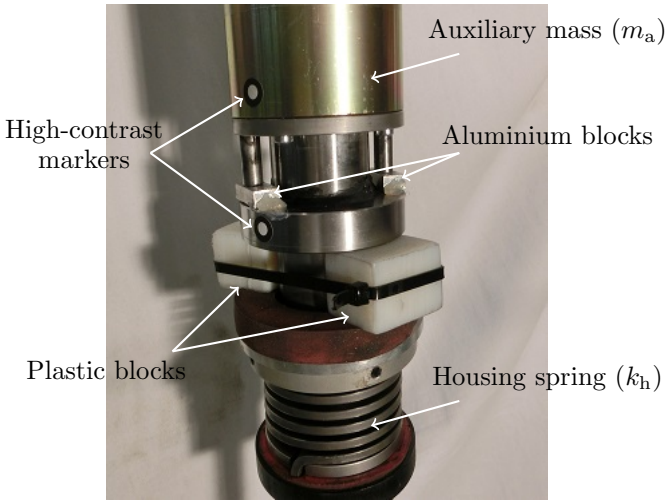

Figure 3.22: Measurement set-up with aluminium blocks to decrease the gap and with high-contrast markers for the video processing software.

FFT analysis was made on the model's displacement response and the raw high-speed video data for both masses, with a Hann window applied to 1.5 seconds of data. The comparison for all three gap lengths $a = 9.65$ mm, 6.07 mm and 3.15 mm can be seen in Figures 3.23, 3.24 and 3.25 respectively. Displacement signals for both masses during half a second are compared between model and and experiment for all three gap lengths in Figures 3.26, 3.27 and 3.28. It is not possible to make a good comparison of the displacement RMS values since there is always some low frequency disturbances in measurements which do not exist in simulation.

The amplitudes in the FFT plots at excitation frequency and third harmonic are mostly quite similar in model and experiment for all three gap lengths. The frequency components below the excitation frequency are mostly due to disturbances in the experiment. For the largest gap, see Figure 3.23, there is however significant frequency components at about 51 Hz and 102 Hz, the second and fourth harmonics respectively, that are not predicted in the model. The second harmonic as well as an additional component between the excitation and second harmonic is significant in the experiments with the two smaller gaps, see Figures 3.24 and 3.25, but again not predicted in simulation. It is interesting though that the simulation for the smallest gap gives a displacement signal with a period much longer than the excitation period, quite similar to the experimental data, cf. Figure 3.28. This is manifested as the two peaks at about 9 Hz and 44 Hz in the FFT plots in Figure 3.25.

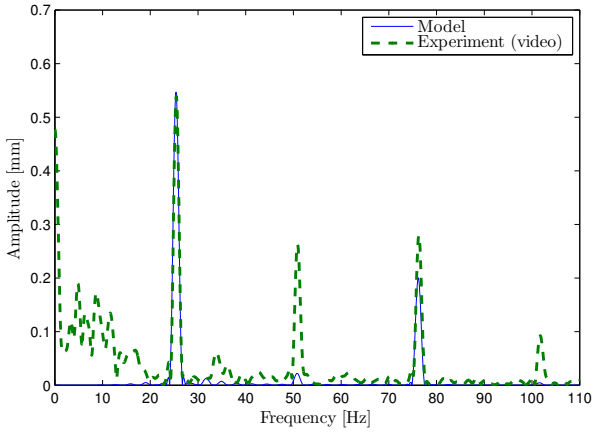

(a) Main mass.

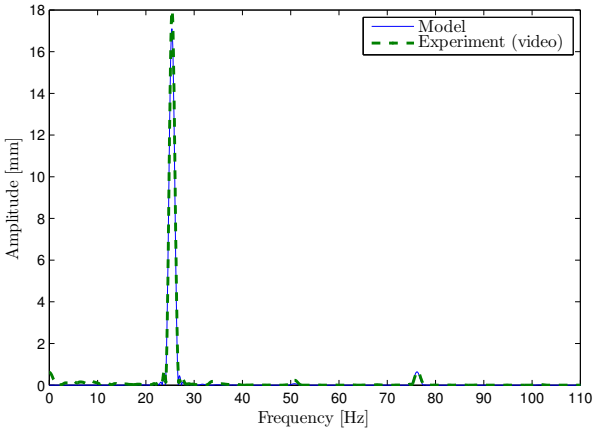

(b) Auxiliary mass.

Figure 3.23: FFT of model response vs. high-speed video data, with gap length $a = 9.65$ mm. Excitation frequency is 25.4 Hz.

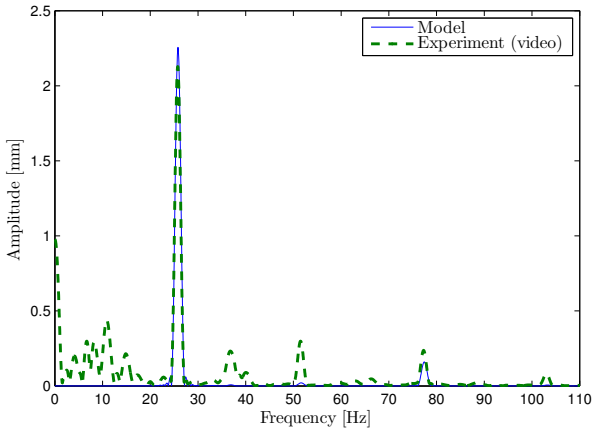

(a) Main mass.

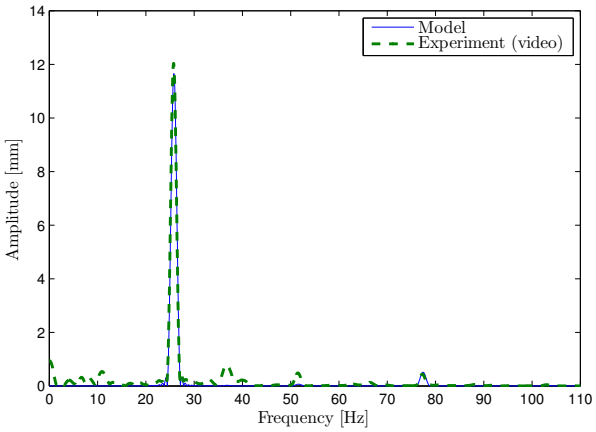

(b) Auxiliary mass.

Figure 3.24: FFT of model response vs. high-speed video data, with gap length $a = 6.07$ mm. Excitation frequency is 25.8 Hz.

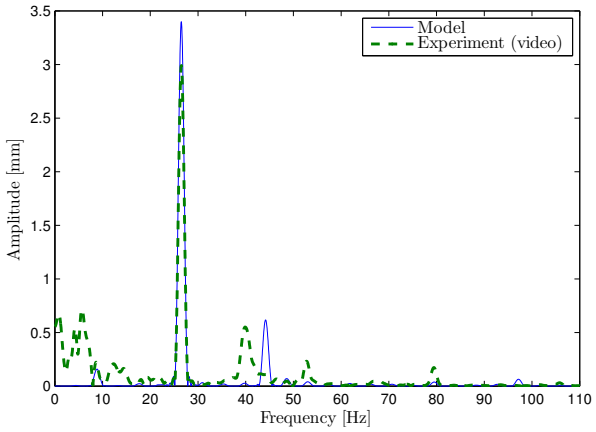

(a) Main mass.

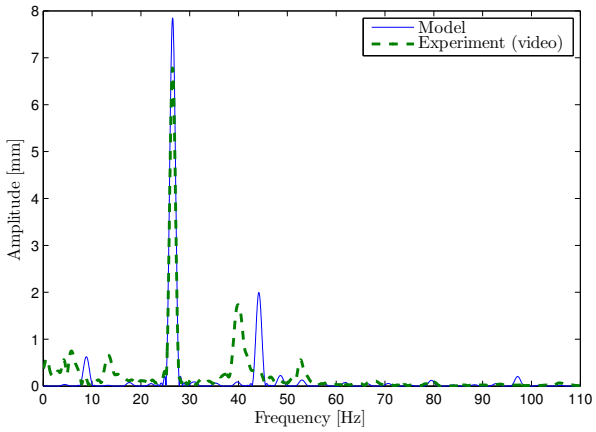

(b) Auxiliary mass.

Figure 3.25: FFT of model response vs. high-speed video data, with gap length $a = 3.15$ mm. Excitation frequency is 26.5 Hz.

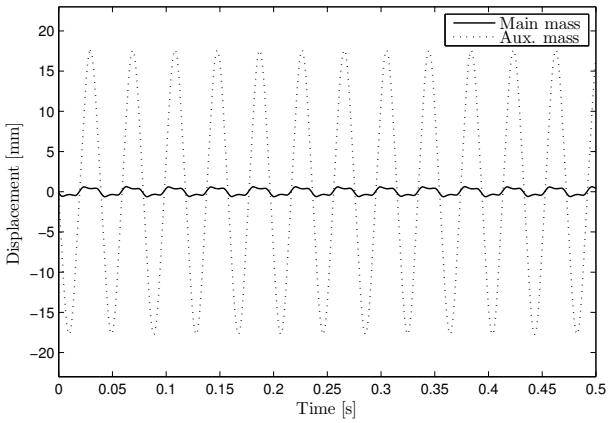

(a) Model.

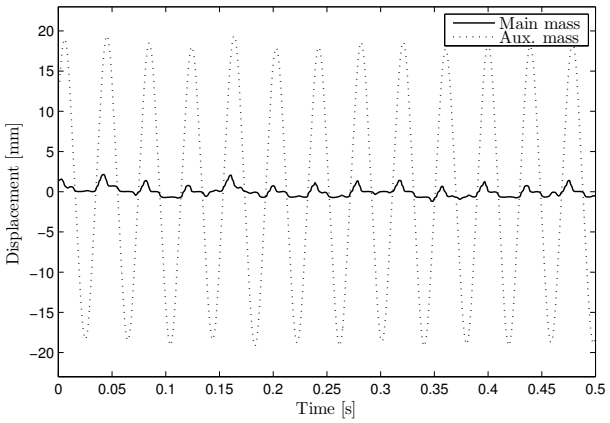

(b) Experiment.

Figure 3.26: Displacement history from model vs. high-speed video data, with gap length $a = 9.65$ mm.

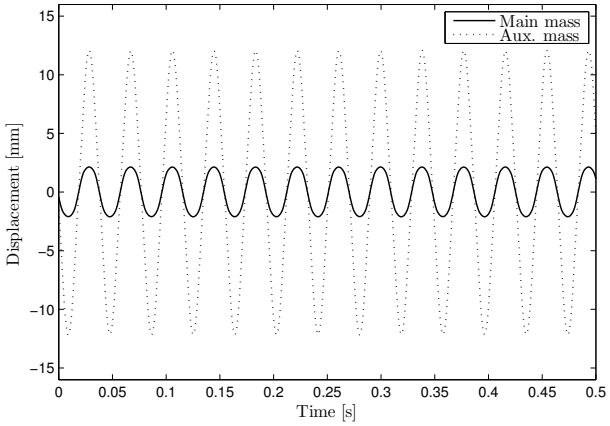

(a) Model.

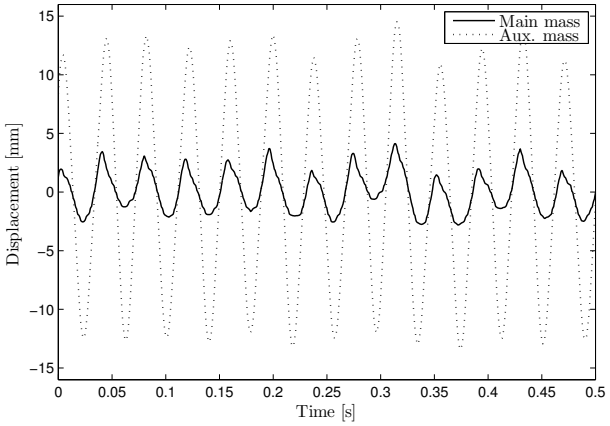

(b) Experiment.

Figure 3.27: Displacement history from model vs. high-speed video data, with gap length $a = 6.07$ mm.

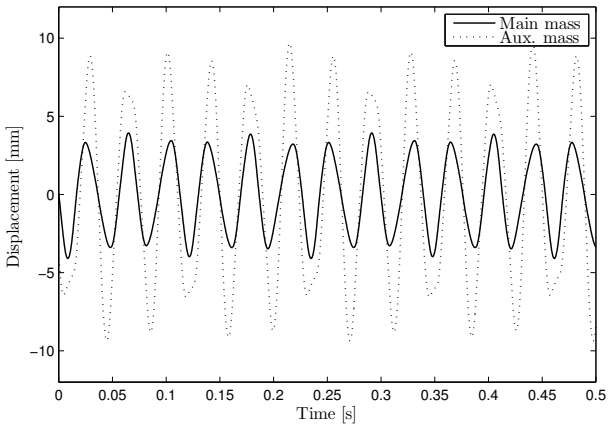

(a) Model.

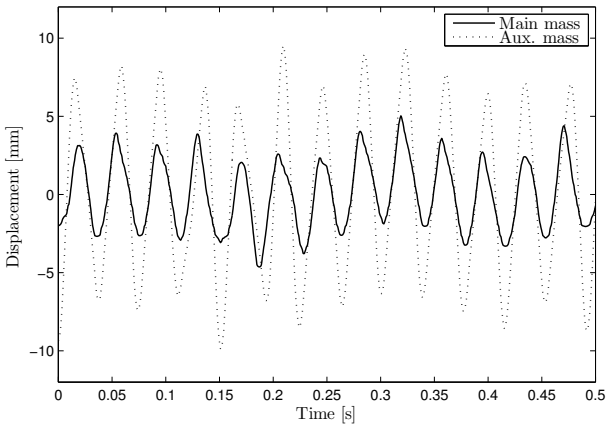

(b) Experiment.

Figure 3.28: Displacement history from model vs. high-speed video data, with gap length $a = 3.15$ mm.

The overall level of vibration, as seen in the displacement signals in Figures 3.26, 3.27 and 3.28, is similar in model and experiment. Even if the model is currently not capable of predicting the full frequency content, this is good enough for the purpose of this project, namely to predict the overall vibration level based on changes in the NLTVA parameters. It is clearly seen that vibration increases with decreased gap length in the experiment, just as it is in the model.

4 Optimisation method

Prior to optimising the NLTVA, there are issues concerning defining the objective function, parametrising the model, choice of optimisation algorithm and computational set-up that need to be addressed.

The initial parametrisation has the following three free parameters: auxiliary spring stiffness k_a, gap length a and spring preload F_0. The optimal performance, as defined by the objective function, will be found with respect to these parameters. In a later stage, it will also be investigated how the mass ratio $\mu = m_\mathrm{a}/m_\mathrm{m}$ influences the performance and how small the auxiliary mass m_a can be made and still be effective. Some additional optimisations will also be run with free auxiliary mass m_a and free auxiliary damping c_a. However, the parametrisation is here explained in a general way to be used in any optimisation case.

The set of free parameters is denoted P. Optimisation is run using the set of normalised parameters p, which is defined by the relation

$$P = P_0 \cdot (p + 1) \tag{4.1}$$

where P_0 is the set of nominal free parameters. Both P and P_0 contain physical values, while p contains normalized values where a 0 simply means the nominal value. The normalisation provides scaling and centring of the problem, i.e. all normalised parameters have the same order of magnitude and have approximately equal effect on the objective function, which is beneficial for the solver to succeed [40]. The optimisation problem is stated as

$$p_\mathrm{optim} = \arg\min_p L(p) \tag{4.2}$$

where p_optim is the optimal parameters (normalised) and L is the value of the objective function which is described below. The goal is to find the global minimum of the objective function, or to come very close to it. Whether any of the found minima is the global minimum will not be possible though. The likelihood to get there increases with the number of optimisation runs of different starting guesses. Therefore, a large number of optimisations are run, each with a starting guess randomised uniformly within the parameter bounds. To increase speed, the starts are run in parallel using the *parfor* statement in MATLAB as recommended in the documentation [41]. The optimisation routine is described further in a flowchart in Appendix C.

4.1 Objective function

A quantitative measure of the performance of the machine is given by the objective function L. It is important to think through exactly what is sought for in the performance and to define the objective function accordingly. The goal here can be seen as a combination of two different objectives: 1) a low vibration level in 2) a wide frequency band. These have to be weighted relatively. For the purpose of minimising vibration around a nominal operating frequency f_nom, the objective function is based on the area under the frequency response curve for a certain predefined range in frequency. Although the frequency can vary considerably for pneumatic machines, the minimum of the response should be concentrated towards the nominal frequency, since that is where most machines are most likely to operate. A weighting function $W(f)$ is therefore used to provide most priority to minimising the response at the nominal point $f = f_\mathrm{nom}$, but to still give some relevance to deviating frequencies. Based on observations of the current prototype machine operating under different conditions, the nominal operating frequency is set to

$$f_\mathrm{nom} = 28 \text{ Hz} \tag{4.3}$$

The frequency response used in the objective function is measured in velocity RMS at the handles, i.e. at the housing mass. It is seen as a function of the operating frequency and the model parameters and is denoted $\dot{x}_{3,\,\mathrm{RMS}}(f,\, p)$. Velocity is used since it is closest to the standardised frequency weighting used to measure hand-arm vibration, cf. Section 2.2.

It was decided to consider frequency variations within ±15 % of the nominal frequency. That means a frequency range of interest of

$$f \in [f_{\text{lb}},\, f_{\text{ub}}] = [0.85 f_{\text{nom}},\, 1.15 f_{\text{nom}}] \tag{4.4}$$

It was also decided that the weight at the lower and upper bound frequencies f_{lb} and f_{ub} should be 1/3 of the weight at the nominal frequency f_{nom}, i.e.

$$W(f_{\text{lb}}) = W(f_{\text{ub}}) = \frac{1}{3} W(f_{\text{nom}}) \tag{4.5}$$

Both these values, 15 % and 1/3, were estimated and do most likely have a great effect on the objective function: how important a low vibration level at the nominal frequency is and how important a wide effective frequency band is. The main thing to remember is that a TVA that suppresses vibration really well at the nominal frequency but has inferior effectiveness or even causes amplified vibration at slight variation in frequency, such as a linear TVA with low damping, is never acceptable.

The weighting function $W(f)$ is a normal distribution centred around the nominal frequency f_{nom}:

$$W(f) = \mathcal{N}(f_{\text{nom}},\, \sigma^2) = \frac{1}{\sigma\sqrt{2\pi}} e^{-\frac{(f-f_{\text{nom}})^2}{2\sigma^2}} \tag{4.6}$$

Its standard deviation σ is derived from (4.6) using the frequency band in (4.4) and the weight condition in (4.5), resulting in

$$\sigma = \sqrt{\frac{(0.15 f_{\text{nom}})^2}{-2\ln(1/3)}} \tag{4.7}$$

For the nominal frequency $f_{\text{nom}} = 28$ Hz in (4.3), this becomes $\sigma \approx 2.83$ Hz.

Instead of discretising a grid of equidistant frequencies and multiplying the response at each frequency with the weighting function, the weighting is realized by concentrating frequency points toward f_{nom}. The grid of frequencies is easiest defined in terms of the intervals Δ_i which are inversely proportional to the weighting function:

$$\begin{aligned} \Delta_i = f_{i+1} - f_i \;&\propto\; W\left(\frac{i-1}{N-2}(f_{\text{ub}} - f_{\text{lb}}) + f_{\text{lb}}\right)^{-1}, \qquad i = 1, 2, \ldots, N-1 \\ f_1 &= f_{\text{lb}} \\ f_N &= f_{\text{ub}} \end{aligned} \tag{4.8}$$

This defines the grid of frequencies $f_i,\ i = 1, 2, \ldots, N$. In this way, the density of grid points at a certain frequency is proportional to the weighting function, cf. Figure 4.1. Note that the number of frequency points N should not be too small for this to work. 15 points are used and that works fine.

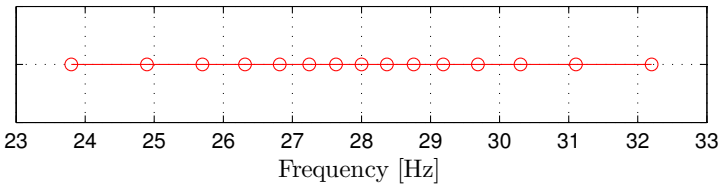

Figure 4.1: Discretisation of the frequency band into $N = 15$ grid points centred around $f_{\text{nom}} = 28$ Hz, with the density of points concentrated towards the middle according to the weighting function.

The objective function L can now be formulated as a function of the set of model parameters p. Trapezoidal integration rule is used for the response curve, but the different frequency intervals are not accounted for in order for the weighting to work. The objective function L is given as

$$L(p) = \frac{1}{2} \sum_{i=1}^{N-1} \dot{x}_{3,\,\text{RMS}}(f_i,\, p) + \dot{x}_{3,\,\text{RMS}}(f_{i+1},\, p) \tag{4.9}$$

where the discrete frequency points f_i are given implicitly in (4.8). This is the objective function used throughout the project to solve the optimisation problem stated above in (4.2).

Great effort has been put into making the objective function continuous and smooth by trying to eliminate numerical and systematic errors as described in Section 3.3. The smoothness is required for the chosen optimisation algorithms to work properly.

4.2 Non-linear least squares formulation

The objective function L in (4.9) is defined as a sum of velocity RMS responses at different frequencies. By creating the vector $\boldsymbol{l}$ that is basically the square root of all responses, then L can be defined as the sum of squares of the elements in $\boldsymbol{l}$. The elements of $\boldsymbol{l}$ are defined by

$$\begin{aligned} l_i(p) &= \sqrt{\dot{x}_{3,\,\mathrm{RMS}}(f_i,\, p)}, && i = 2, \ldots, N-1 \\ l_i(p) &= \sqrt{\frac{1}{2}\dot{x}_{3,\,\mathrm{RMS}}(f_i,\, p)}, && i = 1, N \end{aligned} \tag{4.10}$$

The non-linear least squares formulation of the objective function can then be written as

$$L(p) = \sum_{i=1}^{N} l_i^2(p) \tag{4.11}$$

which is equivalent to (4.9) and minimised according to (4.2).

4.3 Optimisation algorithm

There exist a wide range of built-in optimisation routines for non-linear problems in MATLAB. Mainly two functions were considered: *lsqnonlin* and *fmincon*. They both use gradient-based minimisation methods and are designed to work for problems with an objective function that is continuous and has continuous first partial derivatives. The non-linear least squares solver *lsqnonlin* is in this case advantageous, since the problem can easily be formulated as a least squares problem as in (4.11). It exploits the structure of non-linear least square problems to enhance efficiency compared to general minimisation problems [36]. *fmincon* is a more general minimisation solver for objective functions that are scalar valued, such as L in (4.9). *fmincon* also works for more complicated problems with bounds, linear equalities/inequalities and non-linear constraints, which are not needed in this problem, while *lsqnonlin* only allows for parameter bounds.

The non-linear least squares solver *lsqnonlin* implements two different algorithms; the trust-region-reflective method and the Levenberg-Marquardt method. Trust-region-reflective does not handle underdetermined problems while Levenberg-Marquardt does not handle problems with bounds. The problem requires some bounds on the free parameters; the gap length cannot be negative for example and it is generally desired to keep all values within realistic bounds. Therefore, the trust-region-reflective method is used and the problem must not be underdetermined, i.e. there must be at least as many equations (frequency points) as the number of variables (free parameters).

It should be noted that this is not a global optimisation, but merely a multi-start optimisation giving local optima, some of which are likely to be close to the global optimum due to a large number of randomised starts.

5 Optimisation results

In this chapter, results and discussion from different optimisations of the NLTVA are presented. The first section focuses on optimisation of the NLTVA in the current prototype with nominal auxiliary mass. Comparison is made with an LTVA and the sensitivity of the optimal solution is investigated. The section ends with a comparison of different exciting force assumptions as well as looking into where the NLTVA is operating with respect to the analytical resonance frequency for the different exciting force assumptions. The second section shows the sensitivity to weight of the auxiliary mass. The third section shows the results from an optimisation for a light auxiliary mass where the damping of the NLTVA is optimised as well. The fourth section shows a

case where the weight of the auxiliary mass is optimised. The last section showcases a study where the proposed NLTVA is used for the more traditional task; to suppress vibration at the resonance of a one-mass system.

As a reference, the optimised non-linear system (NLTVA) will often be compared with the corresponding linear system (LTVA). It will also be compared with a system where the TVA is deactivated by fixing it to the main mass (fixed TVA) and with a system where all masses are fixed together (1 mass). The last case (1 mass) corresponds to having no means of vibration reduction. Figure 5.1 summarises how these four configurations were modelled and how they are referred to in the following text.

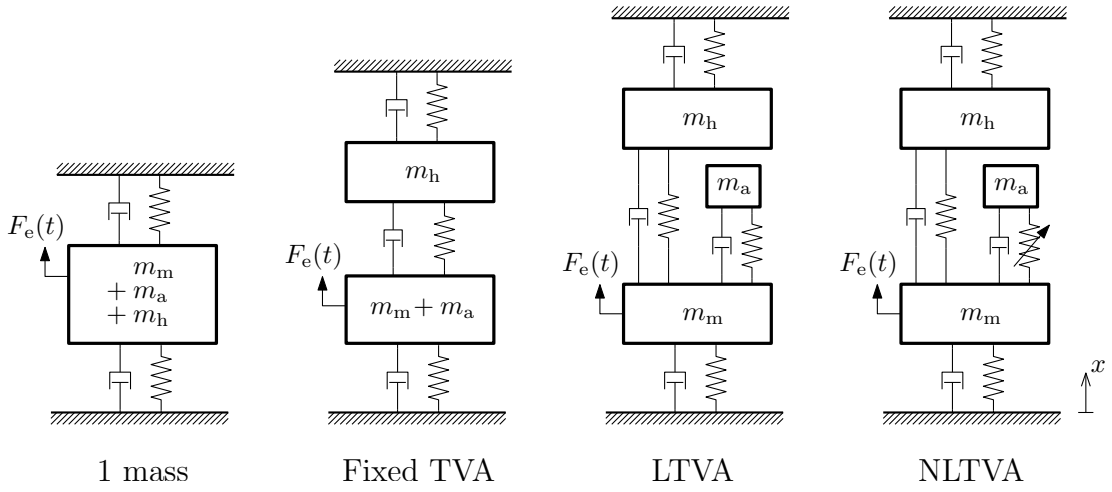

Figure 5.1: Different model configurations used in comparisons of system response. They are referred to as 1 mass, fixed TVA, LTVA and NLTVA. The optimised non-linear system is the rightmost NLTVA.

5.1 Nominal auxiliary mass

In the first optimisation of the prototype's NLTVA, the auxiliary mass m_a was kept fixed at its nominal value of 1 kg. The bound values set in the optimisation for the free parameters are shown in Table 5.1.

Table 5.1: Physical values of the free parameters in optimisation.

Parameter	Nominal value	Lower bound	Upper bound
k_a [kN/m]	40	0	500
a [mm]	5	0	40
F_0 [N]	190	0	500

Figure 5.2 shows the resulting objective function values sorted in ascending order with corresponding normalised parameters for all optimisation starts. The optimal result is thus the first, leftmost in the graph. When looking at Figure 5.2 one sees that 131 out of 262 optimisations resulted in a very low objective function. This shows that although multiple starts are needed to get the best possible parameter values, a relatively good parameter set can be obtained with much fever starts than were used. Another interesting thing to notice is that the stiffness k_a and preload F_0 vary substantially among the results that give a low objective function. These parameters can thus be chosen rather freely and still give essentially the optimal found performance. Variation in the gap a is however much smaller. The key thing is the combination of the three parameters. A combination of k_a, a and F_0 that tunes the NLTVA to a certain operating frequency for a certain exciting force amplitude could be found theoretically using the derived results (2.1) and (2.2). A wide effective frequency band can then be achieved by moving the last resonance far up in frequency, which is done by choosing a high stiffness k_a as noted previously in Section 3.4.4. The best and the 100th best parameter set of the optimisation can be seen in Table 5.2.

The best run (#1) gives the objective function value $L = 0.0878$ and the optimal parameters $k_a = 164.24$ kN/m, $a = 10.21$ mm and $F_0 = 98.22$ N. The 100th best run (#100) gives the objective function value $L = 0.0966$ and

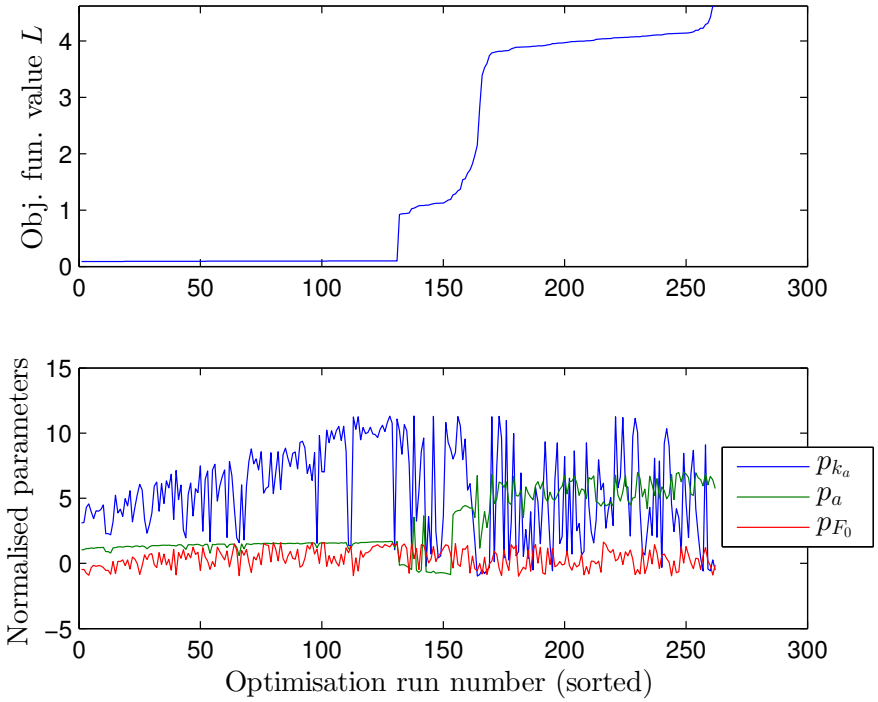

Figure 5.2: Optimisation result from 262 runs with $m_\mathrm{a} = 1.0$ kg, $\mu = 0.37$.

Table 5.2: Comparison of k_a, a and F_0, between the best and the 100th best found solution.

Run number	Obj. func. L	k_a [kN/m]	a [mm]	F_0 [N]
#1	0.0878	164.2357	10.2145	98.2244
#100	0.0966	321.3769	12.9526	486.1319

the optimal parameters $k_\mathrm{a} = 321.38$ kN/m, $a = 12.95$ mm and $F_0 = 486.13$ N. The difference in performance between the two is thus roughly 10 %. All parameters in run #100 are however much higher and the high stiffness and preload are harder to construct, so the best solution is more favourable with respect to performance and applicability.

The optimal auxiliary spring force F_k is plotted in Figure 5.3. It shows an overall hardening characteristic dominated by the gap a and stiffness k_a while the preload F_0 has very little effect.

5.1.1 Comparison with an LTVA

A comparison of displacement RMS response of the handle between the optimised NLTVA and the LTVA, both tuned to $f = 28$ Hz, with nominal auxiliary mass $m_\mathrm{a} = 1.0$ kg is shown in Figure 5.4. As references, the response is also shown for the cases with one mass only (all masses fixed together resulting in no vibration reduction at all) and with the TVA fixed to main mass (only vibration isolation between main mass and housing). First, compare the LTVA with the one mass case and fixed TVA case. The frequency band in which the LTVA is better than both is between 19 and 30 Hz. So the upper boundary is very close to the tuned frequency of 28 Hz. Now compare the previous cases with the NLTVA. Although the two optimised NLTVA cases have quite different parameters, as shown in Table 5.2, they give very similar results in the region of interest; around 28 Hz. The effective frequency band has now widened enormously, covering 15 Hz to over 50 Hz. It clearly shows the benefits of using an NLTVA as opposed to using an LTVA or to not using a TVA at all and only having the vibration isolation between main mass and housing. Especially the upper bound of the effective frequency band has increased dramatically. The last resonance frequency has moved far up, beyond 60 Hz. Note that this is a non-linear resonance and is therefore amplitude dependant. With increasing frequency, the exciting force in the model increases quadratically and the NLTVA's resonance frequency, as

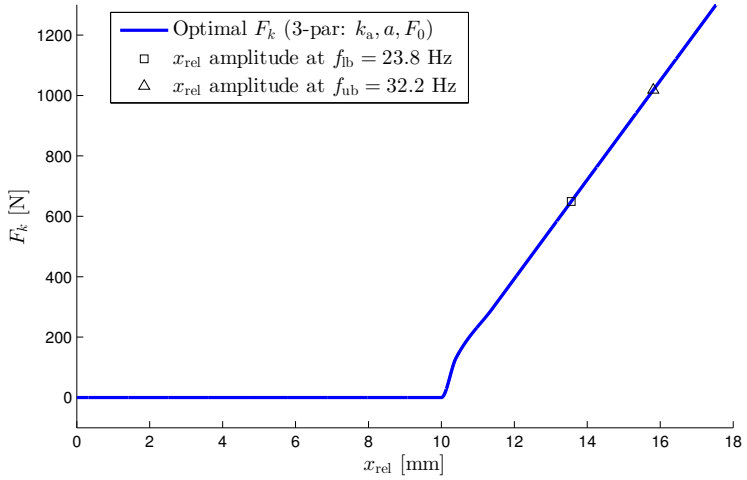

Figure 5.3: Auxiliary spring force F_k for optimal parameter k_a, a and F_0 as given in Table 5.2. The square and triangle markers show the amplitude of the auxiliary mass relative main mass at the lower and upper excitation frequency bounds used in the objective function.

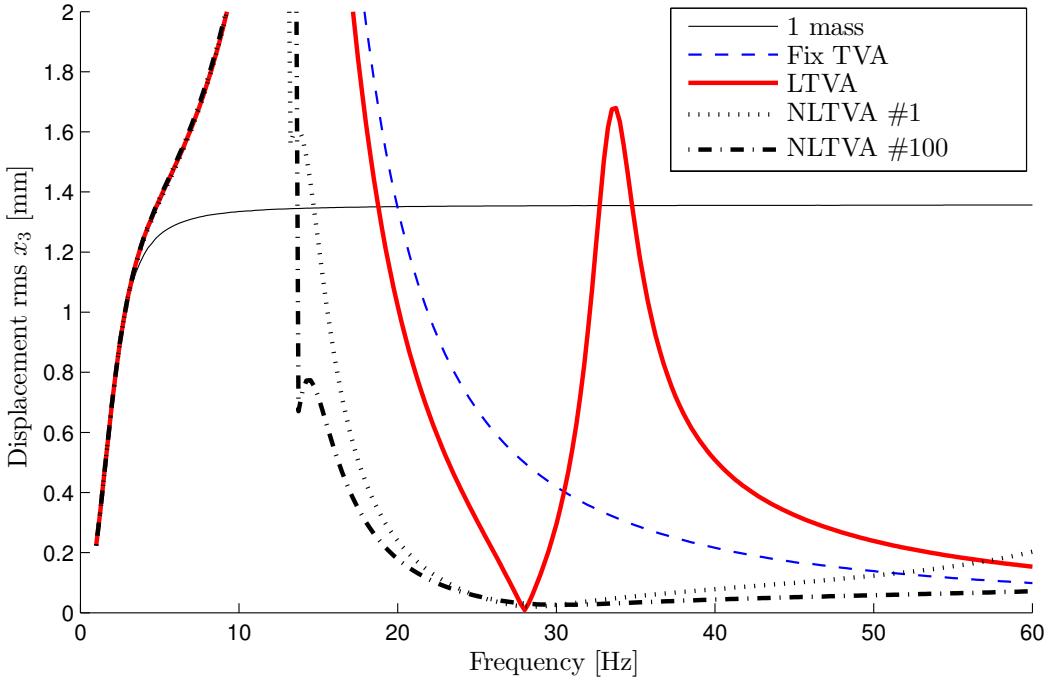

Figure 5.4: Displacement RMS of the handle for five different configurations. 1 mass: the machine is modelled as one single mass of $m_m + m_a + m_h$. Fix TVA: the TVA is deactivated by fixing it to the main mass, so the only vibration reduction is from the isolation between main mass and housing. LTVA: linear system tuned to 28 Hz by adjusting the auxiliary spring k_a. NLTVA: non-linear system using optimised parameter set #1 and #100 from Table 5.2.

stated analytically in (2.1), is expected to increase with it. This should be the reason why the last resonance is moved so far up. A further discussion on the assumption of quadratically increasing exciting force and its consequences is given in Section 5.1.3.

Plotting the phase angles, as seen in Figure 5.5, also shows the superior effect of the NLTVA. At 28 Hz the auxiliary mass is in almost perfect counterphase with the exciting force. Here the main mass (and the housing) makes a 180° phase shift in both the linear and non-linear system, however much more abrupt in the linear system. For the linear system, the last resonance occurs rather soon afterwards, around 34 Hz. At this point, all masses make a 180° shift and the LTVA amplifies vibration since it is no longer in counterphase with the exciting force, cf. the curves for fixed TVA and LTVA in Figure 5.4. The LTVA is thus only effective in a very narrow band above the tuned frequency. For the non-linear system, the last resonance and phase shift comes at a very high frequency. The auxiliary mass can therefore stay close to perfect counterphase (-180°) up to a much higher frequency than in the linear system. With the NLTVA, the lag between main and auxiliary mass around 20 Hz as well as the slower shift around 28 Hz is believed to be caused mainly by the gap length a. The gap and preload are also the reason why vibration is not suppressed as much as with the LTVA exactly at the tuned frequency 28 Hz, cf. Figure 5.4. The non-linearities basically cause a small mismatch between exciting force and auxiliary spring force so that they cannot counteract each other perfectly. In the big picture, however, this is unimportant since the pneumatic machine can never be assured to operate at the tuned frequency exactly.

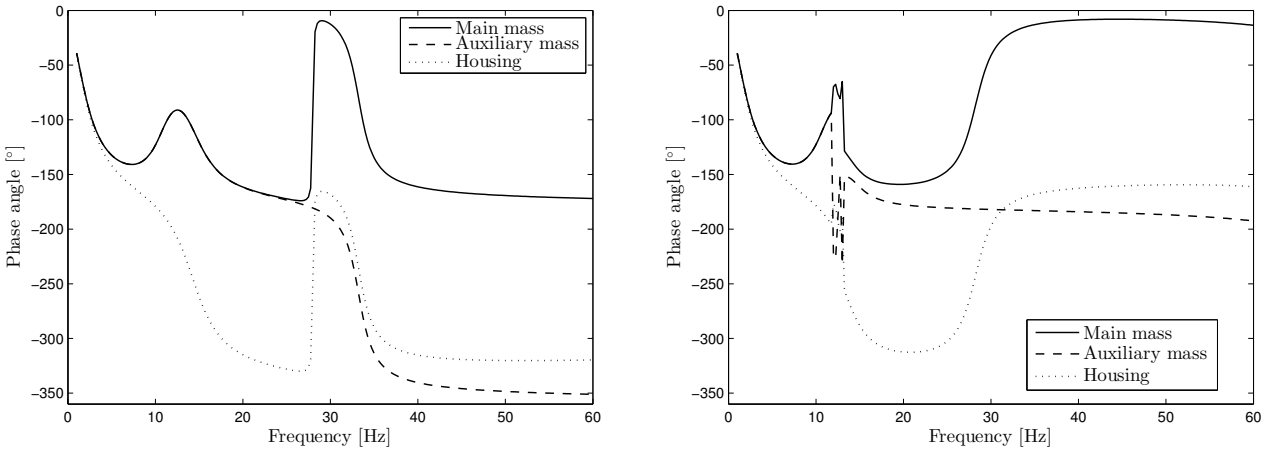

(a) System with LTVA tuned to 28 Hz.

(b) System with optimised NLTVA (#1).

Figure 5.5: Phase angles of all masses taken for the excitation frequency f relative the exciting force, with auxiliary mass $m_\mathrm{a} = 1.0$ kg.

5.1.2 The solution's sensitivity

The optimal parameters are delivered with very high precision from the optimisation. A precision of this kind can of course not be used when manufacturing impact machines. To investigate how sensitive the optimal solution is to variations in the optimal parameters a simple sensitivity analysis was performed. Each parameter was varied from -50 % to +50 % of the optimal value and the objective function L was calculated. The amplitude of the force F_e was also included in the sensitivity analysis because it can be influenced by operating conditions and air pressure and between machines. The results from varying single parameters from the optimal parameters in Table 5.2, with $m_\mathrm{a} = 1$ kg, can be seen in Figure 5.6.

From Figure 5.6 it is clear that, for the optimal parameters used, the objective function is most sensitive to variations in the weight of the auxiliary mass m_a and the length of the gap a. The objective function is significantly less sensitive to the amplitude of the force F_e. The preload F_0 can be varied within ±50 % without any significant changes in the objective function. Although the sensitivity to stiffness k_a is much grater than for the preload there is a rather wide range around 0 where the changes in L are minimal. The greater sensitivity to changes in weight of the auxiliary mass m_a and the gap length a should not be problematic since they are the parameter that are easiest to control. On the other hand the sensitivity to the amplitude of the force can be problematic, since it is hard to measure and control. The forcing amplitude should therefore be measured as

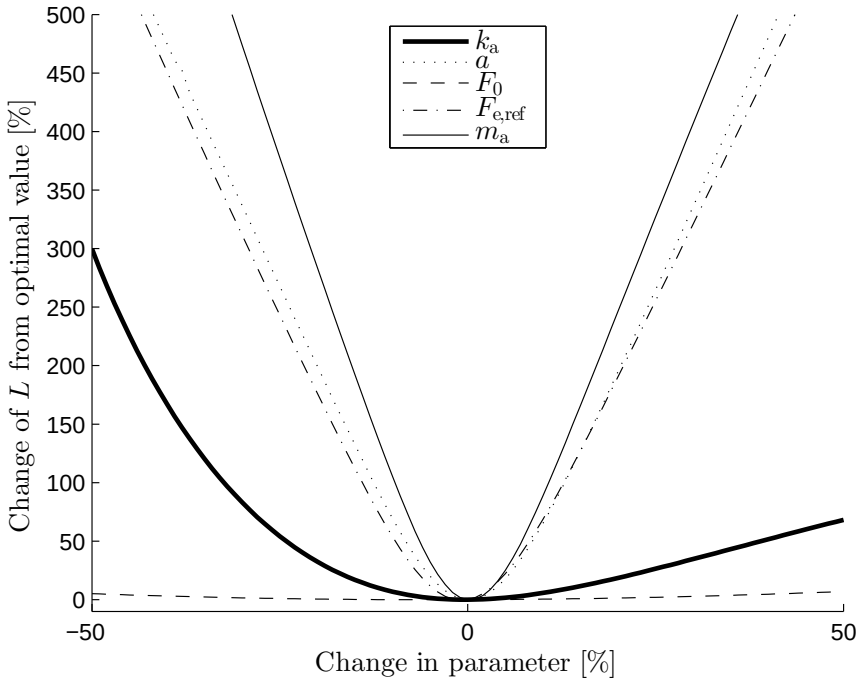

Figure 5.6: Changes in the objective function L when a single parameter and the forcing amplitude are varied from the optimal values #1 from Table 5.2. The amplitude of the force is varied from it's nominal value seen in Table 2.1 and the mass m_a from its nominal value of 1 kg.

well as possible as well as investigating how it varies to be able to use a correct value and possibly include some variation of it in the objective function for future optimisations.

5.1.3 Different exciting force assumptions

As described in Section 3.4.5, the amplitude of the exciting force is assumed to increase quadratically with excitation frequency. To investigate how crucial this assumption is, the proposed NLTVA was also tuned for cases where the amplitude is constant, as well as with a linearly increasing amplitude. The only changes made were that the equation for the exciting force was changed to:

$$|F_e(f)| = F_{e,ref} \tag{5.1}$$

to have a constant force amplitude and

$$|F_e(f)| = F_{e,ref} \cdot (f/f_{ref}) \tag{5.2}$$

to use a linearly increasing amplitude. All other parameters and bounds used were exactly the same as in Section 5.1. The resulting parameters that gave the lowest objective function using all three equations for the amplitude of the force can be seen in Table 5.3.

Table 5.3: The parameters k_a, a and F_0 that gave the lowest objective function value with a constant, linearly increasing and quadratically increasing exciting force amplitude.

	Obj. func. L	k_a [kN/m]	a [mm]	F_0 [N]
Constant $\|F_e(f)\|$	0.1868	256.2161	9.7451	17.3061
Linear $\|F_e(f)\|$	0.1352	253.0793	10.3159	2.1978
Quadratic $\|F_e(f)\|$	0.0878	164.2357	10.2145	98.2244

As can be seen in Table 5.3, the gap length a is similar in all cases. The gap length is slightly lower for a

constant force amplitude and slightly higher when a linearly increasing is used. The stiffness k_a is however much higher for both linear and constant amplitudes than the quadratic. The preload F_0 is only 2 N for the linear case and only 17 N for the constant case. A comparison of the objective function value L for all three cases and for different system configurations can be seen in Table 5.4 and the response of the handle at frequencies around 28 Hz can be seen in Figure 5.7.

Table 5.4: Comparison of the lowest objective function value with a constant, linearly increasing and quadratically increasing exciting force amplitude. The difference in objective function between using the NLTVA and an LTVA is shown on the right.

	Obj. func. L			
	Fixed TVA	LTVA	NLTVA	Reduction of L NLTVA vs LTVA [%]
Constant $\lvert F_e(f)\rvert$	1.1207	0.4880	0.1868	-61.72
Linear $\lvert F_e(f)\rvert$	1.1793	0.5346	0.1352	-74.71
Quadratic $\lvert F_e(f)\rvert$	1.2477	0.5913	0.0878	-85.15

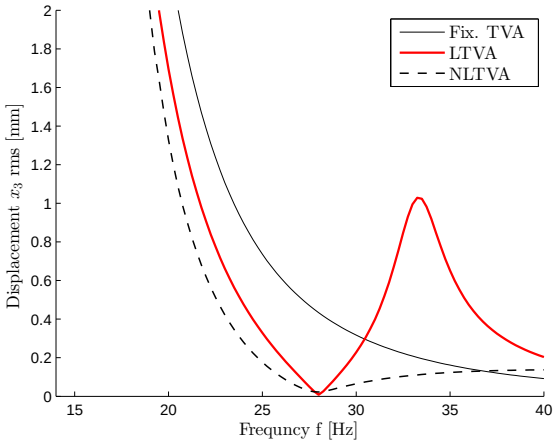

(a) Constant force amplitude $|F_e(f)|$, according to (5.1).

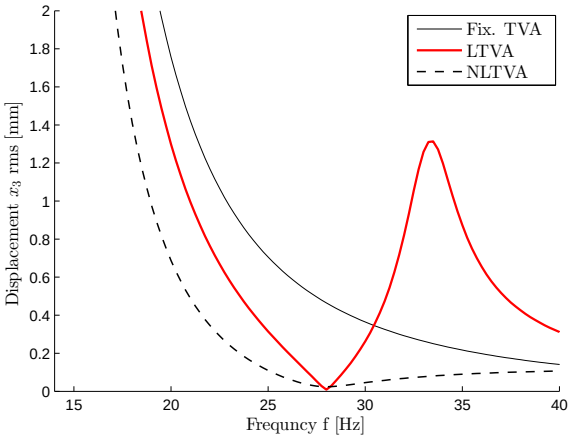

(b) Linearly increasing force amplitude $|F_e(f)|$, according to (5.2).

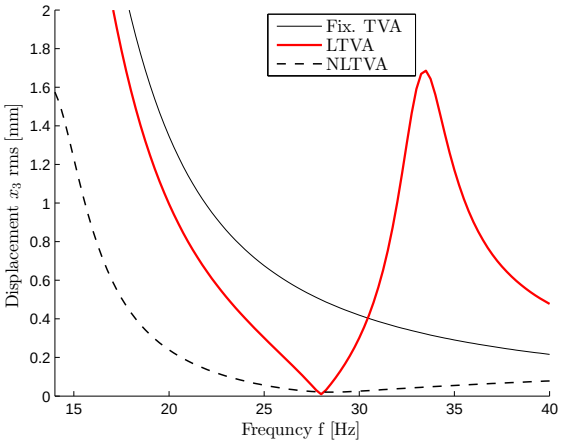

(c) Quadratically increasing force amplitude $|F_e(f)|$, according to (3.18).

Figure 5.7: Response of the housing for different formulations of exciting force amplitude $|F_e(f)|$. Comparison between having the TVA fixed to main mass, LTVA and NLTVA.

Figure 5.7 shows that the NLTVA gives a much wider suppression band than an LTVA for all cases. Table 5.4 shows that the reduction in the objective function is over 60 % for all cases. An interesting finding is that the reduction is lowest for the constant amplitude, a bit greater for the linearly increasing amplitude and greatest for the quadratically increasing amplitude.

Resonance frequency for different exciting force amplitudes

Equation (2.1) shows that the resonance frequency f_{res} of the NLTVA depends on the spring compression b. To investigate where the NLTVA is operating with regards to the resonance frequency, the analytical resonance frequency was calculated. The spring compression b was taken from the simulation and the resonance frequency was calculated using (2.1) for the different force amplitudes $|F_{\text{e}}(f)|$. Comparison between the working frequency and the operating frequency, for all cases using the optimal parameters in Table 5.3, can be seen in Figure 5.8.

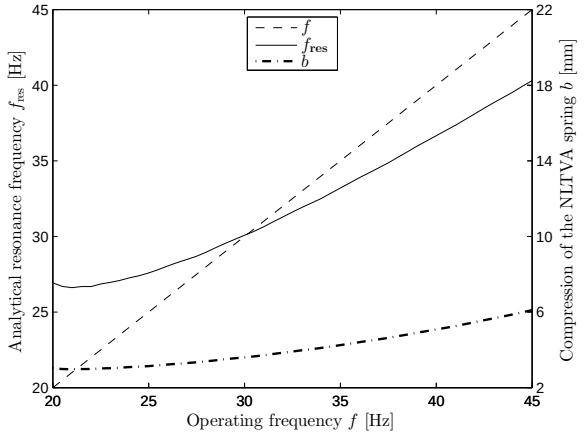

(a) Constant force, according to (5.1).

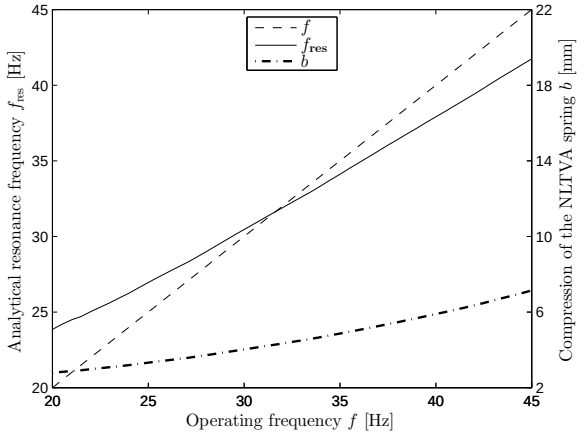

(b) Linearly increasing force, according to (5.2).

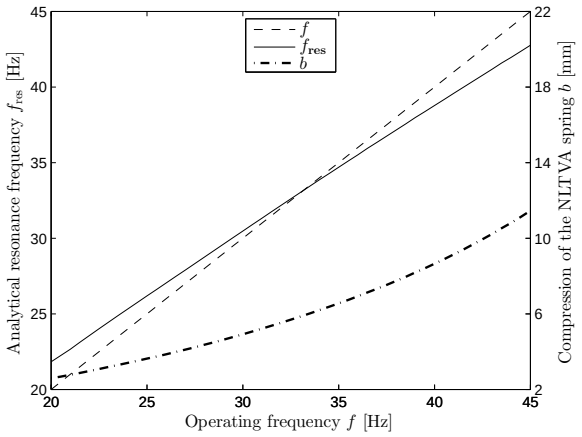

(c) Quadratically increasing force, according to (3.18).

Figure 5.8: Analytical resonance frequency f_{res} versus the operating frequency f, for different formulations of the exciting force amplitude $|F_{\text{e}}(f)|$. The operating frequency is plotted against itself, with a dashed line, as an ideal reference case. The compression of the NLTVA's spring b, which is used to calculate the resonance frequency, is plotted with a dash-dot line. The scale on the right y-axis belongs to b.

The operating frequency is plotted against itself as a reference. This straight line is used as a reference because when the resonance frequency f_{res} is the same as the operating frequency f, the NLTVA gives (theoretically) maximum suppression. The compression b is also plotted with a secondary y-axis on the right.

As can be seen in Figure 5.8c the operating frequency f is very close to the resonance frequency over a wide frequency range when a quadratically increasing exciting force amplitude is used. It is slightly below the

resonance frequency f_{res} when the machine is operated below 33 Hz and when the operating frequency f moves past 33 Hz it overtakes the resonance frequency. When the forcing amplitude grows linearly, cf. Figure 5.8b, the difference between the operating frequency f and the resonance frequency f_{res} is larger for both the lower and higher frequencies and when a constant force amplitude is used, cf. Figure 5.8a, the difference is even greater. This difference between the three cases is most likely the reason for the larger difference between the performance of an NLTVA vs. an LTVA seen in Table 5.4 when a quadratically increasing exciting force amplitude $|F_{\text{e}}(f)|$ is used.

5.2 Sensitivity to mass ratio

To investigate how the weight of the auxiliary mass affects the performance of the NLTVA, the model was optimised multiple times with 9 different values of m_{a}. Lighter masses were chosen because HHIMs in general are desired to be as light as possible for easier handling and better ergonomics. As conventionally done in literature, the weight of the auxiliary mass is expressed relative the main mass as the mass ratio μ defined as:

$$\mu = \frac{m_{\text{a}}}{m_{\text{m}}} \tag{5.3}$$

The optimised parameters, k_{a}, a and F_0, that gave the lowest value of the objective function L for all 9 mass ratios can be seen in Table 5.5 and the value of the objective function versus mass ratio can be seen in Figure 5.9.

Table 5.5: Optimised parameter changes and the corresponding objective function values L for different mass ratios μ. The reference value $L_{\text{ref}} = 1.248$ is the value of the objective function with vibration isolation and a fixed TVA.

m_{a} [kg]	μ	$k_{\text{a,opt}}$ [kN/m]	a_{opt} [mm]	$F_{0,\text{opt}}$ [N]	L	$\Delta L/L_{\text{ref}}$ [%]
1.0	0.3704	164.2357	10.2145	98.2244	0.0878	-92.9659
0.9	0.3333	157.3752	11.3816	76.7169	0.0917	-92.6512
0.8	0.2963	140.5606	12.7339	70.5280	0.0975	-92.1876
0.7	0.2593	105.5335	14.3572	128.8133	0.1072	-91.4087
0.6	0.2222	95.4965	16.3216	74.2882	0.1201	-90.3734
0.5	0.1852	75.4409	18.1274	4.5437	0.1436	-88.4934
0.4	0.1481	49.5826	21.9811	75.6339	0.1893	-84.8247
0.3	0.1111	38.5226	27.3383	28.8508	0.2833	-77.2949
0.2	0.0741	13.1234	27.8495	80.0670	0.5362	-57.0270

When looking at the best parameters for different mass ratios, cf. Table 5.5, two trends can be seen. First the expected reduction in stiffness k_{a} when the mass ratio is decreased and secondly that the gap gets larger when the mass ratio is decreased. No clear trend can be seen for the value of the preload, except that it is always lower than the nominal value of 190 N. The lack of a trend correlates well with the low sensitivity to preload in the case of 1 kg auxiliary mass, as previously seen in Figure 5.6.

Figure 5.9 clearly shows the benefit of having a higher mass ratio. A more surprising finding is however that the growth of L, with decreased mass ratio μ is very gradual down to $\mu = 0.2222$, but when the mass ratio is decreased further the growth becomes much more rapid. To investigate this further, it was necessary to look at the response of the housing, that is used to calculate the objective function, as well as the velocity and displacement of the auxiliary mass. The response, as calculated in the objective function during optimisation, can be seen in Figure 5.10 and the displacement and velocity amplitudes of the auxiliary mass relative to the main mass in Figure 5.11.

Inspection of the response of the housing, for the frequencies used during the optimisation, seen in Figure 5.10, shows that the response is as expected for the higher mass ratios but for the lower mass ratios the NLTVA seems to be out of tune, i.e. the response does not have a minimum at 28 Hz.

Figure 5.11 shows that the amplitudes of both the displacement and velocity of the auxiliary mass relative to the main mass grow with frequency. The displacement and velocity are also higher for lower mass ratio which is expected since a lighter auxiliary mass needs a higher velocity to create the same counter force on the main

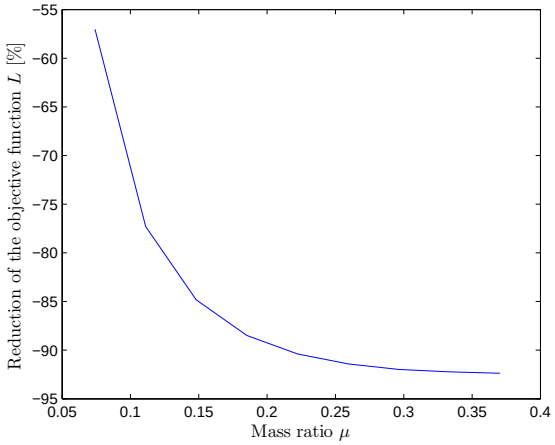

Figure 5.9: Minimised objective function L for different mass ratios μ. Reduction in L is given relative the reference value $L_{\text{ref}} = 1.248$ which is pertinent to a system with vibration isolation and a fixed TVA. The results are obtained from over 250 optimisation starts for each mass ratio.

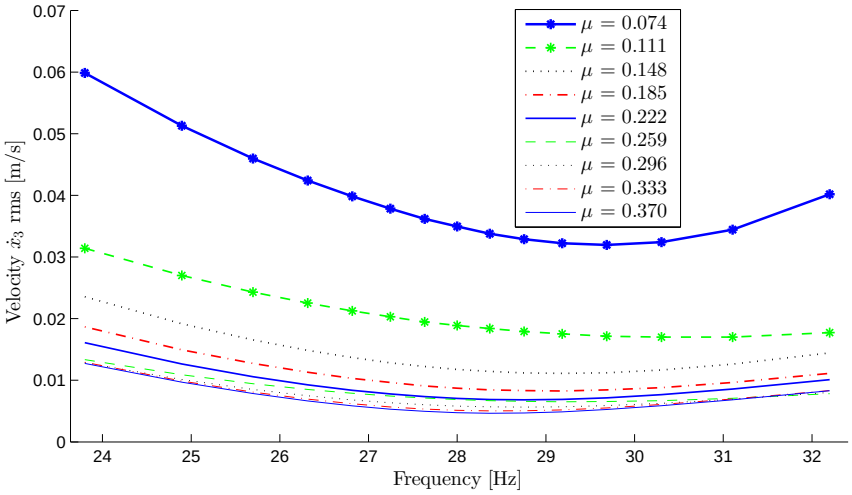

Figure 5.10: Velocity RMS response of the housing in the frequency range of interest for different mass ratios μ. For each mass ratio, the optimal parameters from Table 5.5 are used.

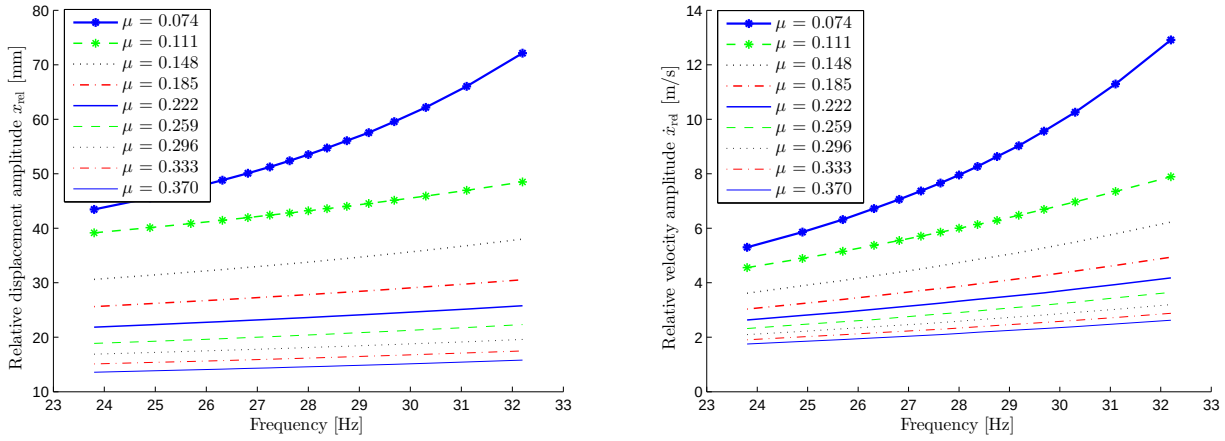

(a) Displacement amplitude.

(b) Velocity amplitude.

Figure 5.11: Amplitudes of the auxiliary mass relative the main mass in the frequency range of interest for different mass ratios μ. For each mass ratio, the optimal parameters from Table 5.5 are used.

mass. Having a higher velocity does however increase the dissipation through viscous damping resulting in less vibration suppression when the mass ratio is lowered. Another interesting thing worth mentioning is that the growth of the auxiliary mass amplitude with frequency is much steeper for lower mass ratio. That depends on the lower optimal stiffnesses $k_{\mathrm{a,opt}}$ obtained for the lower mass ratios as seen in Table 5.5.

5.2.1 Chaotic behaviour with low mass ratios

As described in Section 3.3.2, the response in the computational model is calculated for the first frequency using a defined initial state $\mathbf{z}_0$. When the motion stabilises, the last state at that frequency is used as the initial state at the next frequency to reduce the time needed to stabilise into a limit cycle at each frequency. The stable motion of a non-linear system can however depend heavily on the initial state, i.e. there can exist several limit cycles, and in certain cases the motion will not stabilise at all and instead be chaotic.

To investigate how changes in the initial state affect the solution, two tests were performed. The first approach was to evaluate the response backwards, i.e. starting at the highest frequency of interest (32.2 Hz), with the initial state $\mathbf{z}_0$, and continue to use the final state at that frequency as the initial state at the frequency below. This analysis showed that the response is identical for mass ratios $\mu \geq 0.158$ but for the three lowest mass ratios the response is different. Comparison between beginning at the highest and lowest frequency can be seen in Figure 5.12 for $\mu = 0.074$, 0.111 and 0.148.

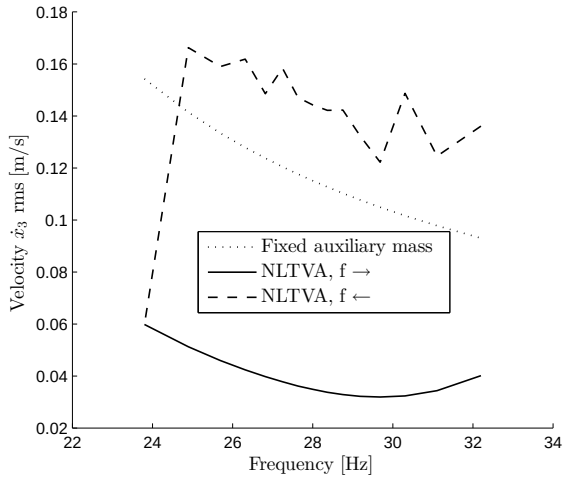

(a) $\mu = 0.074$.

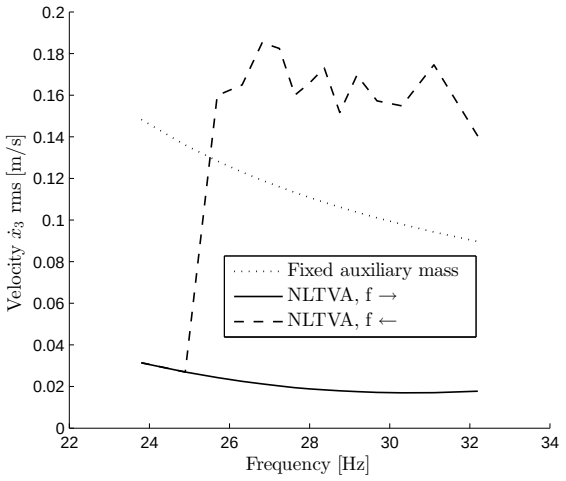

(b) $\mu = 0.111$.

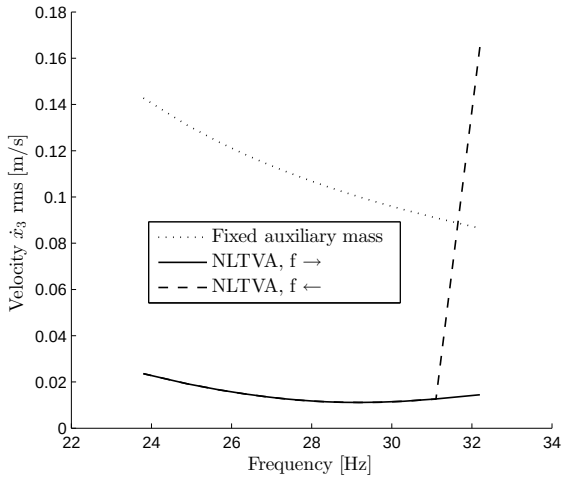

(c) $\mu = 0.148$.

Figure 5.12: Response of the housing within the frequency range of interest by the optimisation for different mass ratios μ. Comparison between starting at the highest frequency vs the lowest.

Figure 5.12 shows that when the simulation goes down the frequency range, different response curves are obtained. When the response, beginning at the highest frequency is compared with the response of the system with fixed auxiliary mass we see that the vibrations are greater, i.e. the TVA has switched from reducing the vibration of the handle to increasing vibration. This unwanted behaviour continues to the second lowest frequency when $\mu = 0.074$, seen in Figure 5.12a. At the lowest frequency, the response drops down to the same value as when the response is calculated from the lowest frequency. Therefore the stability of the vibrations seems to be independent of the initial state for the lowest frequency. This stabilisation similarly happens between 24.9 and 25.7 Hz when $\mu = 0.111$. When $\mu = 0.148$, the chaotic motion only occurs for the highest frequency. Comparison between the highest and second highest frequency, with $\mu = 0.148$ and optimal parameters, can be seen in Figure 5.13. The time history is displayed in Figure 5.13a and 5.13b for 31.11 Hz and 32.2 Hz respectively. Note that the chaotic response at 32.2 Hz is only displayed between 6 and 7.5 s to show the typical chaotic response. Phase space plots from the same data are shown in Figure 5.13c and 5.13d for 31.11 and 32.2 Hz respectively. Note that the phase space plots only include the very last part of the time history that is used to evaluate the RMS during the computation.

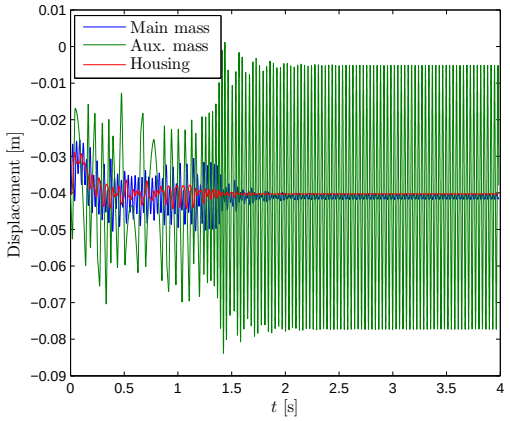

(a) Response of the system at $f = 31.11$ Hz until the vibrations become stable with optimal parameters, $\mu = 0.148$.

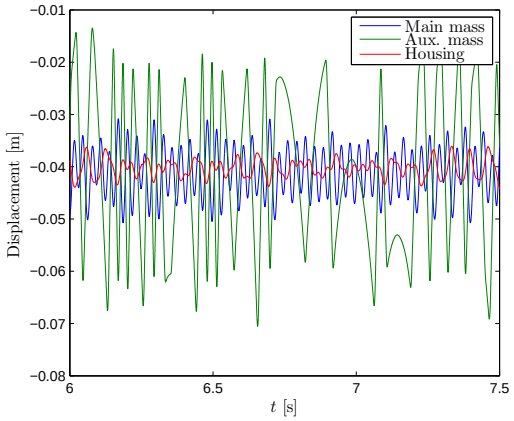

(b) Typical chaotic response of the system at $f = 32.20$ Hz with optimal parameters, $\mu = 0.148$.

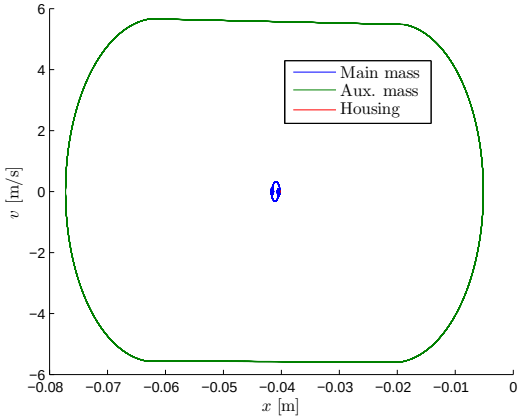

(c) Phase space plot of the vibrations seen in 5.13a.

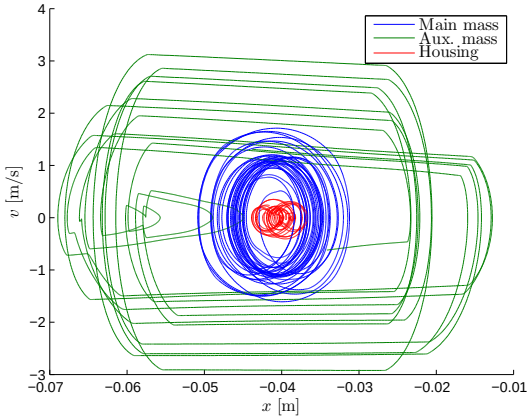

(d) Phase space plot of the vibration seen in 5.13b.

Figure 5.13: Comparison between stable and chaotic vibrations for $\mu = 0.148$. When the system is simulated from the lowest frequency to the highest.

The second test was to calculate the response individually for each frequency always with the initial state $\mathbf{z}_0$. This gave chaotic behaviour at the same frequencies as in the first test for all mass ratios.

Some efforts were made, for the lower mass ratios, to move the minimum of the response lower in frequency, i.e. tuning it to 28 Hz, by increasing the gap and lowering the stiffness manually. These efforts all resulted in a chaotic response within the frequency range of interest, even when starting at the lowest frequency and stepping upwards as usual. This suggests that the optimisation finds the parameters that give the lowest

eigenfrequency, without introducing chaotic response within the frequency range of interest. With the lowest mass ratios though, the system seem to be very sensitive to initial condition and will probably be infeasible in reality.

The results show that the proposed NLTVA can work well for lower mass ratios. Lowering the mass ratio does however reduce the vibration suppression. For very low mass ratios, chaotic response can be an issue and might even cause increased vibration, at least for the large exciting force that is used in this thesis.

5.3 Free damping

The results in the previous section showed that chaotic behaviour can occur when the mass ratio is lowered. As shown in Figure 5.11b, a light auxiliary mass needs to move at a higher velocity and is therefore more affected by the damping. To investigate what would be the optimal damping for the lightest auxiliary mass $m_\mathrm{a} = 0.2$ kg and to see if the chaotic behaviour could be avoided if the damping was lowered further, an optimisation was performed with the damping c_a as a fourth free parameter. The parameter bounds that were used during optimisation can be seen in Table 5.6.

Table 5.6: Physical values of the free parameters in optimisation with free damping c_a.

Parameter	Nominal value	Lower bound	Upper bound
k_a [kN/m]	40	0	500
a [mm]	5	0	40
F_0 [N]	190	0	700
c_a [N s/m]	1	-30	30

Negative damping was allowed due to interest from the supervisor to see if it could improve the performance. The equivalence of negative damping could be achieved by using the outlet air from the impact mechanism to give the auxiliary mass a boost.

The parameter values that minimised the objective function can be seen in Table 5.7 and a comparison between the optimised NLTVA with free damping, nominal damping, LTVA and fixed TVA can be seen in Figure 5.14.

Table 5.7: The parameters that gave the lowest value of the objective function L when the damping c_a was free and the auxiliary mass $m_\mathrm{a} = 0.2$ kg.

$k_{\mathrm{a,opt}}$ [kN/m]	a_opt [mm]	$F_{0,\mathrm{opt}}$ [N]	$c_{\mathrm{a,opt}}$ [N s/m]
11.351	36.7	188	0.0857

As can be seen in Table 5.7, the damping becomes negligibly low but not negative. Very low damping was expected since the performance of TVAs is generally better when there is no damping present. Compared to the previous case where the damping is fixed to its nominal value $c_\mathrm{a} = 1$ N s/m, cf. Table 5.5, the stiffness k_a is slightly lower but approximately the same. The gap length a and preload F_0 are however significantly larger. The increase in the gap length is expected since the auxiliary damping here is close to zero and therefore the NLTVA's dissipation of vibration energy is very low. Figure 5.14 shows that the NLTVA with optimised damping is better tuned to the target frequency, i.e. the minimum lies closer to 28 Hz. The vibration is also significantly lower when the damping is smaller.

Chaotic vibrations appeared at the same frequencies as in Section 5.2.1 if the response was calculated from the highest frequency to the lowest and if single frequencies where calculated, which suggests that lowering the damping c_a does not reduce the risk of chaotic motion.

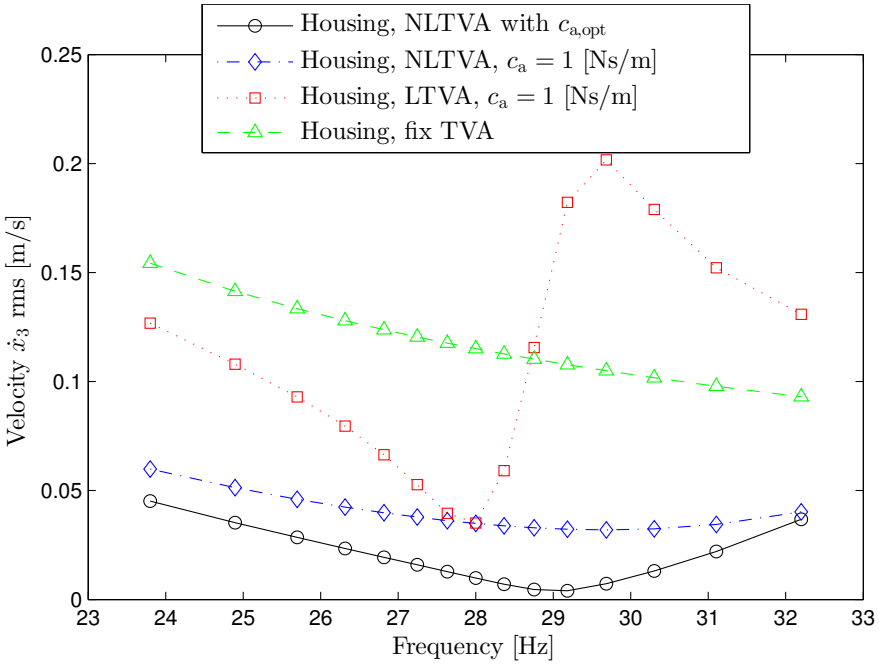

Figure 5.14: Response of the housing within the frequency range of interest. Comparison between optimisation result for the NLTVA with free c_a and the nominal value as well an LTVA and fixed auxiliary mass.

5.4 Free auxiliary mass

In another batch of optimisation runs, the auxiliary mass was allowed free. That is the four parameters k_a, a, F_0 and m_a were allowed to be varied for optimisation. The bound values set in the optimisation for these free parameters are shown in Table 5.8. The resulting sorted objective function values and corresponding parameters are shown in Figure 5.15 and the parameters that minimised the objective function can be seen in Table 5.9.

Table 5.8: Physical values of the free parameters in optimisation.

Parameter	Nominal value	Lower bound	Upper bound
k_a [kN/m]	40	0	500
a [mm]	5	0	40
F_0 [N]	190	0	500
m_a [kg]	1	0.1	3

Table 5.9: The parameters that gave the lowest value of the objective function L when the the auxiliary mass m_a was free.

Obj. func. L	$k_{a,opt}$ [kN/m]	a_{opt} [mm]	$F_{0,opt}$ [N]	$m_{a,opt}$ [kg]
0.0748	273.464	4.5	52	2.0878

The optimisation results seen in Figure 5.15 are similar to the results when m_a was fixed, i.e. a large proportion of the runs resulted in a very low objective function, and the stiffness k_a, and preload F_0 vary significantly among the good results. Another interesting thing is that none of the results with a very low objective function lie on the upper bound of 3 kg for m_a. Most of them do however lie close to a normalised value of $p_{m_a} = 1$ giving an auxiliary mass m_a around 2 kg. As seen in Table 5.9 the best parameter set has $m_a = 2.0878$ kg and gives an objective function value of $L = 0.0748$. This low objective function value fits the trend seen in Section 5.2, i.e. heavier auxiliary mass gives more suppression. The interesting fact is however that the upper bound on the auxiliary mass m_a was set to 3 kg. This suggests that there is a limit to the improvement possible

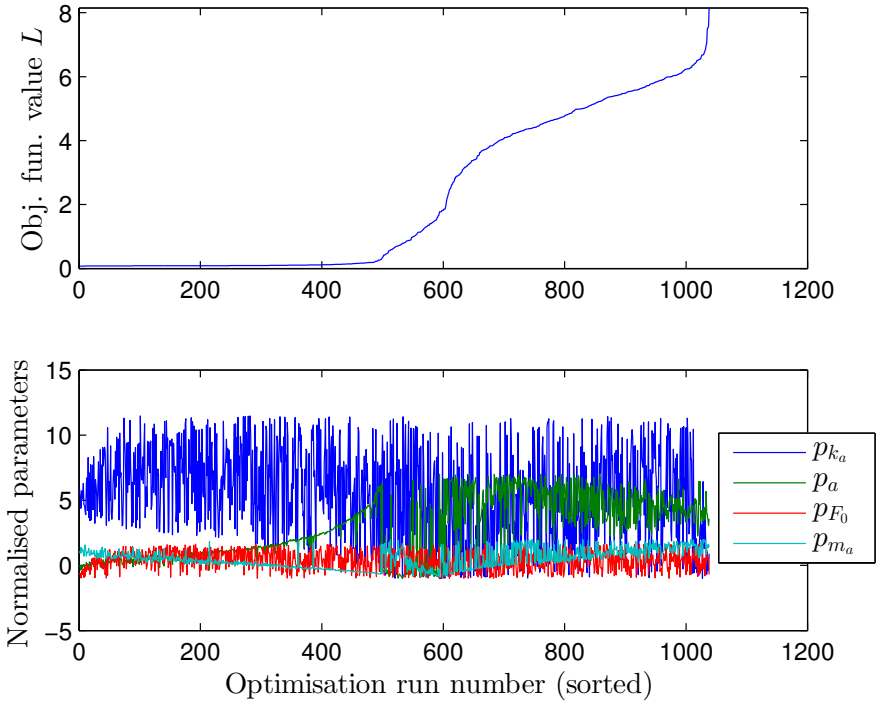

Figure 5.15: Optimisation result from 1038 runs with the weight of the auxiliary mass m_a as a free parameter.

by increasing the auxiliary mass. When put in perspective with the weight of the main mass, the optimal mass ratio is:

$$\mu = \frac{2.0878 \text{ kg}}{2.7 \text{ kg}} = 0.773$$

So the auxiliary mass can hardly be considered an auxiliary mass since its weight is such a large proportion of the total mass of the system.

5.5 Removing a resonance with the proposed NLTVA

Traditionally, the common use of TVAs is to remove or minimise the response at an unwanted resonance. This is desirable when a system is excited at its resonance frequency, as opposed to the studied prototype machine in which the operating frequency is well above all of the primary system's resonances. To investigate the proposed NLTVA's ability to be used in this sense, a case study was performed. All model parameters except the main stiffness k_m were kept the same as in other parts of the project. The housing was however removed from the model to make the study more general. There was thus only two masses in the model as illustrated in Figure 5.16.

The stiffness k_m between the ground and the main mass was set to

$$k_\mathrm{m} = (2\pi \cdot 28)^2 \cdot m_\mathrm{m} \tag{5.4}$$

in order for the eigenfrequency of the primary system to be 28 Hz. The stiffness k_a, gap length a and preload F_0 were then optimised using the same objective function as earlier, for $m_\mathrm{a} = 1.0$, 0.7 and 0.3 kg.

A comparison of the response of the main mass between 1 and 60 Hz with an NLTVA, LTVA and without TVA can be seen in Figures 5.17, 5.18 and 5.19 for $m_\mathrm{a} = 1.0$, 0.7 and 0.3 kg respectively. The wider suppression band of the NLTVA can be seen clearly in these figures. For the lighter mass, a strange peak is shown around 35 Hz. To find the reason for this small peak, the time history was studied at these frequencies. A typical example of the motion can be seen in Figure 5.20. Looking at the time history in Figure 5.20, one sees how the amplitude of the displacement of the main mass varies periodically with a frequency that is one fifth of the

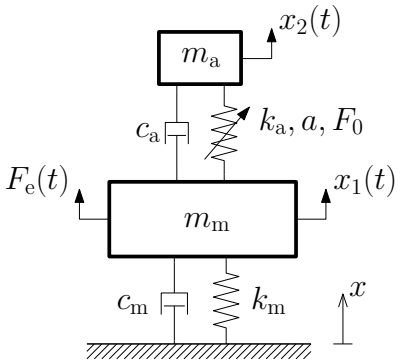

Figure 5.16: 2-DOF model with only main mass and auxiliary mass.

main frequency or 6.5 Hz. Therefore the amplitude of the displacement of main mass varies with the same frequency giving a higher RMS value than at frequencies where the amplitude is constantly low. Although this slight beat is present, the vibration is still much lower than when the LTVA is used up to 50 Hz for both the 0.7 and 0.3 kg auxiliary mass. After the resonance around 55 Hz, the motion becomes chaotic and the level of vibration is slightly higher than when an LTVA or no TVA is used. This shows that the non-linearities present can be beneficial to reduce a resonance, if the system has quadratically increasing excitation as used here and the excitation frequency does not go too high above the resonance frequency. In this case, excitations above 40 Hz give increased vibration compared to the system without the NLTVA.

For more general results and conclusions, this study should be continued by investigating different damping and exciting force scenarios. For example, optimisation should be performed with several different values of main damping c_m and auxiliary damping c_a. It should also include different exciting force assumptions; constant, linearly increasing and quadratically increasing exciting force amplitude.

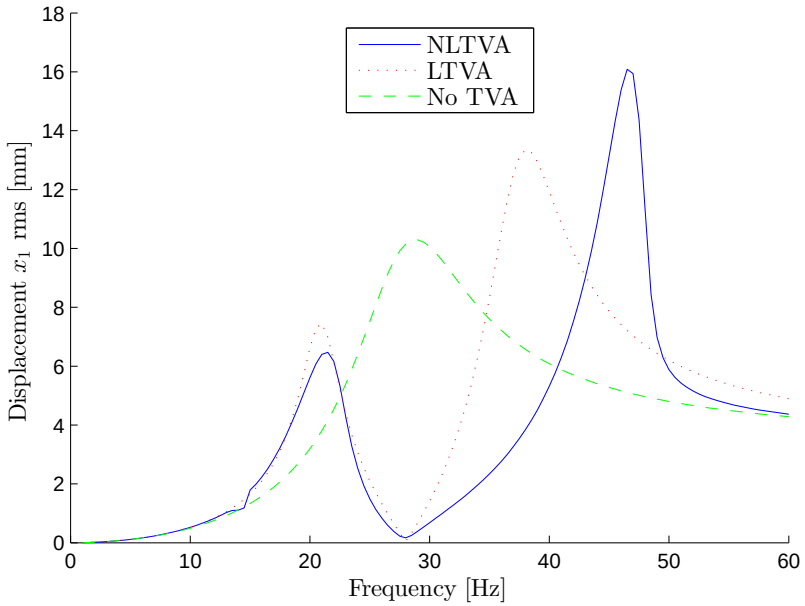

Figure 5.17: Response of the main mass when the resonance between the ground and the main mass has been set to 28 Hz. The response is shown without a TVA, with an optimised NLTVA and an LTVA. $m_\mathrm{a} = 1$ kg. Note that the amplitude of the force grows quadratically.

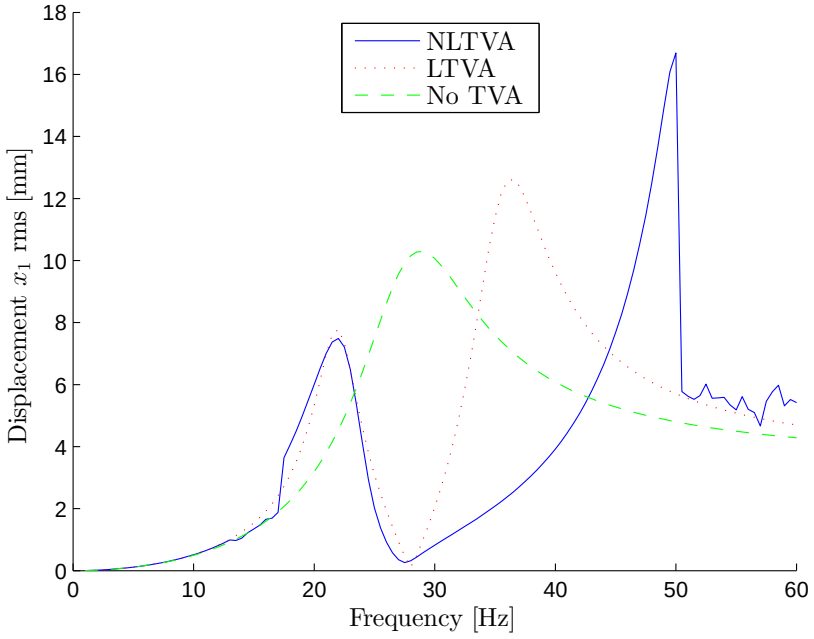

Figure 5.18: Response of the main mass when the resonance between the ground and the main mass has been set to 28 Hz. The response is shown without a TVA, with an optimised NLTVA and LTVA. $m_a = 0.7$ kg. Note that the amplitude of the force grows quadratically.

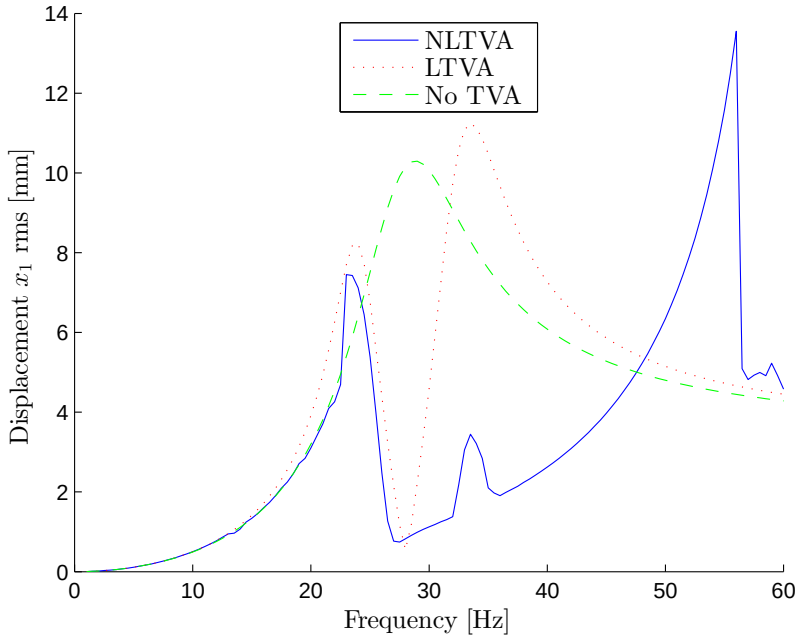

Figure 5.19: Response of the main mass when the resonance between the ground and the main mass has been set to 28 Hz. The response is shown without a TVA, with an optimised NLTVA and LTVA. $m_a = 0.3$ kg. Note that the amplitude of the force grows quadratically.

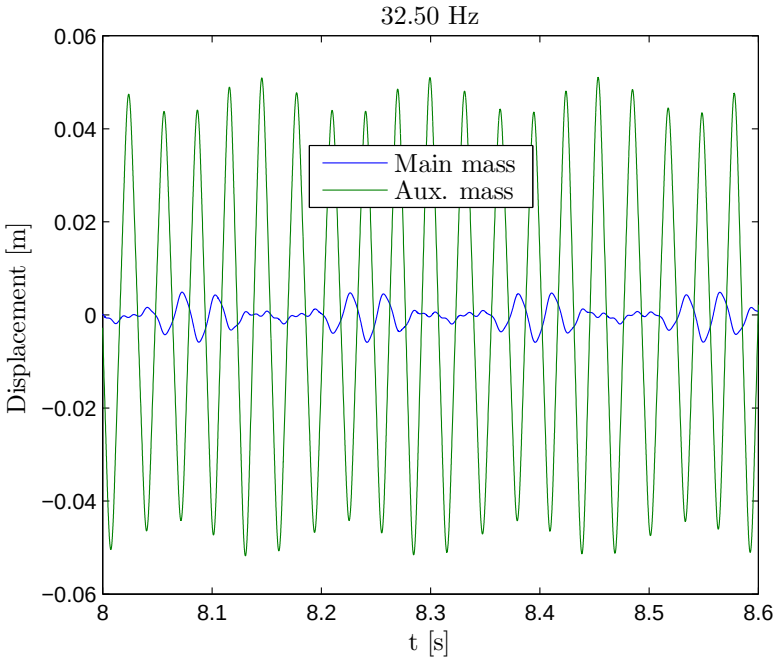

Figure 5.20: Example of time history of the motion at the small peak for $m_a = 0.3$ kg. The amplitude of the displacement of the auxiliary mass varies sinusoidally with a frequency one fifth of the operating frequency.

6 Conclusions

The main goal of the project was to optimise the performance of the NLTVA currently in use in the prototype P3B. A numerical MATLAB model has been built that predicts the vibration of the machine by solving the non-linear 3-DOF equation of motion using a built-in ODE solver. Investigation of the model showed that the error tolerances on the numerical solution had to be tighter than the default ones in MATLAB to give trustworthy results. The model was verified against analytical results and validated against experimental data from the prototype. Comparison of different ODE solvers showed that *ode45* with tightened error tolerances performed best, i.e. it solved the ODE fastest with high accuracy. The calculation time was reduced further by making the auxiliary spring force acting between the auxiliary mass and the main mass continuous and smooth at all points. This was achieved using a third order polynomial in the areas of non-smoothness. The exciting force was measured experimentally to give a realistic input in the model. It was approximated as a sinusoidal force and assumed to increase quadratically in amplitude with excitation frequency.

An objective function was defined in such way that it sums up the level of vibration around the nominal operating frequency, thus taking into account the possible variations in the operating frequency. The frequency points used are distributed around the nominal frequency using a normal distribution, thereby putting more emphasis on minimising the response in the region closest to the nominal operating frequency. The minimisation function *lsqnonlin* was used to minimise the vibration of the handle at the frequencies defined in the objective function. The three parameters subject to optimisation were spring stiffness k_a, gap length a and spring preload F_0. The optimisation results for the current prototype suggests that the level of suppression and the width of the suppression band can be increased significantly. The optimal solutions were highly non-linear and included a significant increase in the gap length a and the spring stiffness k_a which suggests that the best performance is achieved when the auxiliary mass barely compresses the springs to create a counterforce. That means that the auxiliary mass is bouncing against the main mass in an impact-like manner.

A comparison has been made between different ways of varying the amplitude of the exciting force with operating frequency. The formulations used were; quadratically increasing, linearly increasing and a constant amplitude. The results show that the NLTVA gives a much wider suppression band than an LTVA for all the amplitude formulations tested. The superiority of the NLTVA is greatest when a quadratically increasing amplitude is used, slightly less for a linearly increasing amplitude and yet a bit smaller for a constant amplitude.

A likely reason for this superiority of the NLTVA is that its resonance frequency moves up with the operating frequency as it increases. The operating frequency and the resonance frequency stay closest together when the amplitude increases quadratically.

Optimisations with lower mass ratios showed that the vibration suppression decreases with a lighter auxiliary mass. That relation was as expected but the more surprising finding was that the decrease in suppression is very gradual down to $m_{\mathrm{a}} = 0.6$ kg, but below that the performance decreases much more rapidly. For auxiliary mass weights below 0.5 kg the initial state was critical, i.e. the response became chaotic in certain cases. Another interesting finding regarding the weight of the auxiliary mass was that, when the optimisation was performed with the weight of the auxiliary mass as a free parameter with an upper bound at 3 kg, the lowest values of the objective function were obtained when m_{a} was around 2 kg. This suggests that there is a limit on how much the performance of the NLTVA can be improved by increasing the weight of the auxiliary mass.

A study was performed to investigate the proposed NLTVA's performance when it comes to the traditional task, to suppress a resonance in a system. The study showed that, for the exciting force used, the suppression at the target frequency was almost as good as when an LTVA is used but the suppression band is much wider. For lighter auxiliary masses, slight beats were observed above the target frequency but although those beats gave a reduction in vibration suppression, the suppression at these frequencies was still much better than if an LTVA was used. An interesting further investigation would be to consider resonance removal for different excitation forces numerically and validate the results experimentally if they suggest that the NLTVA is superior to the LTVA.

Unfortunately, none of the results from the optimisations have been validated against test data from the prototype. That is a matter for future work. Therefore the question whether the already low vibration of the prototype will decrease significantly in reality if the parameters from the optimisation are used remains unanswered. The results do however strongly suggest that it will. Validation should be done by tuning the available prototype using the optimised parameters and measure if the level of vibration becomes lower than it already is. If these experiments agree with the optimisation results presented, the NLTVA can be optimised and implemented on reciprocating machines of other dimensions and characteristics rather easily with the help of the developed MATLAB code. Since the sensitivity analysis showed that the tuned frequency is sensitive to the amplitude of the exciting force, variations of it should be accounted for in the objective function.

7 Recommendations

The optimisations showed that a very low objective function can be achieved using a variety of parameter sets. The parameter sets are however delivered with such high precision that manufacturing the NLTVA could be problematic. One obvious problem is that manufacturing a spring that has a stiffness over 250 kN/m with a precision of less than 1 kN/m would be very expensive and complex, if possible at all. An approach to solve this problem would be to decide the combination of parameters in three steps:

1. Run an optimisation where all three parameters are free and sufficiently broad bounds.
2. Inspect the parameter sets that give a low objective function value L and pick out a value of k_{a}. The value would then be compared to available springs. Choose the spring with a stiffness closest to the chosen k_{a}.
3. Run another optimisation using the stiffness of the chosen spring as a fixed parameter and the preload F_0 and gap length a as free parameters with rather tight bounds around the values obtained in step 1. This will give more correct values for these parameters to use with the chosen spring.

This method should give good results since the preload F_0 and gap length a are much more controllable than the stiffness k_{a}. Using this method should therefore minimise the loss of vibration suppression due to using a spring that is not exactly as stiff as the solution recommends.

References

[1] T. Nilsson. "Arbete med handhållna vibrerande maskiner och skadlig exponering". *Arbetssjukdom - skadlig inverkan - samband med arbete. Ett vetenskapligt underlag för försäkringsmedicinska bedömningar (sju skadeområden). Arbete och Hälsa*. Ed. by P. Westerholm. 15. Stockholm: Arbetslivsinstitutet, 2002, pp. 245–271.

[2] P. Rehfisch and R. Wålinder. ABC om vibrationsskador. *Läkartidningen* **106**.7 (2009), 439–442.

[3] R. E. Roberson. Synthesis of a nonlinear dynamic vibration absorber. *Journal of the Franklin Institute* **254**.3 (1952), 205–220.

[4] H. Lindell. "Impact machine". WO2014095936A1. 2014.

[5] H. Lindell. Redesign of hand-held impact machines to reduce hand-arm vibration. *Canadian Acoustics* **39**.2 (2011), 80–81.

[6] H. Lindell. *Vibrationer i stenindustrin*. Slutrapport. Swerea IVF, 2012.

[7] H. Frahm. "Device for damping vibrations of bodies". US989958. 1911.

[8] J. Ormondroyd and J. P. Den Hartog. Theory of the dynamic vibration absorber. *Transactions of the American Society of Mechanical Engineers* **50**.7 (1928), 11–22.

[9] J. P. Den Hartog. *Mechanical vibrations*. 4th ed. 1956.

[10] K. Y. Hao, L. X. Mei, and Z. M. Ripin. Tuned vibration absorber for suppression of hand-arm vibration in electric grass trimmer. *International Journal of Industrial Ergonomics* **41**.5 (2011), 494–508.

[11] K. Y. Hao and Z. M. Ripin. Nodal control of grass trimmer handle vibration. *International Journal of Industrial Ergonomics* **43**.1 (2013), 18–30.

[12] L. A. Pipes. Analysis of a nonlinear dynamic vibration absorber. *Journal of Applied Mechanics* **20** (1953), 515–518.

[13] F. R. Arnold. Steady-state behavior of systems provided with nonlinear dynamic vibration absorbers. *Journal of Applied Mechanics* **22**.4 (1955), 487–492.

[14] J. Hunt and J.-C. Nissen. The broadband dynamic vibration absorber. *Journal of Sound and Vibration* **83**.4 (1982), 573–578.

[15] M. Wang. Feasibility study of nonlinear tuned mass damper for machining chatter suppression. *Journal of Sound and Vibration* **330**.9 (2011), 1917–1930.

[16] G. Schlesak et al. "Variation of the natural frequency of vibratory means in electric tools". US20120279741. 2012.

[17] J. Hecht et al. "Hand-held power tool". US8434565. 2013.

[18] F. Moessnang. "Oscillation damper for hand-held power tool". US8066106. 2011.

[19] F. Moessnang. "Hand-held power tool with an oscillation damper". US7712548. 2010.

[20] *The Nonlinear Tuned Vibration Absorber, The European Research Council (ERC)*. URL: `http://erc.europa.eu/nonlinear-tuned-vibration-absorber` (visited on 2015-04-13).

[21] T. Detroux et al. Performance, robustness and sensitivity analysis of the nonlinear tuned vibration absorber. *Mechanical Systems and Signal Processing* **60–61** (2015), 799–809.

[22] G. Habib et al. Nonlinear generalization of Den Hartog's equal-peak method. *Mechanical Systems and Signal Processing* **52–53** (2015), 17–28.

[23] L. Burström, R. Lundström, and A. Sörensson. "Kunskapsunderlag för åtgärder mot skador och besvär i arbete med handhållna vibrerande maskiner. Tekniska Aspekter." *Arbete och Hälsa*. 17. Stockholm: Arbetslivsinstitutet, 2000.

[24] Arbetsmiljöverkets författningssamling. *AFS 2005:15 - Vibrationer*. 2005.

[25] European Parliament, Council of the European Union. *Directive 2002/44/EC - vibration*. 2002. URL: `https://osha.europa.eu/en/legislation/directives/exposure-to-physical-hazards/osh-directives/19` (visited on 2015-01-20).

[26] ISO 5349-1, 2001. *Mechanical vibration – Measurement and evaluation of human exposure to hand-transmitted vibration – Part 1: General Requirements*.

[27] E. Golysheva, V. Babitsky, and A. Veprik. Vibration protection for an operator of a hand-held percussion machine. *Journal of Sound and Vibration* **274**.1–2 (2004), 351–367.

[28] A. Fischer, R. Meuer, and M. Weber. "Hand-held power tool". US8443912. 2013.

[29] S. R. Henriksson and O. B. S. Östenssn. "Impact tool with a movably supported impact mechanism". US7614460. 2009.

[30] N. Hahn. "Vibration dampening mechanism". US7451833. 2008.

[31] V. Babitsky. Hand-held percussion machine as discrete non-linear converter. *Journal of Sound and Vibration* **214**.1 (1998), 165–182.
[32] E. Golycheva, V. Babitsky, and A. Veprik. Dynamic correction of excitation in hand-held electro-pneumatic percussion machines. *Journal of Sound and Vibration* **259**.4 (2003), 829–843.
[33] I. Sokolov, V. Babitsky, and N. Halliwell. Hand-held percussion machines with low emission of hazardous vibration. *Journal of Sound and Vibration* **306**.1–2 (2007), 59–73.
[34] ISO 28927-10, 2009. *Hand-held portable power tools – Test methods for evaluation of vibration emission – Part 10: Percussive drills, hammers and breakers.*
[35] *MATLAB Documentation. ode45.* Version R2015a. Mathworks, 2015. URL: `http://se.mathworks.com/help/matlab/ref/ode45.html` (visited on 2015-02-02).
[36] *MATLAB Documentation. Least-Squares (Model Fitting) Algorithms.* Trust-Region-Reflective Least Squares. Version R2015a. Mathworks, 2015. URL: `http://se.mathworks.com/help/optim/ug/least-squares-model-fitting-algorithms.html#broz0i4` (visited on 2015-04-07).
[37] A. Nilsson and T. Östgårdh. "Verifiering av matematisk modell för vibrationsdämpare". Bachelor's thesis. Chalmers University of Technology, 2014.
[38] F. A. Mussa-Ivaldi, N. Hogan, and E. Bizzi. Neural, mechanical, and geometric factors subserving arm posture in humans. *The Journal of Neuroscience* **5**.10 (1985), 2732–2743.
[39] T. Tsuji et al. Human hand impedance characteristics during maintained posture. *Biological Cybernetics* **72**.6 (1995), 475–485.
[40] *MATLAB Documentation. When the Solver Fails.* Version R2015a. Mathworks, 2015. URL: `http://se.mathworks.com/help/optim/ug/when-the-solver-fails.html` (visited on 2015-04-07).
[41] *MATLAB Documentation. Improving Performance with Parallel Computing.* Version R2015a. Mathworks, 2015. URL: `http://se.mathworks.com/help/optim/ug/improving-performance-with-parallel-computing.html` (visited on 2015-02-02).

A Derivation of analytical formulas for the non-linear auxiliary system

In this chapter, an exact analytical formula for the resonance frequency of the non-linear auxiliary system with spring stiffness k_a, gap a and preload F_0 is derived for the case of no damping or gravity. Due to the non-linearity, the resonance frequency depends on the vibration amplitude. Assuming that the main mass is completely still when considering the 2-DOF case (both main mass and auxiliary mass) leads to a formula for the vibration amplitude of the auxiliary mass as a function of exciting force amplitude. These results can be used to tune a non-linear TVA to a certain frequency at a certain exciting force amplitude.

Consider free vibration of the auxiliary system in Figure A.1, i.e. without damping and exciting force. Also neglect gravity force. One vibration period time T can be divided into two distinct parts: when the auxiliary mass is not in contact with the main mass and when the auxiliary spring is compressing. Denote the time between positions I and II in Figure A.1 as t_a. Denote the time from position II to position III and back as t_b, cf. Figure A.2. A complete period is then given by

$$T = 2t_a + 2t_b \tag{A.1}$$

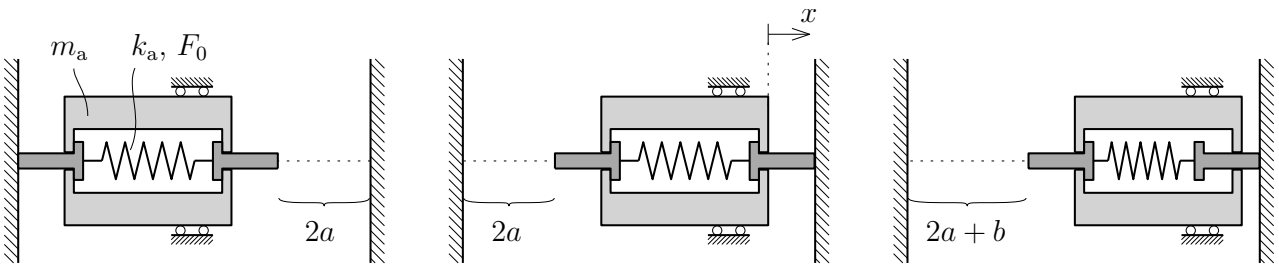

(a) Position I. **(b)** Position II, $x = 0$. **(c)** Position III, $x = b$, $\dot{x} = 0$.

Figure A.1: Auxiliary system at three distinct positions, with the helping coordinate x introduced.

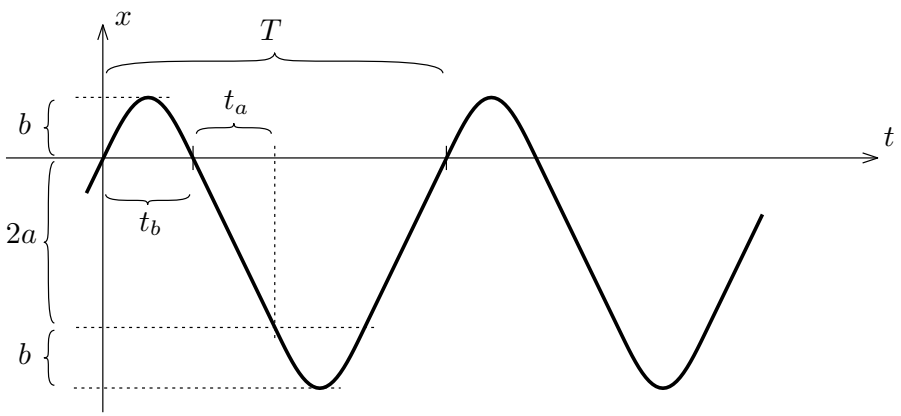

Figure A.2: Motion of the free vibrating non-linear auxiliary system, in terms of the helping coordinate x.

First, consider only the part in which the auxiliary spring is compressing, i.e. for $0 \leq t \leq t_b$. The auxiliary spring force is $F_k = k_\mathrm{a}x + F_0$. Setting up the equation of motion, with the helper coordinate x defined in Figure A.1b, gives

$$m_\mathrm{a}\ddot{x} + k_\mathrm{a}x = -F_0 \tag{A.2}$$

The solution to this equation is

$$x(t) = C\sin(\omega_\mathrm{a}t + \varphi) - \frac{F_0}{k_\mathrm{a}} \tag{A.3}$$

where C and φ are constants from integration and $\omega_\mathrm{a} = \sqrt{k_\mathrm{a}/m_\mathrm{a}}$ is the eigenfrequency if no gap or preload is present. From (A.3) and the extreme point $x = b$ in Figure A.1c, it is seen that $\max\big(x(t)\big) = C - F_0/k_\mathrm{a} = b$, which gives

$$C = \frac{F_0}{k_\mathrm{a}} + b \tag{A.4}$$

From position II in Figure A.1b, $x(0) = 0$, it is seen that

$$\begin{aligned} x(0) = \left(\frac{F_0}{k_\mathrm{a}} + b\right)\sin(\varphi) - \frac{F_0}{k_\mathrm{a}} = 0 \quad \Longrightarrow \\ \varphi = \arcsin\left(\frac{F_0}{F_0 + k_\mathrm{a} b}\right) \end{aligned} \tag{A.5}$$

Now the motion when the auxiliary spring is compressing is completely known. Remember that this is only valid for $0 \leq t \leq t_b$. Inserting (A.4) and (A.5) into (A.3) gives the motion as

$$x(t) = \left(\frac{F_0}{k_\mathrm{a}} + b\right)\sin\left(\omega_\mathrm{a} t + \arcsin\left(\frac{F_0}{F_0 + k_\mathrm{a} b}\right)\right) - \frac{F_0}{k_\mathrm{a}}, \qquad 0 \leq t \leq t_b \tag{A.6}$$

Now it is possible to determine the velocity $\dot{x}(0)$ just as the auxiliary mass touches the wall, and thereby also the time t_a since the velocity is constant while the auxiliary mass is not in contact.

$$\begin{aligned} \dot{x}(t) &= \omega_\mathrm{a}\left(\frac{F_0}{k_\mathrm{a}} + b\right)\cos(\omega_\mathrm{a} t + \varphi), \qquad 0 \leq t \leq t_b \\ \dot{x}(0) &= \omega_\mathrm{a}\left(\frac{F_0}{k_\mathrm{a}} + b\right)\cos(\varphi) = \omega_\mathrm{a}\left(\frac{F_0}{k_\mathrm{a}} + b\right)\frac{\sqrt{k_\mathrm{a}^2 b^2 + 2F_0 k_\mathrm{a} b}}{F_0 + k_\mathrm{a} b} = \omega_\mathrm{a}\sqrt{\frac{k_\mathrm{a} b^2 + 2F_0 b}{k_\mathrm{a}}} \\ t_a &= \frac{2a}{\dot{x}(0)} = \frac{2a}{\omega_\mathrm{a}}\sqrt{\frac{k_\mathrm{a}}{k_\mathrm{a} b^2 + 2F_0 b}} \end{aligned} \tag{A.7}$$

The time t_b is determined by solving $x(t) = 0$ for a time that fulfil $0 < t \leq \pi/\omega_\mathrm{a}$. See $t = t_b$ in Figure A.2. The following solutions exist for $x(t) = 0$ from (A.6):

$$\begin{cases} \omega_\mathrm{a} t + \varphi = \varphi + 2\pi n & \Longrightarrow t = \dfrac{2\pi n}{\omega_\mathrm{a}} \\ \omega_\mathrm{a} t + \varphi = \pi - \varphi + 2\pi n & \Longrightarrow t = \dfrac{\pi(1 + 2n) - 2\varphi}{\omega_\mathrm{a}} \end{cases} \tag{A.8}$$

where n is any integer. The only interesting solution is in the second row of (A.8) for $n = 0$, which gives

$$t_b = \frac{1}{\omega_\mathrm{a}}\left(\pi - 2\arcsin\left(\frac{F_0}{F_0 + k_\mathrm{a} b}\right)\right) \tag{A.9}$$

The total period time T can now be formed from (A.1) with (A.7) and (A.9). The corresponding resonance frequency of the free vibrating auxiliary system is $f_\mathrm{res} = T^{-1} = (2t_a + 2t_b)^{-1}$. This is the exact result for the auxiliary system when the main mass is fixed as ground and there is no damping or gravity. It is written explicitly as

$$f_\mathrm{res} = \sqrt{\frac{k_\mathrm{a}}{m_\mathrm{a}}}\left[2\pi - 4\arcsin\left(\frac{F_0}{F_0 + k_\mathrm{a} b}\right) + 4a\sqrt{\frac{k_\mathrm{a}}{k_\mathrm{a} b^2 + 2F_0 b}}\right]^{-1} \tag{A.10}$$

Note that if both gap a and preload F_0 are zero, the auxiliary system is linear and its resonance frequency is of course $f_\mathrm{res} = \omega_\mathrm{a}/2\pi$.

Finding tuned frequency with main mass included

Now consider the case with both main mass and auxiliary mass. Since this is a non-linear system, the resonance frequency in (A.10) depends on the vibration amplitude $a + b$, while the spring compression b is in turn depending on the exciting force amplitude $|F_\mathrm{e}|$, which depends quadratically on the exciting frequency f as discussed in Section 3.4.5. What is left is to find is the spring compression b as a function of the exciting force

amplitude $|F_\mathrm{e}|$, assuming sinusoidal exciting force.

Consider vibration when excitation frequency f and resonance frequency f_res are equal, still neglecting damping and gravity. It is assumed that vibration in the main mass is suppressed completely, as if it was simply attached to ground, cf. Figure A.1. This is not entirely correct since the exciting force and the auxiliary spring force does not have exactly the same shape and therefore cannot cancel each other. The assumption implies that the momentum of the main mass is constant and equal to zero. This in turn implies that the impulses acting on the main mass from exciting force and spring force must be equal opposites:

$$I_\mathrm{e} + I_k = 0 \tag{A.11}$$

The impulse from the exciting force during one half period is

$$I_\mathrm{e} = \int_0^{T/2} F_\mathrm{e}(t)\ \mathrm{d}x = |F_\mathrm{e}| \int_0^{1/2f} \sin(2\pi f t)\ \mathrm{d}x = \frac{|F_\mathrm{e}|}{\pi f} \tag{A.12}$$

The impulse from the spring force is obtained by deriving the spring force as a function of time. This force is of course zero when the auxiliary mass is not in contact. When in contact, the spring force is $F_k(t) = \ddot{x}(t) m_\mathrm{a}$. Acceleration $\ddot{x}(t)$ of the auxiliary mass when in contact is calculated from the motion in (A.6). The spring force is then given as

$$F_k(t) = -m_\mathrm{a}\omega_\mathrm{a}^2 \left(\frac{F_0}{k_\mathrm{a}} + b\right) \sin(\omega_\mathrm{a} t + \varphi) = -(F_0 + k_\mathrm{a} b) \sin(\omega_\mathrm{a} t + \varphi) \tag{A.13}$$

The impulse from the spring force during one half period is calculated as

$$I_k = \int_0^{T/2} F_k(t)\ \mathrm{d}x = -(F_0 + k_\mathrm{a} b) \int_0^{t_b} \sin(\omega_\mathrm{a} t + \varphi)\ \mathrm{d}x = -\frac{2}{\omega_\mathrm{a}} \sqrt{k_\mathrm{a}^2 b^2 + 2F_0 k_\mathrm{a} b} \tag{A.14}$$

where t_b is taken from (A.9). Using the cancelling impulses from (A.11) and the results from (A.12) and (A.14), an expression for the spring compression b as a function of exciting force amplitude $|F_\mathrm{e}|$ can be obtained as

$$\begin{aligned}
\frac{|F_\mathrm{e}|}{\pi f} &= \frac{2}{\omega_\mathrm{a}} \sqrt{k_\mathrm{a}^2 b^2 + 2F_0 k_\mathrm{a} b} \\
\frac{k_\mathrm{a}}{m_\mathrm{a}} \left(\frac{|F_\mathrm{e}|}{2\pi f}\right)^2 &= k_\mathrm{a}^2 b^2 + 2F_0 k_\mathrm{a} b \\
\frac{k_\mathrm{a}}{m_\mathrm{a}} \left(\frac{|F_\mathrm{e}|}{2\pi f}\right)^2 + F_0^2 &= (F_0 + k_\mathrm{a} b)^2 \\
b &= \frac{1}{k_\mathrm{a}} \left[\sqrt{\frac{k_\mathrm{a}}{m_\mathrm{a}} \left(\frac{|F_\mathrm{e}|}{2\pi f}\right)^2 + F_0^2} - F_0\right]
\end{aligned} \tag{A.15}$$

Note that (A.15) is based on the assumption of perfectly cancelling impulses in (A.11), which is not exactly the case in reality.

The vibration amplitude $a + b$ is now known as a function of exciting force amplitude. To find the resonance frequency for a given exciting force, one has to solve a system of non-linear equations consisting of (A.10), (A.15) and a relation between exciting force amplitude $|F_\mathrm{e}|$ and excitation frequency f.

B Pictures of measurement set-up

Below are some pictures from the measurements on the HHIM prototype without housing in the ball absorber test rig.

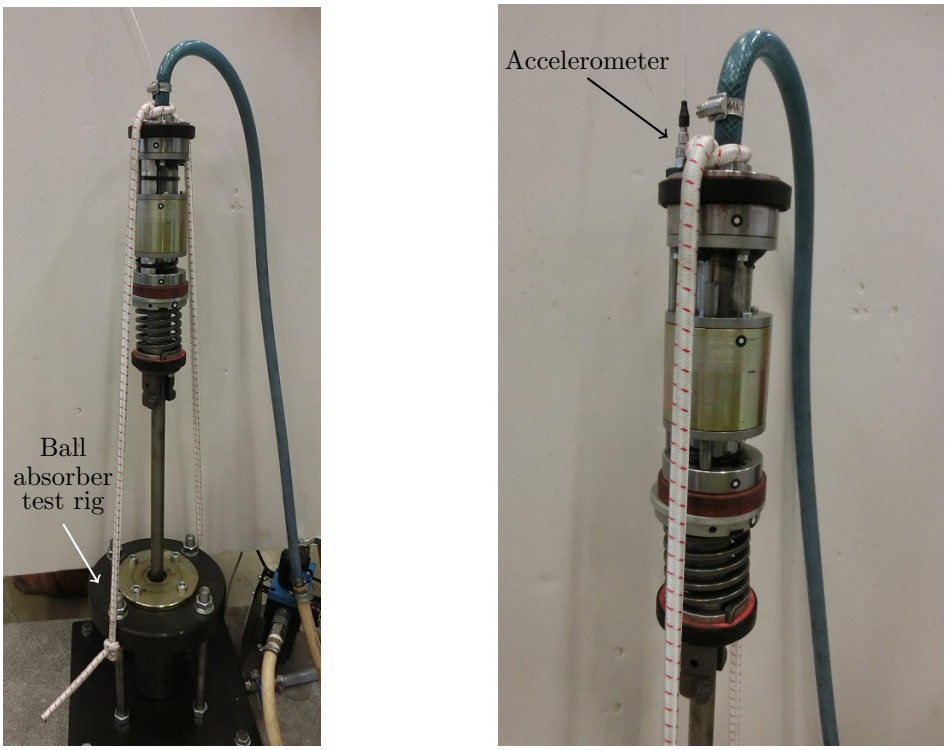

(a) The prototype machine in the ball absorber test rig.

(b) Close up with the accelerometer on the top surface next to the air intake.

Figure B.1: Measurement set-up with elastic bands keeping the prototype machine in place vertically.

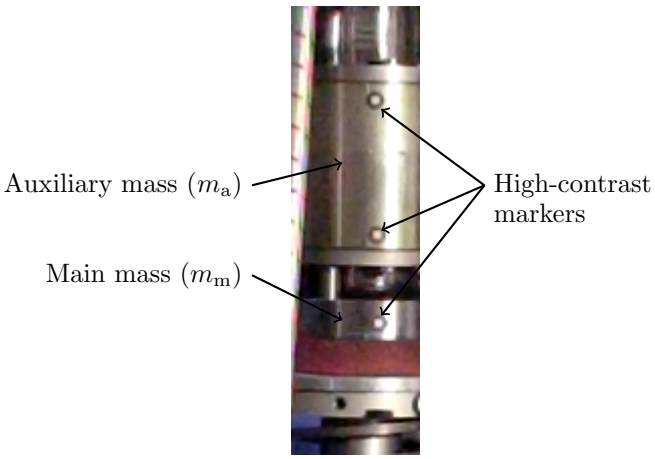

Figure B.2: High-speed video footage at 1000 fps. Resolution is authentic; 224×64. The housing was removed and the auxiliary mass is seen in the upper half. High-contrast markers were used to measure motion in Tracker.

C Flowchart of the optimisation routine

Figure C.1 illustrates the optimisation routine that is implemented in MATLAB using the built-in least squares solver *lsqnonlin* together with the following customised scripts/function files: *TVA3_main.m*, *TVA3_obj.m* and *TVA3_fr.m*. Note that not all details in the methodology are included.

In short, *TVA3_main.m* is where the model parameters are defined as well as the optimisation settings for maximum number of optimisation runs, maximum total computation time, which parameters to optimise (the free parameters) and the bounds for the free parameters. After that, the parallel pool is started if it is available. Before the optimisation starts, detailed settings for *lsqnonlin* are made such as which algorithm to use and the change in parameters when calculating finite difference gradients. Results from all completed starts together with other relevant data such as model parameters in use, bounds, randomised starting values etc. are saved to a .mat file named with a time stamp according to *optrun_YYYY-MM-DD_hh.mm.ss.mat*.

TVA3_obj.m computes a vector of weighted velocity RMS responses at the handle, the sum of which is defined as the objective function value L. The nominal operating frequency (28 Hz default), the relative frequency range to consider (± 15 % default) and settings for the weighting function are defined here.

In *TVA3_fr.m*, the response of the 3-DOF system is computed given the model parameters and a vector of excitation frequencies. The response can be returned as displacement RMS, velocity RMS, acceleration RMS and phase angle at the main mass, the auxiliary mass and the housing. Time signals of all masses can also be retrieved and plotted from this function. The system can also be easily configured as a 2-DOF or 1-DOF system by putting rigid links between two or all three of the masses.

Since the optimisation runs are independent from each other, they can be run in parallel if the computer has multiple cores in the CPU and if the Parallel Computing Toolbox is available in MATLAB. This also means that one can run the main script simultaneously on different computers. When several batches of these runs have been performed, a convenient script called *gather_optruns.m* is used to gather the data from all optimisations with the same model parameter values and the same free parameters during optimisation. The script sorts all obtained objective function values in ascending order and allows for an easy overview of the resulting optimised parameters from the best runs.

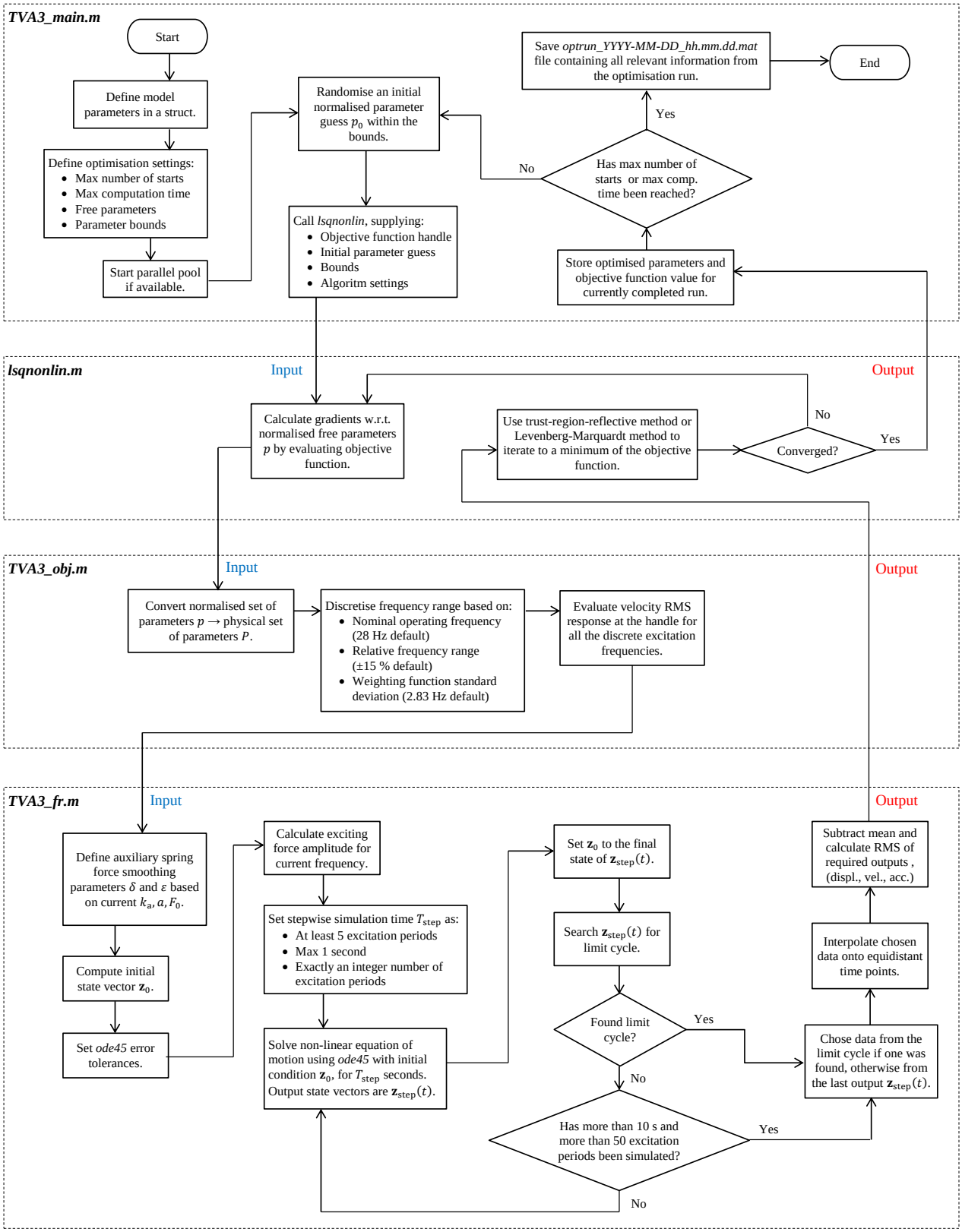

Figure C.1: Flowchart of the optimisation routine in MATLAB.